ΠΑΝΕΠΙΣΤΗΜΙΟ ΘΕΣΣΑΛΙΑΣ
ΣΧΟΛΗ ΕΠΙΣΤΗΜΩΝ ΥΓΕΙΑΣ
ΤΜΗΜΑ ΙΑΤΡΙΚΗΣ

ΕΡΓΑΣΤΗΡΙΟ ΦΥΣΙΟΛΟΓΙΑΣ

Διευθύντρια: Καθηγήτρια Χρυσή Χατζόγλου

Διδακτορική Διατριβή

«Dissecting the role of aquaporin-1 (AQP1) and amiloride sensitive epithelial sodium channel (ENaC) in pleural mesothelioma biology»

υπό

RAJESH M. JAGIRDAR

MICROBIOLOGIST

Υπεβλήθη για την εκπλήρωση μέρους των

απαιτήσεων για την απόκτηση του

Διδακτορικού Διπλώματος

Λάρισα, 2018

Η έγκριση της διδακτορικής διατριβής από το Τμήμα Ιατρικής της Σχολής Επιστημών Υγείας του Πανεπιστημίου Θεσσαλίας δεν υποδηλώνει αποδοχή των απόψεων του συγγραφέα (σύμφωνα με τις διατάξεις του άρθρου 202, παράγραφος 2 του Ν.5343/1932).

Εγκρίθηκε από τα Μέλη της Επταμελούς Εξεταστικής Επιτροπής (6η/21-11-2018 ΓΣΕΣ):

1ος Εξεταστής (Επιβλέπων)	**Ζαρογιάννης Σωτήριος** Επίκουρος Καθηγητής Φυσιολογίας, Τμήμα Ιατρικής, Πανεπιστήμιο Θεσσαλίας
2ος Εξεταστής	**Γουργουλιάνης Κωνσταντίνος** Καθηγητής Πνευμονολογίας, Τμήμα Ιατρικής, Πανεπιστήμιο Θεσσαλίας
3ος Εξεταστής	**Μολυβδάς Πασχάλης-Αδάμ** Ομότιμος Καθηγητής Φυσιολογίας, Τμήμα Ιατρικής, Πανεπιστήμιο Θεσσαλίας
4ος Εξεταστής	**Γερμενής Αναστάσιος** Καθηγητής Εργαστηριακής Ανοσολογίας, Τμήμα Ιατρικής, Πανεπιστήμιο Θεσσαλίας
5ος Εξεταστής	**Δανιήλ Ζωή** Καθηγήτρια Πνευμονολογίας, Τμήμα Ιατρικής, Πανεπιστήμιο Θεσσαλίας
6ος Εξεταστής	**Χατζόγλου Χρυσή** Καθηγήτρια Ιατρικής Φυσιολογίας, Τμήμα Ιατρικής, Πανεπιστήμιο Θεσσαλίας
7ος Εξεταστής	**Παρασκευά Ευφροσύνη** Αναπληρώτρια Καθηγήτρια Κυτταρικής Φυσιολογίας, Τμήμα Ιατρικής, Πανεπιστήμιο Θεσσαλίας

ACKNOWLEDGEMENTS

My education is a reflection of support, from my mother Mrs. Ranjana Jagirdar, my father Mr. Mukund Jagirdar, my very loving and understanding family that encouraged work and curiosity. My younger sister, Mrs Roopa Jagirdar Podicheti and Dr. Ram Podicheti, thanks for the appreciation you've shown.

Among my mentors, I count Assistant Professor of Physiology Sotirios Zarogiannis, also as my friend, my Guru, a rock who never wavered in his faith of science, of doing the right thing and, above all else being a man of his own accomplishments. I am delighted to be your first Ph.D. student.

To the Professor of Respiratory Medicine Konstantinos Gourgoulianis, my deepest respect and a heartfelt thank You. No words will suffice the depth of my gratitude to you. Your support and guidance stimulated me to think in a more broad scientific way. Thank You, Emeritus Professor Paschalis-Adam Molyvdas for the constant encourgement and support and for the very fruitful scientific discussions that we had.

To the Professor of Medical Physiology and Chair of the Department of Physiology, Dr. Chrissi Hatzoglou, a great thanks for everything, from scientific guidance and discussions to letters of support to the Greek embassy and to helping me with the lab needs even on weekends. Your help is always invaluable.

Also I would like to thank the Associate Professor of Cellular Physiology Efrosini Paraskeva, for orientation and help when needed especially during my initial days in Larissa.

I would also like to thank the members of my examination committee, Professor of Laboratory Immunology Anastasios Germenis, Professor of Respiratory Medicine Zoi

Daniil and Associate Professor of Cellular Physiology Efrosyni Paraskeva for stimulating discussions and for taking the time to read and assess my PhD Thesis.

Many thanks to Dr. Ioannis Kalomendis, Dr. Sofia Magkouta for the kind gifts of the cell lines.

I would also like to thank Dr. Konstantinos Dimas and Dr. Ilias Begas for the kind provision of the rat tails in order to conduct the gel contraction experiments.

Last but not least, my lab members, the finest minions of science I've met, Dr. Erasmia Rouka, Dr. Ourania Kotsiou, Mr. Eleftherios Papazoglou, Ms. Eleanna Pitaraki, Ms. Lydia Giannakou, Ms. Olympia Kouliou and Mr. Stefanos Giannopoulos, your help and every bit of patience, kindness and the will to work as a team, I wish you all Thanks, many times over.

My friends from childhood Mr. Kaushal Clarence, Mr. Vijay Cirium, every vacation in India, during my studies in Ph.D. they loved, understood, and helped every way they could so I could go on.

My peers, colleagues and acquaintances who helped every way they could, Dr. Giorgos Pisas, Ms. Gerasimina Tsinti, Dr. Adam Molyvdas, Ms. Rafaela Beta, Mr. Dionisis. Antonopoulos, and Mr Ioannis Makantasis, to all of you I say, the minion network is a great help in difficult times. Thank You all.

The rent I owe to Science, a part of it, is now paid.

Rajesh M. Jagirdar

SHORT CURRICULUM VITAE

Name: Rajesh M Jagirdar
Date of Birth: 27th February 1974
Present: PhD candidate, Department of Physiology, Faculty of Medicine, School of Health Sciences, University of Thessaly, BIOPOLIS, Larissa, Greece

Research Experience	
Dates	**Appointment**
July 2013-Present	**Ph.D. Candidate**, Department of Physiology, University of Thessaly, Larissa, Greece ***Title:*** "Dissecting the role of aquaporin-1 (AQP1) and amiloride sensitive epithelial sodium channel (ENaC) in pleural mesothelioma biology" ***Anticipated Defence in December 2018***
November 2010 – December 2011	**Laboratory Manager**, Veena Antony Laboratory, Department of Medicine, University of Alabama, Birmingham, Alabama, USA
June 2008 – October 2010	**Research Associate II**, Arul Chinnayan Laboratory, University of Michigan, Ann Arbor, Michigan, USA
June 2008 – October 2010	**Research Associate II**, Max Wicha Laboratory, University of Michigan, Ann Arbor, Michigan, USA
December 2005 – May 2008	**Research Associate II**, Victor Thannickal Laboratory, University of Michigan, Ann Arbor, Michigan, USA
August 2003 – November 2005	**Research Assistant II**, Gabriel Nunez Laboratory, University of Michigan, Ann Arbor, Michigan, USA

Academic Degrees			
Date	Title of Award	Subject	Awarding Body
August 2001 – August 2008	MSc	Cellular & Molecular Biology	Eastern Michigan University, Ypsilanti, Michigan, USA
August 1996 – July 1998	MSc	Biotechnology	University of Calicut, Calicut, India
Aug 1993 -Jul 1996	BSc	Botany, Chemistry, Microbiology	Osmania University, Hyderabad, India

Publication Track Record (2006-2018)
Number of Publications: ***11***
1st Author: ***4;*** *Other Author position:* ***7***
Citations: ***2307***
*h-Index****: 8;*** *i10-Index:* ***8***

Publications:

1. Katkova LE, Baturina GS, Bodnar AA, **Jagirdar RM**, Hatzoglou C, Gourgoulianis KI, Solenov EI, Zarogiannis SG. Benign pleural mesothelial cells have higher osmotic water permeability than malignant pleural mesothelioma cells and differentially respond to hyperosmolarity. ***Cell Physiol Biochem. In Press.***

2. Jagirdar RM, Apostolidou E, Molyvdas PA, Gourgoulianis KI, Hatzoglou C, Zarogiannis SG. Influence of AQP1 on cell adhesion, migration and tumor sphere formation in malignant pleural mesothelioma is substratum and histological type dependent. ***Am J Physiol Lung Cell Mol Physiol***. 2016;310:489-95.

3. Peppa VI, Arsenopoulou ZV, Zarogiannis SG, Deligiorgi T, **Jagirdar R**, Makantasis I, Stefanidis I, Liakopoulos V, Molyvdas PA, Gourgoulianis KI, Hatzoglou C. VEGF increases the permeability of sheep pleura ex vivo through VEGFR2 stimulation. ***Cytokine.*** 2014;69:284-8.

4. Zolak JS*, **Jagirdar R***, Surolia R, Karki S, Oliva O, Hock T, Guroji P, Ding Q, Liu RM, Bolisetty S, Agarwal A, Thannickal VJ, Antony VB. Pleural mesothelial cell differentiation and invasion in fibrogenic lung injury.
Am J Pathol. 2013;182:1239-47. * Equal first authorship.

5. Jagirdar R, Solenov EI, Hatzoglou C, Molyvdas PA, Gourgoulianis KI, Zarogiannis SG. Gene expression profile of aquaporin 1 and associated interactors in malignant pleural mesothelioma. ***Gene.*** 2013;517:99-105.

6. Hecker L*, **Jagirdar R***, Jin T, Thannickal VJ. Reversible differentiation of myofibroblasts by MyoD. ***Exp Cell Res.*** 2011;317:1914-21. * Equal first authorship.

7. Hecker L, Vittal R, Jones T, **Jagirdar R**, Luckhardt TR, Horowitz JC, Pennathur S, Martinez FJ, Thannickal VJ.NADPH oxidase-4 mediates myofibroblast activation and fibrogenic responses to lung injury. ***Nat Med.*** 2009;15:1077-81.

8. Chung J, Serezani CH, Huang SK, Stern JN, Keskin DB, **Jagirdar R**, Brock TG, Aronoff DM, Peters-Golden M.Rap1 activation is required for Fc-g receptor-dependent phagocytosis. ***J Immunol.*** 2008;181:5501-9.

9. Amer A, Franchi L, Kanneganti TD, Body-Malapel M, Ozören N, Brady G, Meshinchi S, **Jagirdar R**, Gewirtz A, Akira S, Núñez G. Regulation of Legionella phagosome maturation and infection through flagellin and host Ipaf. ***J Biol Chem.*** 2006;281:35217-23.

10. Franchi L, Amer A, Body-Malapel M, Kanneganti TD, Ozören N, **Jagirdar R**, Inohara N, Vandenabeele P, Bertin J, Coyle A, Grant EP, Núñez G. Cytosolic flagellin requires Ipaf for activation of caspase-1 and interleukin 1beta in salmonella-infected macrophages. ***Nat Immunol***. 2006;7:576-82.

11. Distinct roles of TLR2 and the adaptor ASC in IL-1beta/IL-18 secretion in response to Listeria monocytogenes. Ozören N, Masumoto J, Franchi L, Kanneganti TD, Body-Malapel M, Ertürk I, **Jagirdar R**, Zhu L, Inohara N, Bertin J, Coyle A, Grant EP, Núñez G. ***J Immunol.*** 2006;176:4337-42.

Master Thesis:

1. "Myo-D is a critical switch in fibroblast to myofibroblast differentiation"
M.Sc. Cellular and Molecular Biology - Eastern Michigan University, Ipsilanti, Michigan, USA, 2008

2. "Epidemiological studies of Coxsackie viruses using virus neutralization tests with Vero cell line"
M.Sc Biotechnology - University of Calicut, Calicut, India, 1998

Awards:

1. Research spotlight at University of Alabama, Birmingham USA http://www.dom.uab.edu/2011/05/may-2011-research-spotlight-louise-hecker-ph-d-rajesh-jagirdar-m-s/

2. Meta Hellwig research award for Graduate studies in Cell, Molecular Biology, Eastern Michigan University, USA, 2002

3. Graduate teaching assistant scholarship Molecular Biology BIOL 110 and 120 Introductory Level Biology courses, Department of Biology, Eastern Michigan University, USA, 2001, 2002.

4. JNU National Scholarship: Program sponsored by the Department of Biotechnology. University of Calicut from July 1996 to Aug 1998.

Selected Poster presentations:

1. R. Jagirdar, E. Pitaraki, E. Papazoglou, C. Hatzoglou, K. Gourgoulianis, S. Zarogiannis. Effects of 2-Deoxy-glucose with Cisplatin-Pemetrexed in mesothelioma sphere formation. ***European Respiratory Society International Congress, September 2018, Paris, France.***

2. R. Jagirdar, VB Cirium, E Papazoglou, R.K. Tangirala, N.K. Mohare, E. Rouka, R. Podicheti, C. Hatzoglou, K. Gourgoulianis and S. Zarogiannis. RAG recombinase and DNA sequence dependant interactors promote recurrent gene fusions in solid tumors. ***European Conference on Computational Biology, September 2018, Athens, Greece.***

3. R Jagirdar, S Zarogiannis, PA Molyvdas, C Hatzoglou, K Gourgoulianis. The role of Epithelial sodium channel (ENaC) in cell proliferation and tunneling nanotube (TnT) formation in benign mesothelial cells and malignant pleural mesothelioma. ***European Respiratory Society International Congress, September 2017, MIlan, Italy.***

4. R. Jagirdar, PA Molyvdas, K. Gourgoulianis, C. Hatzoglou, S. Zarogiannis**.** The role of amiloride sensitive epithelial sodium channel (ENaC) in cell migration of mesothelioma cells is dependent on the cell type and the extracellular matrix. ***European Respiratory Society International Congress, September 2016, London, UK.***

5. O. Kotsiou**, R. Jagirdar**, C. Hatzoglou, K. Gourgoulianis, S. Zarogiannis**.** IL-33 levels in pleural fluids from various etiologies differentially alter mesothelial cell adhesion and migration. ***European Respiratory Society International Congress, September 2016, London, UK.***

6. R. Jagirdar, E. Apostolidou, P.A. Molyvdas, K. Gourgoulianis, C. Hatzoglou, S. Zarogiannis. The role of aquaporin-1 (AQP1) and amiloride sensitive epithelial sodium (ENaC) in cell adhesion of mesothelioma cells is cell and extracellular matrix type dependent. ***European Respiratory Society International Congress, September 2015, Amsterdam, The Netherlands.***

7. S. Zarogiannis, A. Grammatikopoulos, **R. Jagirdar**, D. Magouliotis, V. Peppa, Z. Arsenopoulou, I. Makantasis, P.A. Molyvdas, K. Gourgoulianis, C. Hatzoglou. Electrophysiological study of the ENaC function of sheep tracheal epithelium with and without cigarette smoke extract exposure. ***European Respiratory Society International Congress, September 2015, Amsterdam, The Netherlands.***

«Dissecting the role of aquaporin-1 (AQP1) and amiloride sensitive epithelial sodium channel (ENaC) in pleural mesothelioma biology»

Rajesh M. Jagirdar

Πανεπιστήμιο Θεσσαλίας, Τμήμα Ιατρικής, 2018

ΤΡΙΜΕΛΗΣ ΣΥΜΒΟΥΛΕΥΤΙΚΗ ΕΠΙΤΡΟΠΗ

1. **Σωτήριος Ζαρογιάννης** Επίκουρος Καθηγητής Φυσιολογίας, Τμήμα Ιατρικής, Πανεπιστήμιο Θεσσαλίας **(Επιβλέπων)**
2. **Κωνσταντίνος Γουργουλιάνης** Καθηγητής Πνευμονολογίας, Τμήμα Ιατρικής, Πανεπιστήμιο Θεσσαλίας
3. **Πασχάλης-Αδάμ Μολυβδάς** Ομότιμος Καθηγητής Φυσιολογίας, Τμήμα Ιατρικής, Πανεπιστήμιο Θεσσαλίας

Περίληψη

Το Κακόηθες Μεσοθηλίωμα του Υπεζωκότα (ΚΜΥ) που προκαλείται από περιβαλλοντική έκθεση σε αμίαντο, είναι ένας επιθετικός καρκίνος της υπεζωκοτικής κοιλότητας του θώρακα. Ο ρόλος της Υδατοπορίνης-1 (AQP1) και του επιθηλιακού διάυλου νατρίου (ENaC) χαρακτηρίστηκε στα πλαίσια της βιολογίας του ΚΜΥ. Η αναστολή της λειτουργίας της AQP1 και του ENaC σε κύτταρα μεσοθηλιώματος με Χλωριούχο Υδράργυρο ($HgCl_2$) και Αμιλορίδη αντίστοιχα, εξετάστηκαν στα πλαίσια της κυτταρικής προσκόλλησης, κυτταρικής μετανάστευσης, σχηματισμού σηραγγωδών νανοσωλινίσκων (TnT), κυτταρικού πολλαπλασιασμού, σχηματισμού σφαιροειδών, διήθησης σφαιροειδών και συστολής γέλης κολλαγόνου. Καλοήθη μεσοθηλιακά κύτταρα (MeT-5A), κύτταρα επιθηλιοειδούς (M14K), διφασικού (MSTO) και σαρκωματώδους (ZL34) τύπου ΚΜΥ χρησιμοποιήθηκαν για να χαρακτηριστούν οι παραπάνω φαινότυποι σε υπόστρωμα ομόλογης κυτταρικά προερχόμενης εξωκυττάρια μήτρα (ECM) ή ινωδονεκτίνης (FN). Η αναστολής της AQP1 με $HgCl_2$ μείωσε την κυτταρική προσκόλληση των κυττάρων MeT-5A και M14K, την κυτταρική μετανάστευση των κυττάρων ZL34, τον σχηματισμό TnT στα κύτταρα MeT-5A, τον κυτταρικό πολλαπλασιασμό και τον σχηματισμό σφαιροειδών σε όλους τους κυτταρικούς τύπους. Η διήθηση σφαιροειδών και η συστολής γέλης μειώθηκε επίσης σημαντικά. Η αναστολή του ENaC με αμιλορίδη αύξησε την κυτταρική προσκόλληση των κυττάρων ΚΜΥ αλλά μείωσε την κυτταρική μετανάστευση των κυττάρων MeT-5A, MSTO και ZL34. Επίσης μείωσε το σχηματισμό TnT στα κύτταρα ZL34 καθώς και τον κυτταρικό πολλαπλασιασμό και σχηματισμό σφαιροειδών των κυττάρων MeT-5A, M14K και ZL34. Η διήθηση σφαιροειδών μειώθηκε μόνο στην περίπτωση των κυττάρων MSTO. Η συστολή γέλης κολλαγόνου μειώθηκε σε όλους τους κυτταρικούς τύπους. Τα παραπάνω

αποτελέσματα αναδεικνύουν ένα σημαντικό ρόλο για την AQP1 και το ENaC στη βιολογία του ΚΜΥ.

Abstract

Malignant Pleural Mesothelioma (MPM) caused by environmental exposure to asbestos, is an aggressive neoplasm of the thoracic pleural cavity. The role of Aquaporin1 (AQP1) and Epithelial Sodium Channel (ENaC) was characterized in the context of MPM biology. AQP1 and ENaC activity was evaluated by blockade with Mercuric (II) Chloride ($HgCl_2$) and amiloride respectively in order to assess their role in MPM cell adhesion, cell migration, TnT formation, cell proliferation, spheroid formation, spheroid invasion, and gel contraction. Benign mesothelial cells (MeT-5A), epithelioid type MPM (M14K), biphasc MPM (MSTO) and sarcomatoid MPM (ZL34) cells were used to characterize the phenotypes on homologous cell derived ECM or FN treated substratum. AQP1 inhibition with $HgCl_2$ abolished cell adhesion in MeT-5A and M14K cells. Cell migration was lowered in ZL34 cells, TnT formation was lowered in MeT-5A cells, in all cell types cell proliferation and spheroid formation was impacted negatively. Spheroid invasion and gel contraction was also diminished significantly. ENaC blockade with amiloride enhanced cell adhesion in MPM cells, cell migration was lowered in MeT-5A, MSTO and ZL34 cells. ENaC blockade lowered TnT formation in ZL34 cells. Cell proliferation, spheroid formation was negatively influenced in MeT-5A, M14K and ZL34 cells and spheroid invasion was lowered only in MSTO cells. Gel contraction was significantly reduced in all cell types during ENaC activity blockade with amiloride. These results highlight the important role of AQP1 and ENaC in MPM biology.

List of abbreviations

AE	asbestos exposure
Akt	RAC-alpha serine/threonine-protein kinase
AQP1	Aquaporin1
Arp2/3	Actin related protein 2/3
ASCL-1	Achete-Scute homolog 1
ASIC1	Acid Sensing Ion Channel 1
AUC	Area under curve
BAP1	BRCA1 associated protein 1
bFGF	basic Fibroblast Growth Factor
BPLAE	benign pleural lesions due to asbestos exposure
BRCA1	breast cancer type 1 susceptibility protein
BRN2	Brain-2
cIV	Collagen type IV
CAP1	Channel activating protease
CADM1	Cell Adhesion Molecule 1
CCNA2	Cyclin A2
CD44	Cluster of Differetiation 44, a cell surface receptor
CDC20	Cell Division Cycle 20
CDH1	Cadherin 1, epithelial Cadherin
CDH3	Cadherin 3, placental Cadherin
CHO	Chinese hamster ovary
CDK2	Cyclin Dependent Kinase 2
CDKN2A	Cyclin Dependent Kinase Inhibitor 2A

CDKN3	Cyclin Dependent Kinase Inhibitor 3
CD-DST	Collagen Drop – Drug Sensitivity Test
CDDP	Cisplatin
CMRA	Chloro Methyl RhodAmine
CTCs	Circulating Tumor Cells
E2F1	A transcription factor
E47/TCF3	Transcription Factor 3
ECM	Extra-Cellular Matrix
EGFR	Epidermal Growth Factor Receptor
EMT	Epithelial mesenchymal transition
ENaC	Epithelial sodium channel
EPA	ethyl-propyl modification to amiloride base
EPP	Extrapleural Pneumonectomy
FAK	Focal Adhesion Kinase
FBLN3	Fibulin-3
Fn/FN	Fibronectin
FOXC1	Forkhead Box C1
FOXC2	Forkhead Box C2
GFAP	Glial Fibrillary Acidic Protein
HA	Hyaluronan
HAPLN1	Hyaluronan-And-Proteoglycan linked protein 1
HM	Human Mesothelial cells
HMGA2	High Mobility Group AT-Hook 2
HMGB1	High Mobility Group Box1 protein 1

HSV1	Herpes Simplex Virus 1
IHC	Immuno-histo-chemistry
ILK	Integrin Linked Kinase
KEGG	Kyoto encyclopedia of genes and genomes
LDH	Lactate dehydrogenase
LLC	Lewis Lung Carcinoma
LM	Laminin
LIF	Leukemia Inhibitory Factor
Lin7	Protein lin-7 homolog A
LS	Long-term survivors
MAbK1	Monoclonal antibody K1
Mets	Metastasis
MI	Migration index
MIPs	Membrane Intrinsic Proteins
miR	microRNA
MITF	Melanogenesis Associated Transcription Factor
MLC	Myosin Light Chain
MLCK	Myosin Light Chain Kinase
MLCP	Myosin Light Chain Phosphatase
MMP	Matrix Metalloprotease
MMP2	Matrix Metallo Protease 2
MMT	Mesothelial Mesenchymal Transition
MPF	Mesothelin/megakaryocyte potentiating factor
MPM	Malignant pleural mesothelioma

MSLN	Mesothelin
MTT	3-(4,5-dimethylthiazol-2-yl)-2,5-diphenyltetrazolium bromide
NHE1	Sodium/hydrogen exchanger 1
OPN	Osteopotin
OS	Overall survival
P/D	Pleurectomy/Decortication
PE-SMRP	Pleural effusion SMRP
PTEN	Phosphatase and Tensin homolog
qPCR	quantitative PCR
Rho	A trascription factor
ROC	Receiver Operator Characteristic
ROCK	Rho-associated protein kinase
RSV-M	Rous Sarcoma Virus mutant M
RSV-TM	Rous Sarcoma Virus mutant TM
SCNN1A	Amiloride-sensitive sodium channel subunit alpha
SCNN1B	Amiloride-sensitive sodium channel subunit beta
SCNN1D	Amiloride-sensitive sodium channel subunit delta
SCNN1D	Amiloride-sensitive sodium channel subunit alpha
SEZ	Sub-Ependymal zone
shRNA	short hairpin RNA
siRNA	small interfering RNA
SMRP	Soluble Mesothelin Related Peptides
S-SMRP	Serum SMRP
SNAI1	Zinc finger protein SNAI1

SNAI2	Zinc finger protein SNAI2
SS	Short-term Survivors
SV40	Simian Virus 40
TCF4	Transcription factor 4
TNF α	Tumor Necrosis Factor α
TIMPs	Tissue Inhibitors of MetalloProteases
Tn	Tenascin
TNM	Tumor Node Metastasis
TnTs	Tunneling nanotubes
TPE	Tuberculous pleural effusion
TWIST1	Twist-related protein 1
uPA	Urokinase-type plasminogen activator
VACC	Voltage Activated Calcium Channel
VEGFA	Vasculo Endothelial Growth Factor A
VEGFR	Vascular Endothelial Growth Factor Receptor
WT1	Wilms Tumor 1
ZEB1	Zinc finger E-box-binding homeobox 1
ZEB2	Zinc finger E-box-binding homeobox 2
3’ UTR	3’ UnTranslated Region

Table of contents **Page number**

INTRODUCTION

1. The pleural cavity.

1.1 Anatomy and histology of the pleura.

The human respiratory system in the thoracic cavity is a gas exchange compartment with remarkable mechanical strength, encapsulated in two halves. The hilum of the lung (root) seals the extra-pulmonary space between lungs and the chest wall with a serous membrane, called the pleura. The pleura is a serosal membrane of mesodermal origin that covers the surface of the chest cavity and the outer surface of the lungs and anatomically they are separated by the mediastinum thus isolating the two pleural cavities [1]. The parietal layer of the pleura lines the inner surface of the thoracic wall and the diaphragm. The visceral layer of the pleura covers the lungs and dips into the fissures that separate the lobes. Between the two layers of the pleura there is a virtual cavity that is termed as the pleural cavity and contains a small amount of fluid that is constantly recycled and is termed as the pleural fluid. The total surface area of the human visceral and parietal pleura is nearly the same [2]. The visceral pleura (25-85 μm thick) is supported by a bed of vascular capillaries of the bronchial circulation [2]. The parietal pleura (30-40 micron thick) receives its blood supply from the intercostal arteries and also has lymphatic openings or lacunae preferentially at the sternum and spinal chord caudal regions which have characteristic “stomata” (small pores between mesothelial cells) of 2-12 μm in diameter that allow the direct communication of the pleural cavity with the lymphatic vessels [2]. The parietal pleura is innervated by the phrenic and intercostal nerves while the visceral pleura receives autonomic innervation from the pulmonary plexus. The parietal pleura is sensitive to pain, temperature and pressure while the visceral one only detects stretch and is not sensitive to the above [3].

The pleura as a membrane consists of five distinct layers, the outer one being a monolayer of mesothelial cells that face the pleural cavity and sits on a basal lamina with thin connective tissue. Below there is thin elastic layer that is on top of a layer of loose connective tissue that contains blood and lymphatic vessels, nerves and fibroblasts. Finally, the last layer is a fibroelastic layer (Wang, 1998). Within the loose connective tissue of pleura, below the mesothelial cell, there are also found cellular components of the immune system such as mast cells, macrophages and lymphocytes [4].

1.2 Pleural mesothelial cells.

The pleural mesothelial cells form a monolayer that constitutes the outer layer of the pleura. The mesothelial cells are derived from mesodermal layer during development but possess intermediate filaments that are constituents of both epithelial (cytokeratins) and mesenchymal cells (e.g. vimentin) rendering them unique. They can be found with two different morphological features, the flattened ones that are the most frequent and the cuboidal ones that are more active metabolically [6]. The location of these two mesothelial cells types varies, but it seems that in the parietal layer of the diaphragm the cuboidal cells are more frequent as compared to the caudal parietal pleural layer where more flattended cells are found [5]. Cuboidal cells are also found in the parietal pleura lications where there are stomata, so the population of mesothelial cells that surrounds the stomata consists of cuboidal cells [6]. The pleural mesothelial cells do not comprise a population of highly renewing cells under normal conditions but when primed by such a stimulus (i.e. in case of pleural inflammation) the mitotic activity is increased drastically [6]. Mesothelial cells have a well-developed microvillous border

and there is a primary cilium present [7]. Altough the role of the pleural mesothelium was thought to be mainly that of a physical barrier protecting from physical injury by the provision of a smooth, low friction contact during respiratory tribological movements of the lung within the chest cavity, in the past two decades many other roles have been identified [6]. The primary role of the mesothelial layer of the pleura is indeed to maintain the serosal integrity and function by providing a surface that is rich in secretions consisting of proteoglycans and glycosaminoglycans, predominantly Hyaluronan (HA), that allow for low friction during respiration [8]. Through this secretory function, they deter the adhesion of cancer cells to the mesothelium preventing malignant dissemination [6]. Moreover, they are equipped with all the molecular machinery required for active transport of water and solutes that allows them to contribute to the turnover of the pleural fluid. Additionally, apart from protecting from invading pathogens by their barrier function, they participate in the immunological response to invaders. The mesothelial cells present antigens to T cells and secrete a wide range of cytokines, growth factors, constituents of the extracellular matrix and mediators that facilitate the induction as well as the resolution of inflammation and participate in the tissue repair following inflammation. Finally, the mesothelial cells also contribute in the regulation of the fibrin turnover in cases of pleural insult [6].

1.3 Physiology of the pleural fluid and pleural membrane.

In humans the volume of pleural fluid approximates 0.26 mL/kg [9]. The pleural cavity is a sealed space and functions to mechanically couple the lung with the chest wall. The tribological movement (liquid friction) between pleural surfaces mainly arises due to

pleural fluid formation due to two constituents, water and proteins and metabolites (carbohydrates, dissolved gases etc) in the blood. The pleural fluid production in the pleural space is governed by Starling trans-capillary pressure defined as: $Qf = Lp \times A [(P_{cap} - P_{pl}) - \sigma_d (\pi_{cap} - \pi_{pl})]$. Simply stated Qf – liquid movement is dependant on hydrostatic partial pressure of capillaries (P_{cap}) and pleura (P_{pl}) and solute reflection coefficient σ, the ability of large molecule to impede free movement of smaller molecules and oncotic pressure π (pressure exerted by dissolved solutes in capillaries (π_{cap}) or pleura (π_{pl}) [3]. Pleurl fluid production arises from ultrafiltration of plasma from the parietal pleura capillary bed [10]. As shown in **Picture 1** pleural fluid absorption is a process that is achieved by Starling forces through the visceral pleura, by lymphatic drainage through the parietal pleural lymphatic stomata and through solute coupled liquid absorption though the mesothelial cells of the parietal and visceral pleura. Endocytosis of proteins by both visceral and parietal pleura mesothelial cells has also been shown to mediate transcellular fluid transport to some small extent [10].

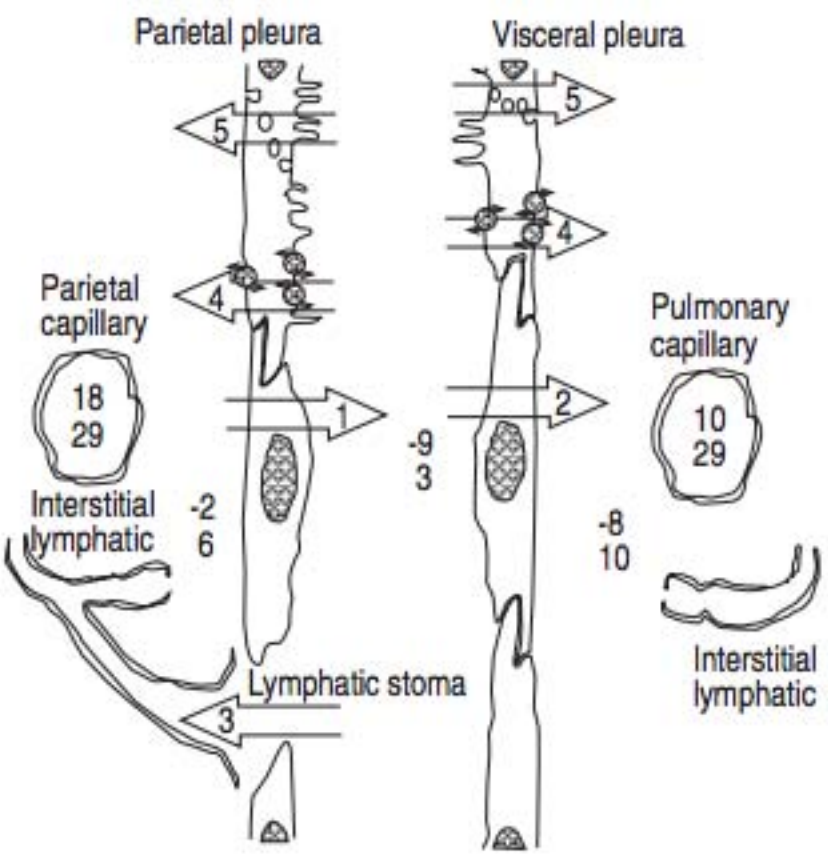

Picture 1: Depiction of pleural fluid turnover mechanisms in the rabbit. Mesothelial cells, pleural capillaries and lymphatcis are shown in parietal and visceral pleura. The pleural fluid arises as a filtrate from the parietal pleura capillaries by Starling forces (1), and is absorbed through several pathways. By the visceral pleura through Starling forces (2), by the parietal pleura lymphatic stomata (3), by solute coupled absorption by the mesothelial cells of both pleurae (4) and by transcytosis by the mesothelial cells of both pleurae (Zocchi, 2002).

With respect to the properties of the pleural membrane in terms of ion transporting capacity sheep pleural membranes have provided useful insights by their virtue of electro-physiological properties. There exists a natural polarity in the visceral and parietal pleural membranes in terms of apical side that faces pleural cavity and the basolateral side that either lines the parenchyma or the chest wall depending upon on lung or chest wall pleura respectively. In the context of Ussing chamber experiments, transmembrane ionic permeability can be measured as a resistance to the movement of ions when known quantities of applied current. The presence of mercuric chloride

sensitive Aquaporin channel activity was demonstrated in sheep peritoneal membranes. It was determined that with the application of mercuric chloride on either apical or basolateral side of the peritoneal membrane led to a significant lowered ohmic resistance indicating an increased ionic current permeability [11]. Elsewhere the direct evidence of AQP1 protein expression in the pleural cavity was determined in a rat model during tuberculous pleural effusion (TPE). Expression was detected on both visceral and parietal pleura. The expression of AQP1 transcript was significantly increased on both visceral and parietal pleurae of rats receiving an inoculum of tuberculosis bacilli. The forced expression of AQP1 recombinant adenovirus conferred significantly better pleural fluid clearance in the TPE model [12]. This demonstrates the presence of water channel proteins among which functionally AQP1 is suggestive of playing an important role.

Human and sheep parietal pleura have been characterized for their electrical resistance properties in Ussing chamber experiments. In both species the applied potential difference showed a linear relationship when resistance was calculated. Further with the exposure of amiloride on the apical side the transmesothelial resistance was significantly higher while on the basolateral surface the changes were not significantly affected [13, 14]. These effects were also demonstrated in studies involving sheep and human peritoneum that indirectly points to the presence of amiloride sensitive ENaC channels in this serosal membrane as well [15, 16].

The transmembrane electrical resistance properties have been characterized with sheep thoracic cavity pleura of the intercostal area and the diaphragmatic pleura. It was demonstrated that there is a significantly higher innate resistance in the diaphragmatic pleura in the sheep and further that there are cellular morphologies that

differ, with more dense and cuboidal cells apparent in diaphragmatic pleura compared to parietal intercostal pleura [17]. Similarly, human pleura from different locations of the chest cavity i.e. cranial, caudal and mediastinal locations show important differences in permeability during Ussing chamber experiments. Of the 3 different locations, pleural membrane in the caudal region demonstrated significantly least resistance. Addition of amiloride (inhibiton of Na^+ transport channel ENaC) or ouabain (inhibition of Na^+-K^+ pump) led to significant differential in caudal parietal pleura but not cranial or mediastinal pleura [18].

Visceral and parietal pleura from sheep were demonstrated to be responsive to dexamethasone treatment such that their transmembrane electrical resistance was lowered significantly. Mifepristone, an antagonist of dexamethasone had no effect alone, but when co-treated along with dexamethasone the drop in electrical resistance was rescued. This effect was uniform in both visceral and parietal pleura and also in terms of the apical or basolateral exposure to dexamethasone and/or mifeprestone. This observation supports the notion that dexamethasone induces the translocation of channel proteins to the plasma membrane that take in solute movements [19]. The Vascular Endothelial Growth Factor (VEGF), a cytokine that stimulates neo-angeniogenesis and vascular permeability, has also been reported for its role on the pleural membranes. VEGF exposure renders lower resistance in sheep pleura leading to a higher permeability as assessed by Ussing chamber experiments [20]. This is particularly important as VEGF secretion is well established in inflammatory and malignant pleural effusions.

The expression of AQP1 has been demonstrated during the embryonic development of rat in the visceral pleura at E21 (embryonic day 21) stage of

development as assessed by western blot [21]. The expression of AQP family of proteins in the pleura has been reported in a mouse model. AQP1, AQP3 and AQP7 and AQP9 have been shown be expressed in the mouse pleura. In the absence of AQP1 expression (germline deletion mutant) instillation of 500 mOsm fluid into the pleural space led to accumulation of less fluid in the pleural space as compared to wild type mice, indicating the role of AQP1 in osmotic balancing of pleural fluid. Equilibration of pleural fluid osmolarity with plasma osmolarity due to osmotically imbalanced fluid in pleural space was slower in AQP1 mutant compared to AQP1 wild type mice. This demonstrated the importance of AQP1 expression in pleural fluid physiology [22]. In AQP1 null mice when high osmolarity (5% BSA, 500 mOsm/kg) fluid was instilled into pleural cavity the osmolarity of pleural fluid was significantly higher compared to that of AQP1 wild type mice. When both wild type or AQP1 knockout mice were osmotically challenged with sodium channel activator terbutaline or inhibitor Amiloride, the osmotic imbalance over time was significantly higher compared to controls irrespective of AQP1 expression and further that pleural fluid volumes were also significantly high (with amiloride) and significantly lower (with terbutaline) depending on inhibition or activation of sodium channel transporter activity [23]. In a comparative study including hyperosmolar and iso-osmolar pleural fluid clearance in wild type and AQP1 knockout mice, it was demonstrated that with the AQP1 deletion, osmotic water transport was significantly reduced by two fold (50%) while in wild type mice treated with Mercuric Chloride, an inhibitor of AQP1 pore channel there was a 43% lower water osomotic transport as assessed by osomolarity measurements of pleurally injected hyperosmotic challenge. Conversely the prior stimulation of AQP1 with dexamethasone, significantly enhanced osmotic balance of pleural fluid challenge

in wild type mice. The hyperosmotic challenge equilibration in the presence of amiloride or terbutaline was unaffected. When iso-osmolar pleural fluid was used a challenge with the inclusion of terbutaline or amiloride, the pleural fluid volume clearance was significantly higher or lower respectively. In contrast the expression of AQP1 or the inhibition of AQP1 did not demonstrate any significant changes in volume of the pleural fluid clearance after injection into pleural cavity [24]. This demonstrates a context dependant function of pleural surfaces for their role in pleural fluid turnover during an osmotic challenge. The role of AQP1 in iso-osmolar fluid challenge is suggestive to be minimal in nature while that of sodium channel activators is significant. In the context of hyper osmotic challenge, the activity of both AQP1 and sodium channels is a necessity.

1.4 Pathologies of the pleura.

Pleural space obstruction due to fluid accumulation is the most common symptomatic ailment of the pleura. Effusions in the pleural space are commonly described in transudative and exudative terms. Transudative pleural effusions arise due to factors that influence an imbalance in hydrostatic pressures that govern pleural fluid production. In transudative pleural effuisons due to congestive heart failure, the rate of accumulation outpaces the rate of drainage resulting in benign pleural effusions [3]. In the context of Nephrotic syndrome (kidney damage) pleural effusion of transudative nature are also presented. This occurs mainly due to increased hydrostatic pressure (due to salt retention) and decreased oncotic pressure due to protein loss via urinary excretion [25]. Hepatic hydrothorax is yet another manifestation of transudative pleural effusion due to complications from hepatic cirrhosis. This occurs due to ascitic fluid

movement from peritoneal cavity into the pleural cavity through the porous diaphragm [26]. The mechanism appears to be due to decreased oncotic pressure of the plasma compared to pleural fluid oncotic pressure resulting in a compensatory effusion. While these are select instances of pleural effusions of transudative nature, it is apparent that Starling transcapillary pressure based on hydrostatic and oncotic components are critical to understanding benign pleural effusions. A key characteristic of transudative pleural effusions defined in Light's criteria is the component of protein content in pleural fluid lesser than that of serum and thus increased hydrostatic pressure.

Pleural effusions that arise due to infectious disease or malignant metastasis of the pleural space are classified as exudative pleural effusions. The key feature of this type of pleural effusion is due to vascular permeability of the capillaries during infection or malignancy. The literuature indicates a host of infectious agents such as parasitic protozoa Entamoeba, Echinococcus, Paragonimus infections and in most cases either, liver abscess (pus build up) or at times parasitic infestation into the pleural space through the lung. Other rare but notable parasitic contagions such as Ascaris, Strongyloides, Taenia, Trichinella, Ancylostoma, Necator, Wuchereria, Brugia are also reported in the context of pleural space involvement [27]. Viruses have also been reported to cause pleural infections leading to pleural inflammation. HHV8, Dengue virus, Coxsackie B5, HTLV1, Adenovirus, Cytomegalo virus, Parovirus, Respiratory syncitial virus, Varicella zoster virus, Herpes simplex and influenza virus are well reported in the literature which present as pleural effusions. Of particular interest is SV40 viral infection of the pleura leading to malignant pleural mesothelioma of biphasic or sarcomatoid histotype [28]. Bacterial lung infections leading to pneumonia also contribute to pleural effusions. A variety of aerobic, anaerobic, gram-positive and

gram-negative bacteria have been reported in the literature. Pleural effusions are most frequently observed in infections with Streptococcus pneumoniae (40-60% of cases), Staphylococcus aureus (40-70%), Streptococcus pyogens (55-95%) and with Bacillus anthracis (90-100%). These bacteria are anerobic and gram positive. Escherichia coli (40%), Pseudomonas species (25-50%), Haemophillus influenzae (45-75%) and Legionella species (25-60%) are representative, aerobic, gram negative bacteria reported to cause exudative pleural effusions. The intervention of immune effector cells due to secreted chemotactic factors from the pleural mesothelial cells are thought to be the primary mechanism of these pleural effusions [3].

In the context of malignant pleural effusions lung cancer, breast cancer and lymphomas figure prominently [3]. Lactate dehydrogenase (LDH) release is a clinically employed marker to assess tissue damage indicating LDH presence in pleural fluid. Accumulation of pleural fluid after metastasis to the pleural cavity are attributed lymphatic blockade of the stoma to lymphatic drainage or due blockage of mediastinal lymph node blockage due to neoplastic involvement. Mechanistically, the ratio of pleural fluid protein to serum protein is lowered thereby starling forces prevail in exerting hydrostatic pressure. Another important characteristic of malignant pleural effusions is the presence of a wide variety immune effector cells and metastatic non-adherent cancer cells. A predominant fraction of white blood cells consisting of lymphocytes, mononuclear cells and polymorphic nuclear leukocytes are found upon pleural fluid cytology. The increased infiltration of pleural space with cells is attributed to increased capillary permeability and leading to fluid accumulation [29]. It has been reported that about 40% of pleural effusions arise due to malignant metastasis, and that

lung and breast cancer metastasis contribute to as much as 75% of pleural infusions [30].

2. Malignant pleural mesothelioma (MPM).

MPM is a well-recognized neoplastic disease of the pleura due to asbestos exposure with a prolonged latency of 20-40 years between initial exposure to clinical presentation [31]. MPM is a therapy resistant cancer of the pleura. Histological subtypes of MPM are cytologically and pathologically well characterized and the most frequently presented as epithelioid, biphasic or sarcomatoid MPM and further epithelioid MPM histotype favors a prolonged survival in contrast to sarcomatoid MPM [32].

2.1 Etiology of MPM.

Malignant pleural mesothelioma is a neoplasm of the pleural cavity etiologically linked to asbestos exposure. Asbestos exposure mainly occurs due to occupational reasons or due to use of asbestos material products in domestic use such as construction, surface paving, whitewash raw material or habitation near asbestos rich mineralogical deposits. An emergence of 33 malignant pleural mesothelioma cases was reported in an area of crocidolite mining industry in Asbestos hills, a region of Cape Province, South Africa. Majority of cases consisted of mixed type of tumor histology characteristic of epithelial and mesenchymal like appearance [33].

The global incidence of mesothelioma due to occupational exposure to many forms of asbestos (Chrysotile, Crocidolite, Amosite) has since been actively reported in developed and developing countries such as Australia [34], Japan [35], China [36],

Turkey [37], Greece [38, 39], Italy [40] and USA [41] to name a few. Non-asbestos related mesothelioma is also reported in the literature. Serpentine material such as erionite (fibrous zeolite mineral of potassium aluminum silicate) is reported for its use in construction of roads and whitewash materials. Fluoro-edenite, another non-asbestos mineral fiber is mined for its use in construction of roads, buildings and in plaster and mortar material. Non-asbestos material exposure to these minerals, have been associated with mesothelioma incidence. Carbon nanotubes are a new age material, with fibrous properties. They have wide applications in industry but have been reported to cause mesothelioma in rat models. X-ray irradiaton exposure in Hodgkin and non-Hodgkin lymphomas in childhood is also correlated for mesothelioma development after a latency of 5-50 years. Occupational exposure to radiation among radiation technologists, atomic energy industry and research personnel and nuclear energy processing industry workers has also been reported as a causative of mesothelioma. Simian Virus 40 (SV40) has also been debated. The exposure to this virus mainly occurred through vaccine preparation against poliovirus. The attenuated live vaccines were mainly produced in monkey kidney cell culture. The confirmatory assays for such viral exposure harboring SV40 contaminant has been reported to be inconsistent. Synthetic plastics polyurethane and polysilicone preparations have been demonstrated to cause neoplasms including mesothelioma in rat models in vivo [42, 43].

2.2 Clinical presentation of MPM.

Malignant pleural mesothelioma symptoms presents as breathlessness, chest pain, weight loss and fatigue. Shortness of breath occurs due to pleural effusion, encasement due to tumor growth. Thoracic pain may occur due to invasion of the tumor into chest

wall, bone pain and neuropathic pain due to invasion into neural intercostal, paravertebral or brachial plexus structures. Chest X-ray findings indicate pleural effusions, nodular plural thickening. Ultrasound of the thoracic cavity often reveals pleural fluid volumes, pleural lesions and thickenings. Computed tomography reveals plural effusion at the disease site, interlobular and chest invasion sites, magnetic resonance imaging is employed to determine response to treatment as this procedure reflects density variation and loss while positron emission tomography – computed tomography is useful in determining uptake of radio-labeled fluoro-2-deoxyglucose which reveals high metabolic activity of neoplastic tissue and is helpful in determining staging and as a guide for surgical biopsy [44]. Examination of the pleural space by videography is often helpful in determining the extent of neoplastic growth in addition to cytological examination of pleural effusion fluid. Pleural effusion volume ranges from 300mL to > 800 mL. Pleural adhesion and pleural plaques as revealed by thoracoscopy are considered to be negative pronostic factors of survival [45]. Diagnosis and prognosis using molecular markers in mesothelioma studies are discussed separately. Staging of mesothelioma disease progression has been well established based on Tumor Node Metastasis (TNM) evaluation. TNM determination involves the use of computed tomography scans. The T descriptor defines the extent of tumor appearance, localization on the pleural surfaces, diaphragm and mediastinal areas is denoted as T1, T2 stage involves both pleural surfaces, invasion into diaphragmatic muscle and at times extension from visceral pleura into the lung parenchyma. T3 stage involves locally advanced but resectable appearance and invasion into soft tissue of chest wall, non-transmural pericardial invasion (superficial). T4 stage disease is non resectable with invasive features as in T3 and transdiaphragmatic invasion, spine and

mediastinal organs. N1 refers to nodal metastasis in ipsilateral bronchopulmonary, hilar and mediastinal lymph nodes, N2 refers to further extension of N1 into contra lateral bronchopulmonary, hilar and mediastinal and/or into supraclavicular lymph nodes [46].

2.3 Clinical management of MPM.

Tumor removal when possible is a preferred option for managing tumor burden by physical eradication of the tumor mass. Historically surgical resection is limited to early stage of disease, which confers a longer survival for curative intent procedures as compared to palliative procedures. Pleurectomy/Decortication (P/D) involves removal of all visible tumor irrespective of the pleural surface wherever the tumor is located, while Extrapleural Pneumonectomy (EPP) involves removal of tumor along with supposedly benign areas surrounding the site of the tumor, that is part of the pericardium, of the diaphragm and the parietal pleura. Survival with P/D is better compared to EPP and futher that there is a higher risk of mortality due to operative procedure in EPP. Radiation is usally employed prior to or after surgical therapy primarily to limit the spread or the development of new tumor nodules. Chemotherapy primarily consists of a combination of Cisplatin and Pemetrexed [47, 48]. Radiation therapy is also considered to be beneficial but only in instances as an adjunct to surgery, and/or chemotherapy. In fact, when all three-treatment options are considered together, i.e., trimodality treatment has been shown to be significantly associated with prolonged survival. Some key observations from an institutional review indicate that trimodal therapy patients were most likely early-diagnosed cases, and had an epithelioid histology [49].

2.4 Predictive markers of MPM.

Biomarkers in disease diagnosis and prognosis are a useful tool for the clinical management. Some important criteria to consider during biomarker evaluation are the ease of obtaining analytical sample (blood versus biopsy specimen), application within routine laboratory techniques such as ELISA or Immunohistochemistry analyses or DNA/RNA based method of detecting a biomarker (DNA for sequencing and identifying mutations, microarray detection etc). The biomarker analysis reagent should also demonstrate high sensitivity to detect low amounts of the target biomarker and high specificity to discriminate the target biomarker from other similar biomarkers such as isoforms. In the context of mesothelioma molecular diagnosis Mesothelin, Osteopontin, Fibulin3, HMGB1 are a few noteworthy biomarkers well reported in the literature.

Mesothelin: Malignant pleural mesothelioma diagnosis with the aid of biomarkers is primarily reported in the context of Mesothelin (MSLN) and more specifically, soluble Mesothelin related peptides (SMRP). SMRP is a product of post-translational modification of Mesothelin protein (molecular weight, 69 kDa) that is cleaved by proteolysis into N terminal Mesothelin/megakaryocyte potentiating factor (MPF) and the C terminal peptide is retained on the cell surface as mesothelin (approximately 40-43 kDA). Mesothelin cDNA and its deduced protein sequence were first reported based on a monoclonal antibody K1 (MAbK1), and the over-expression of the cDNA in NIH-3T3 fibroblasts demonstrated that the protein was localized on the cell surface as determined by immuno florescence staining. The expression of mesothelin on the cell surface was lost when transfected cultures were treated with phosphatidyl inositol- specific phospho lipase C [50]. This demonstrates membrane

anchoring of the protein through glyco-phosphatidyl-inositol anchoring. Mesothelin has been reported in clinical settings of mesothelioma diagnosis as a biomarker evaluation reagent, under the brand of MESOMARK^{TM}. Serum samples from various cancers (lung, ovarian, pancreatic, endometrial and colon cancer) diagnosed patients and from healthy controls exposed to asbestos, had significantly lower concentrations than in the serum of mesothelioma patients. Further to the utility of the assay reagent and the procedure, it demonstrated stability, irrespective of analysis material that may be subject to artifacts due to improper storage and handling and the co-efficient of variation was demonstrated to be low [51]. Pleural effusions arising from mesothelioma, benign pleural effusions and malignant pleural effusions due to lung, breast, ovarian cancers, lymphoma and sarcoma were assessed with MESOMARK to evaluate pleural effusion SMRP (PE-SMRP) along with matched serum SMRP (S-SMRP). It was demonstrated that PE-SMRP was higher than S-SRMP in MPM cases and also PE-SMRP were higher compared to PE-SMRP of non-MPM and benign effusions. A receiver operator characteristic (ROC) curve analysis (true positive rate versus false positive rate) to calculate the specificity and sensitivity was performed in an MPM versus non-MPM+benign setting. The PE-SMRP area under curve (AUC) for MPM (81.6%) versus non-MPM+benign effusions (70.5%) and MPM versus benign effusions (81.5% vs 72.9%) and in MPM versus non-MPM effusions (81.7% versus 66.9%) demonstrated a consistent pattern of bigger AUCs [52].

In effusion samples, when cytological analysis was un-informative, matched pleural and serum SMRP were performed. More than 70% of cytology negative samples from conventional diagnosis were SMRP positive for both effusion and serum in mesothelioma-diagnosed patients [53]. The utility of Mesothelin as a diagnostic

biomarker of MPM is therefore robust and reliable. The prognostic value of Mesothelin as a biomarker in MPM progression, histology specific correlation and therapy based on Mesothelin profile has also been described. In a large cohort of 218 tumor samples Immuno-histo-chemistry (IHC) analysis with mouse monoclonal antibodies against Mesothelin and MPF has been reported. It was demonstrated that Mesothelin staining for histological examination was robust with antibodies (5B2 and MN-1 clones) directed against membrane bound antigen (Mesothelin) rather than staining for the soluble fraction that was retained within the cytoplasm during post-translational modification of Mesothelin nascent peptide. Further when a large cohort of 1562 cancer samples was assessed using 5B2 and MN-1 antibodies, 90% positive staining (with 5B2) and 100% (MN-1) in ovarian cancers, 87% (5B2) and 71% (MN-1) in invasive ductal carcinoma of pancreas, 61% (5B2) and 41% (MN-1) in adenocarcinoma of the colorectum, 49% with 5B2 and 38% with MN-1 in adenocarcinoma of the stomach. In malignant mesothelioma, it was demonstrated that 75% and 78% were stained as Mesothelin positive samples. Further, among the mesothelioma samples the there was a 81% (5B2) and 84% (MN-1) staining in epithelioid MPM compared to 20% with both antibodies in sarcomatoid samples and 65%in biphasic mesothelioma (with 5B2 and MN-1). The statistical differences were significant between epithelioid-sarcomatoid and epithelioid versus biphasic comparisons. Among the mesothelioma group survival was 36 months in 100% positive stained (all cells in the tumor) compared to heterogeneous and non-positive stain where survival was 10 months. When the stain was diffuse from both 5B2 and MN-1 IHC along the plasma membrane, multivariable Cox regression analysis revealed a favorable prognosis [54]. This demonstrates the

potential of Mesothelin as a potential marker with application in cancers other than mesothelioma and further that it needs further evaluation as a prognostic factor.

Mesothelin targeting through monoclonal antibodies (amatuximab) infusion along with classical Cisplatin and Pemetrexed chemotherapy has been reported in the literature. It was demonstrated that the median overall survival (OS) was 14.8 months as compared to OS of 13.3 months from previous reports in the literature that involved only chemotherapy. Of particular note was the fact that the majority of study participants were diagnosed as stage IV, epithelioid histology [55]. The rationale of targeting Mesothelin biomarker on the tumor cells was thus adapted for specific cell targeting although it still relied on the natural immune system to engage via antigen dependant cell ctyotoxicity through the ligation of amatuximab antibodies and mesothelin.

Osteopontin: Osteopotin (OPN) is a yet another biomarker evaluated for use in mesothelioma diagnosis and prognosis. The method of evaluation was based on histological staining of mesothelioma tumor tissues using a immuno histological (IHC) staining score (HScore). In a cohort of 101 mesothelioma patient samples divided into two categories based on survival >24 months as long term survivors (LS) and <24 months as short term survivors (SS), it was demonstrated that LS had a significantly low HScore for OPN staining compared to SS and further that univariate analysis demonstrated to be a significant prognostic factor for survival. The drawback was that OPN expression had no significant correlation with age, sex, histotype of MPM, or asbestos exposure [56]. The performance of OPN as a diagnostic marker by ELISA method, along with MESOMARK has also been reported. The study involved human subjects who had occupational asbestos exposure (AE), confirmed mesothelioma

patients, patients with benign pleural lesions due to asbestos exposure (BPLAE), and patients with pleural effusions due to metastasis (Mets) from cancers other than mesothelioma. It was demonstrated that OPN expression was significantly lower in asbestos exposed group compared to all other groups consisting of MPM, benign lesions and Mets. Serum OPN was able to distinguish between MPM, MeTs, BPLAE versus healthy asbestos exposed (AE), and between MPM or Mets with BPLAE. Pleural OPN was also assessed but did not demonstrate any significant differences between the groups tested. In contrast with MESOMARK, it was demonstrated that MSLN could distinguish between AE, BPLAE, Mets and MPM, but no differences were observed with AE, BLPAE and Mets comparisons. MSLN could also distinguish comparisons between MPM and AE or between MPM and BPLAE. A combination of OPN and MSLN for a multivariate analysis was also performed but there were no significant results that could support the utility of OPN and MESOMARK as an improved method of MPM prognosis [57]. The significance of OPN expression in mesothelioma cell models has also been reported. It was shown that OPN over expression confers multidrug resistance to vinorelbin (a mitotic poison that disrupts microtubule stability; VNB), etoposide (a topoisomerase inhibitor; VP-16), Gemcitabine (a DNA analog that disrupts DNA replication; Gem) and Cisplatin (CDDP). With the overexpression of OPN, IC_{50} (inhibitory concentration for 50% reduction in proliferation) for the compunds tested were significantly higher along with an almost 50% increase in resistance to apoptosis at IC_{50} lethal to wild type OPN expressing cells. OPN being a component of the ECM was also investigated to determine if cell interactions with OPN would have an effect on cell adhesion. OPN over expressing (compared to wild type OPN expression) cells demonstrated

significantly higher cell adhesion on Hyaluronan (HA) treated substratum but not on OPN treated substratum and conversely silencing of OPN in OPN overexpressing cells abolished cell adhesion significantly to HA treated surfaces. The mechanism behind OPN overexpression induced drug resistance was demonstrated through the expression of alternatively spliced CD44 receptor expression that in turn binds HA. Ligation of CD44-HA interaction leads to Akt activation that rescues cells from apoptotic initiation by inhibiting caspase activation [58]. Although OPN has been assessed for its diagnostic and prognostic value, its use as a specific diagnostic/prognostic marker is clinical MPM assessment remains to be adopted.

High Mobility Group Box1 protein (HMGB1): HMGB1 is a versatile protein with many functions. It primarily acts as a cellular damage signal transducer. In the context of mesothelioma, it has been demonstrated to show a number of properties that enable oncogenic transformation and selection at the cellular level. HMGB1 protein expression was demonstrated by western blot analysis of human mesothelial (HM) cells exposed to both crocidolite and chrysotile to be dose dependent and further that HM cells expressed secreted and ctyoplasmic HMGB1. In the context of cellular damage due to asbestos uptake cells release Tumor Necrosis Factor α (TNFα), that signals cellular stress and confers cell survival. It was demonstrated that chrysotile induces a more robust response in generating significantly higher TNFα mRNA and protein. Next when HM cells were pretreated with TNFα for 24 hours, followed by stimulus with either forms of asbestos there was a significantly higher cell viability compared to asbestos alone treatment. In a time course format with HM cells, combinations of asbestos exposure along with macrophage co-culture or TNFα co-stimulation were performed at 48 hours or 5 weeks. It was demonstrated that HMGB1 was the upstream

regulator of top 57 differentially expressed genes. Additionally when genes from TNFα downstream signaling were identified there was a complete overlap of differentially expressed genes with those of HMGB1 influenced genes. Thus it was apparent that HMGB1 signaling precedes TNFα responsive genes. HMGB1 plays a similar role *in vivo*, as shown in mice injected with low, medium or high dose of chrysotile or crocidolite by the intraperitoneal route. Blood were subject to HMGB1 analysis. With crocidolite treatment, serum HMGB1 levels were high after 1 week of exposure and up to 10 weeks. In contrast Chrysotile exposure led to higher HMGB1 levels in a transient manner [59]. This finding is a key in illuminating the molecular events during asbestos exposure in that HMGB1 and TNFα play critical roles in rescuing cells exposed to asbestos.

HMGB1 in its native state is found in the nucleus and participates in chromatin remodeling for transcriptional purposes. HM cells upon stimulus with asbestos (crocidolite, 5 $\mu g/cm^2$) actively secreted HMGB1. The level of secreted HMGB1 from HM compared to that from mesothelioma cells was significantly lower and further the mesothelioma cells also secreted hyper acetylated HMGB1 (post translational acetyl modification at lysine residues in nuclear localization signal motif). Comparisons of sera between healthy and asbestos exposed individuals and malignant mesothelioma diagnosed patients with pleural effusion also demonstrated a significantly higher HMGB1 total protein and acetylated HMGB1. Moreover total HMGB1 was significantly higher in exposed individuals as compared to healthy samples. Total and acetylated HMGB1 comparisons between different stages of disease progression revealed no statistically viable pattern. Pleural effusion samples subject to HMGB1 analyses demonstrated significantly higher total HMGB1 and acetylated HMGB1 in

mesothelioma patients compared to pleural effusions from non-malignant or malignant pleural effusions from other cancers. Sensitivity versus specificity analyses were also performed in order to estimate AUC and to develop minimal cutoff in order to discriminate between groups based on health status, nature of effusion and type of malignancy (mesothelioma versus non-mesothelioma). It was demonstrated that the AUC of >0.80 and AUC=1.0 resulted at a cut off 11.35 ng/ml, 9.7 ng/ml for total HMGB1 and acetylated HMGB1 for comparisons between mesothelioma and asbestos exposed individuals. AUC analyses were also performed with other biomarkers panel consisting of Fibulin 3 (AUC =0.92), Mesothelin (AUC=0.79) and Osteopontin (AUC=0.50). However when combined plots were performed against total or acetylated HMGB1 with Fibulin3, Mesothelin or Osteopontin, no significant correlation was found. The combination of Total or acetylated HMGB1 with Fibulin 3 demonstrated significant differences for comparisons between mesothelioma and benign pleural effusions as well as between mesothelioma and pleural effusions from non mesothelioma cancers. When AUCs from the combined Total HMGB1 or acetylated HMGB1 and Fibulin 3 were plotted, the AUCs were 0.987 and 0.981 when effusions from mesothelioma versus non-mesothelioma were analyzed [60]. This demonstrates the utility of HMGB1 for the binary discrimination between MPM and non-MPM diagnosis and further that the combined analysis of HMGB1 and Fibulin 3 sets a valuable insight into the adoption of biomarkers in combinations as a means to gain certainty of diagnosis.

The expression of HMGB1 at the protein and mRNA level has also been investigated in clinical samples. In a large cohort of 170, clinically diagnosed mesothelioma patients, protein expression by IHC and mRNA expression by RT PCR

analyses were performed. HMGB1 IHC analyses revealed cytoplasmic, nuclear staining or both. RNA expression of HMGB1 transcript was significantly higher in patients on chemotherapy, and, the protein expression was significantly higher in clinical stages III and IV. Kaplan-Meier curves were analyzed based on high or low expression of HMGB1. Patients with total (nuclear and cytoplasmic) high HMGB1 staining had a significantly worse survival than low staining. Similar findings were reported only in cases of high cytoplasmic stain. In patients undergoing chemotherapy treatment (with cisplatin or cisplatin+pemetrexed) high HMGB1 stain was associated with a worse prognosis compared to low stain with chemotherapy or non-medicated patients. Low HMGB1 expression was well correlated with longer survival in both epithelioid and non-epithelioid histotypes of mesothelioma patients [61]. Taken together these data indicates the role of HMGB1 (protein) as a predictor of survival, i.e. high expression is negatively associated with survival. The observation that low HMGB1 staining as observed in patients on chemotherapy is an important aspect of clinical management and drugging strategy for patient benefit. In a large cohort of 497 individuals, HMGB1 from serum were analyzed in order to gain insights into asbestos exclusive stratification. Median HMGB1 differed significantly in comparisons of healthy versus asbestos exposed (AE) individuals with exposure of <10 and >10 years. In patients symptomatic of pleural plaque development HMGB1 was significantly compared to normal sera but significantly lower than patients with asbestosis and mesothelioma diagnosed patients. AUC analyses of various MPM with the asbestos exposure state (0.81) or healthy individuals (0.94) had significant p values <0.001 [62]. This demonstrates an important characteristic of HMGB1 in serum of patients with asbestos exposure without malignant disease (asbestosis), with pleural plaques. The

discriminating power and diagnostic accuracy are valuable in assessing overall disease type of pleura in the context of asbestos exposure.

Fibulin-3 (FBLN3): Fibulin 3 is an extracellular matrix protein. In an exploratory study matched mesothelioma with normal pleural samples were subject to microarray analyses that demonstrated FBLN3 was ranked 37th on a genome wide assay with significantly higher expression (7.36 fold) in mesothelioma versus normal comparison. Plasma and pleural effusion samples were assessed for FBLN3 by ELISA assay on two patient and normal controls cohorts from two different centers. FBLN3 was significantly higher in mesothelioma patient compared to asbestos exposed individuals and also in comparison to patients with pleural effusions due to malignancy other than mesothelioma. AUC curve analyses of study were performed to compare serum FBLN3 in the context of malignant mesothelioma versus asbestos exposed. The AUCs were identical in studies performed at two centers (1.00 and 0.99) and further that Fibulin3 cut off levels based on combined AUC of 0.99 (cutoff at 52.8 ng/ml) were significantly higher in mesothelioma patients such that there was a statistical higher mean compared to that of other cancer with pleural effusions or with cancers and no pleural effusions. Serum FBLN3 levels were reduced after cytoreductive surgical procedure (18 of 18 patients) and concomitantly increased trend was observed during disease progression in 6 patients. When plasma and pleural effusion FBLN3 were compared there was no statistical correlation for any of the disease status wise comparisons. In pleural effusion FBLN3 from mesothelioma patients versus non-mesothelioma patient, AUC was 0.88 at a cutoff level of 346.01 ng/ml but at sensitivity and specificity was lower than% 83 and 92% analyzed. In context of benign versus mesothelioma effusions the AUC was 0.86 at cutoff level of 378.33 ng/ml. Pleural

effusion FBLN3 in patients with cytoreduction therapy were significantly higher in stage III, IV compared to stage I, II and further that survival curves were significantly different between patients at a cutoff of 733 ng/ml (>733 ng/ml had a worse prognosis). IHC analyses were also performed to evaluate nuclear and cytoplasmic staining on mesothelioma biopsies however histological scoring was not significantly different when nuclear or cytoplasmic stain alone was used across epithelioid, biphasic-sarcomatoid histologies. However the comparison between neoplastic mesothelioma cell versus non-neoplastic plurae were significantly different [63]. FBLN3 expression thus is well correlated with asbestos exposure, mesothelioma diagnosis and pleural effusion from non-mesothelioma malignancies. FBLN3 being an ECM component though is prone to enzymatic modification. As there was no correlation between pleural effusion and plasma FBLN3, it is suggestive of the biomarker subject to degradation during transit through peripheral circulation by humoral proteases. An important part of FBLN3 sensitivity and specificity to long-term stored samples (>10 years) was that the AUC were significantly lower compared to stored samples from 2 years or less. This demonstrates FBLN3 marker to be labile to long term storage. Recently, a study comparing the diagnostic performance between MSLN and FBLN3 in pleural effusions (PE) of mesothelioma patients with those of benign PEs or from other non-mesothelioma PEs was reported. FBLN3 levels did not different significantly however MESOMARK SRMP consistently discrimated between mesothelioma patients with benign PEs and non-mesothelioma PEs. AUC of FBLN3 was 0.42 compared to 0.82 on benign pleural effusions, AUC of FBLN3 was 0.49 compared to 0.69 (SMRP) in non-MPM PEs. When benign and nonMPM PEs were combined for AUC analyses the AUC of FBLN3 was 0.44 compared to 0.79 of SMRP. In all instances the p values of

SRMP was <0.007 or lower [64]. Taken together from these studies involving multiple biomarkers for diagnostic accuracy comparisons and the one published by Pass et al., it is apparent that there are inherent limitations for FBLN3 as a biomarker for diagnostic and prognostic purposes in mesothelioma patients.

3. Cell phenotypes relevant to the understanding of MPM biology.

Given the physiology, biomarker development and its uses in diagnosis as well as classical *in vitro* and *in vivo* models of study in mesothelioma, it is imperative to draw attention to a few important features of patho-physiological aspects of mesothelioma development and progression. The tumor micro-environment has long drawn attention it the terms of its intricate complexity of cell-cell interactions, cell-ECM interactions and selection advantages such as resistance to apoptosis, proliferation potential and immune evasive ability [65]. Important features of healthy pleural physiology provide valuable insights into the mechanisms underlying pathological pleural effusions commonly noted in the epithelioid histotype of MPM are critical to MPM therapy. Therefore, below conceptual framework of experimental design, avenues to adopt in vivo feature of the extracellular matrix and pleural fluid turnover mechanism through the involvement of AQP1 and Epithelial sodium channel are briefly described.

3.1. Mesothelioma cell adhesion, migration, proliferation, spheroid formation-invasion, tunneling nanotube formation and EMT: important phenotypes with clinical and biological implications.

The process of cell adhesion is a critical first step that “implants” an oncogenically transformed cell, which subsequently grows, and forms characteristic tumor foci as

observed in clinical observations. Disease modeling of pleural metastasis using orthotopic modeling is technically and anatomically appropriate research method. In this regards a malignant pleural effusion model has been well described in literature using Lewis Lung Carcinoma (LLC) cells where in a suspension of cells ($1.5x10^5$) in 50 μL PBS is directly injected into the pleural cavity. Eventually, after 14 days post transplantation tumor growth is visible on both parietal and visceral pleura [66]. The process of disseminated single tumor cells within the pleural space and their implantation is reliant upon the ability of mesothelioma cells to interact with mesothelial cell proteins. This is achieved through the production of CA125 (MUC16) a glycosylated peptide that binds with high specificity to Mesothelin protein on nearby cell as well as on mesothelioma cells. The interactions of CA125 with N terminus of Mesothelin protein is a key component for favorable cell adhesion and further that functional blockade of CA125 with single chain immunoglobulin has significant deleterious affects on mesothelioma cell adhesion to cell monolayers expressing Mesothelin of ovarian and mesothelioma origin [67]. The process of adhesion in regards to mesothelioma cell models when grown on benign omental cell monolayers or fibroblast monolayers has been reported in an *in-vitro* model. This method incorporated green fluorescence labeled mesothelioma cells. Cell Adhesion Molecule 1 (CADM1) mediates interaction between mesothelioma cells and is demonstrated to be well expressed either on the membrane or within the cytosol. Of remarkable interest are two important features of CADM1 expression. 1) CADM1 expression when detectable at the cell-cell contacts, the tumor histology tended to show cells spread out and scatter over benign tissue and 2) while diffuse CADM1 expression in the cytosol led to a “stacking” of cells [68]. Thus cell adhesion with neighboring cells during tumor

development is an important consequence that may eventually lead to tumor cell sloughing resulting in a metastatic cascade.

3.2. Indicators of distant metastasis in MPM.

The utility of detecting circulating tumor cells (CTCs) is an important diagnostic advancement. This is particularly relevant in differential diagnosis of CTC counts to discriminate between non-malignant and malignant pleural effusions from human clinical studies. The method exploited antibody mediated capture of CTCs expressing Epithelial Cell Adhesion Molecule (EpCAM) which were isolated from peripheral blood draw samples although specific discrimination based on AUC-ROC analyses was statistically insignificant. However, there remained three features of particular interest 1) statistically higher significant counts in epithelioid as compared with biphasic and sarcomatoid histotypes and 2) increasing CTCs during disease progression in epithelioid histotype [69]. As the disease severity is dependant on the histotype, CTC count is a generalized indicator of stronger cell adhesion and therefore the lower incidence of CTCs in peripheral blood in biphasic and sarcomatoid histotypes. As mentioned earlier Mesothelin remains a gold standard in clinical practice to reliably diagnose the incidence of mesothelioma. There has been an active interest in exploiting the marker as a target of therapeutic efforts by Pastan group. A single chain "scFv antibody" peptide reactive against mesothelin was developed followed by in-frame fusion with Psuedomonas exotoxin A (MORAb-009). This recombinant peptide therapeutic demonstrated considerable toxicity towards cervical cancer cells genetically modified for the expression of Mesothelin, in gastric adenocarcinoma and ovarian carcinoma cells at very low IC50 range of 6-16 ng/ml concentration [70]. This

antibody was also shown to significantly reduce cell adhesion of Mesothelin positive cells during adhesion to cell monolayers expressing CA125, a cognate receptor of Mesothelin N terminal domain [71]. MORAb-009 has been subject to clinical trials with the intent of blocking Mesothelin and CA125 interaction thus affection cell adhesion and that the rationale being to limit early stages of tumor metastasis [72].

3.3. A special case of cell-cell adhesion – tumor spheroids.

In-vivo model of mesothelioma in peritoneal cavity by crocidolite and chrysotile injection has been demonstrated in a rat model. The neoplasms were demonstrated by histology to be minimally invasive, with no metastasis observed into other organs and the neoplastic tissue retained a spherical morphology. Isolates from clinical tissue specimens of humans were cultured on human fibronectin or rat collagen demonstrated similar characteristics of isolated monolayers giving rise to a spheroid cell mass [73]. Taken together this demonstrates an interesting aspect of morphological similarities of tumor growth retained in cell cultures derived from mesothelioma tumor tissue. This is thought to be a process that relies on progressive loss of cell adhesion with the substratum while maintaining intimate contact with neighboring cells and eventually giving rise to a cellular, spheroid cell mass that is viable. During cell culture of tumor explants, predominantly spheroid populations are observed when non-adhesive plastic surfaces were used. The histology of the spheroids demonstrated a collagen core supporting the multi-cellular structure. The cell-cell adhesion remains while cells undergo mitotic division, this is an indication of a native mechanism that drives tumor proliferation and tumor size. When cells grown in monolayers and spheroidal cultures were subject to apoptotic agents TRAIL (a cell death inducing protein ligand) and

cycloheximide (protein synthesis inhibitor) the monolayers showed complete apoptosis while the spheroids remained viable with apoptotic cells interspersed in the multi-cellular structure [74]. Therefore cell adhesion processes whether between the cells and the substratum or between the cells themselves is an important aspect that is suggestive of organization of cells in 2 and 3 dimensions, and, it impacts cellular biochemistry that regulates response to apoptotic stimuli therefore sensitivity to chemotherapeutics.

3.4. Tumor growth and invasion.

In the settings of malignant pleural effusion modeling in mouse, it has been demonstrated that infusing cancer cell suspensions in the pleural space leads a to a pleural effusion phenotype with Lewis Lung Carcinoma cells (LLC). *In vivo* growth of such pleural inoculums of malignant cells is an orthotopic model of study. It mimics the essence of pleural effusions in malignant pleural mesothelioma patients. Moreover, the tumor development was evident when assessed by small animal computed tomography studies, visible neoplastic tumor foci upon anatomical examination and further the histological characteristic of such foci has been demonstrated to invade visceral pleural, parietal pleura, diaphragm along with characteristic neo-angiogenesis [66]. Orthotopic, syngenic allograft model in rat has also been demonstrated. II-45, a sarcomatoid cell line derived from a asbestos induced mesothelioma model in rat was developed further to repeated exposure to clinically applied mesothelioma chemotherapy drugs consisting a panel of cisplatin, pemetrexed, vinorelbine, gemcitabine and cisplatin+pemetrexed in cell culture. The resulting pemetrexed chemo-resistant cell lines were shown to significantly reduce rat survival after inoculation into naïve host animals [75]. This demonstrated acquired chemo-resistance

through prolonged selection with cytotoxic drugs and reproducible tumor development in vivo upon transplantation. Taken together, tumor growth of malignant pleural effusion and by orthotropic xenograft represents the development of pathological tissue initiated by implantation of single cell suspension. Given that tumors were observed after a period of 2-3 weeks of incubation, it is indicative of robust growth en-masse due to high cell proliferation. *In vivo* tumor growth is a complex phenomenon involving rapid localized growth, interaction of tumor cells with benign tissue, association of local fibroblasts, interaction with immune cells and the development of tumor supportive vasculature. Among these varying interactions the core phenomenon of cell proliferation and invasion into naïve tissue is an overall mechanism that leads to disease progression. Therefore in order to assess cell proliferation and invasion specific to cancer cells, *in vitro* phenotypes of cell proliferation over defined periods of time is a useful model to assess therapeutic molecules that reduce cell proliferation. In the context of invasion, wound healing assay after infliction of a scratch on a monolayer of cells is a convenient *in vitro* technique. It represents the growth at the edge of a proliferative population of cells in a cell cycle synchronized state. The *in vitro* phenotypes of cell proliferation and invasion that provide an assessment of tumor growth are by design individual phenotypes and are restricted in 2 dimensions. Tumor spheroids *in vitro* are a representative model that incorporates cell proliferation and invasion. The spheroid cultures are a simple yet highly reproducible model of investigation for growth and invasion given that individual cells are typical starter population and are observed days to weeks of time. Spheroid cultures grown on polyHEMA substratum (inert biocompatible polymer) when subject to various apoptotic stimuli demonstrated higher resistance to apoptosis compared to that of

monolayer cultures. The resistance was demonstrated to be mediated through mammalian Target of Rapamycin (mTOR) mechanism that demonstrated upregulation of anti-apoptotic panel of genes consisting of Bcl-Xl, Bcl2, FLIP, surviving and down regulation of pro-apoptotic genes Bad, Bid, Bax, Bak, Bim genes [76]. Elsewhere, the genetic expression of various pathways as assessed by microarray analysis demonstrated that in 3D spheroid cultures, functional categories of immune response, wound response, lymphocyte stimulation and response to cytokine stimulation genes were up-regulated while genes associated with apoptosis were significantly downregulated [74]. The spheroid cultures are a close approximation of 3D dimensional nature of organs and they represent near *in vivo* conditions. The aspect of tumor proliferation-invasion has been demonstrated in patient explants of mesothelioma in a collagen drop – drug sensitivity test (CD-DST). In this method live tumor samples ex vivo are subject to culture in a collagenous matrix as a mimic of basement membrane of the tissue where the tumor grows with a contiguous invasion into benign area. This represents an important technique where *ex vivo* drug sensitivity can be assessed during patient care and in clinical follow up appropriate chemotherapeutic strategy to manage patient care. In a small cohort of 10 patients with mesothelioma, it demonstrated that with CD-DST, at least one chemo-sensitive agent was useful in accomplishing partial response to treatment, 5 patients showed stable disease and 2 patients showed progressive. A panel of 9 chemotherapeutic agents was used to assess chemosensitivity in the study. Gemcitabine (45% of samples) and Docetaxel (40% of samples) showed highest activity against samples tested [77].

3.5. Tunneling nanotubes formation.

Tunneling nanotubes (TnTs) are cellular appenndages continuous to the cytoplasm and act as intercellular communication tubes. TnTs are F actin supported structures, open at both ends when connecting two cells a few cell diameters apart and capable of transferring biological materials, as well as cell organelles like Golgi bodies and mitochondria. TnTs are produced during cellular stress due to acidic pH and connect only between pathological cell types or between benign cells, but not between benign and pathological cells. The TnT formation is sensitive to metabolic poison Metformin that inhibits mitochondrial respiratory chain, Evrolimus that inhibited mTOR mediated actin assembly and Latrunuclin A that de-polymerized actin assembly, at the base of TnTs. Further the TnTs were shown to be present for the first time in solid mesothelioma tumors as demonstrated by 3 dimensional re-construction from serial slices of fixed tissue [78]. The induction of TnTs in cell culture by exogenous, membranous vesicles termed exosomes has also been demonstrated. Co-culture with exogenous exosomes induced a significantly higher number of TnTs within a span of 2 days, further enchanced by low pH culture media. The exosomes were demonstrated to be physically embedded into the base of TnT structures with increased lipid raft content. The induction of TnT formation and membrane specific components was associated with lipid drafts stained with biotinylated chlorea toxin B stained by immunofloresecne [79]. This demonstrated the exosomes function as diffusible stimulus, and that it promoted TnT formation. TnT formation and persistence during cell culture was also assessed. It was demonstrated that malignant mesothelioma cells generate significantly higher TnTs compared to benign mesothelial cells. Further that malignant cells tended to sustain an increased TnT formation as opposed to lowered

TnT formation in mesothelial cells over time. Pleural effusion samples from mesothelioma and primary cultures from pleural fluids demonstrated presence of TnT structures *in vivo* as well their recapitulation when cultured *in vitro*. TnT were induced (low pH and high glucose) in MSTO-211H. Stressed cells when xenografted and compared to cells from regular culture conditions, demonstrated decreased overall survival along with significant weight loss. Further that, when the cells were cultured in TnT inducing conditions or normal media it was demonstrated that the expression of genes influencing cell cycle regulation (E2F1, CCNA2, CDC20, CDKN3) were lowered and increased expression of genes (Tenascin, CD44, Osteopontin, Mesothelin) associated with increased malignancy [80]. TnTs are a feature that exist *in vivo* and *in vitro*, can be influenced with pH and higher TnT production demonstrated be associated with decreased survival. The role of TnT in terms of adapting TnT as conduits of biological material has been described. When cells were infected with GFP producing viruses, transference of GFP was demonstrated over a period of 14 hours during interaction between fluorescence negative and virally infected fluorescent cell. Moreover with use of onoclytic, attenuated HSV1 viruses harbor genes that convert pro-drug into an active form a bystander lysis effect of was also demonstrated as assessed by TUNEL assays [81]. Taken together these data demonstrate the formation of TnTs in mesothelioma tumors, primary cultures from pleural effusions, in mesothelioma cell models. Given the fact that pH and high glucose conditions induce their formation, response to biochemical stress, histology type, TnT development could be modeled and studied as indicators of cellular stress during pharmacological studies. The properties and correlations of TnTs with mesothelioma tumors *in vivo* animal model where higher TnT forming cells diminished survival, combined with the

observation that TnT induction is higher in mesothelioma cells is suggestive of TnT formation with pathological condition of the tumor cells. It demonstrates that TnTs recapitulation of cell morphology irrespective of culture conditions; TnTs are a native feature of cellular physiology.

3.6. Epithelial mesenchymal transition (EMT).

EMT is an important developmental maneuver that enables oncogenic tissue development and homeostasis. It is a morphological and genetic adaptation that enables trans-differentiation i.e. mesothelial origin cells invading the visceral, parietal pleura or the diaphragm and metastasizing to the lymph nodes in the context of mesothelioma. These features of invasion and metastasis, are thought to be driven by a process that aids a developmental selection process favoring tumor development and survival. The EMT in MPM axis has been described in a putative model consisting of Periostin, Epidermal Growth Factor Receptor (EGFR), integrin β1, Phosphatase and Tensin homolog (PTEN), integrin linked kinase (ILK) and two cell cycle regulator proteins p21 and p27. All the EMT markers were detectable by histology to varying degrees in MPM histology preparations in a large cohort of 128 patients. The high expression of cytoplasmic and stromal staining for perisotin was associated with sarcomatoid histotype whereas high membranous expression of EGFR, integrin β1 and nuclear p27 was significant in epithelioid histotype. EGFR, integrin β1, PTEN, ILK, p21 and p27 were well correlated when assessed for dual expression for all combinations however periostin high expression was correlated with high stromal EGFR, membranous integrin, PTEN and p27. Overall survival was higher in low cytosolic perisotin expressing tumors [82]. The entire EMT axis components from periostin signaling

though integrin receptor complex, and down stream integin linked kinase is upregulated as a pathway enmasse. PTEN regulates the ILK activation downstream of integrin activation of ILK and the EMT signaling terminates with p21, p27 proteins regulating cell cycle progression specific to periostin-EMT axis. Thus, the EMT component of mesothelioma development and its clinical relevance is important. Similar analyses with EMT markers consisting of γ catenin, vimentin, fibronectin, Twist1 and YB-1 has also been reported. It was reported that individual EMT markers do not demonstrate significant over-expression with Twist1 being the only exception with higher expression in sarcomatoid histotype compared to epithelioid. In multivariate analysis a combination of low γ catenin along with high Twist1 expression was significantly associated with increased risk of death [83]. A transcriptome based classification of malignant mesothelioma cell lines and MPM biopsy samples has been reported in the settings of EMT evaluation. Initially RNA from MPM cell cultures were analyzed by microarray assay and were allowed to cluster based on genetic changes which demonstrated 2 clusters 1) epithelioid (C1) and 2) sarcomatoid and epithelioid like (C2). Genetic alterations were exclusively detected in CDKN2A, BAP1, genes that were significantly represented in C1. The same clustering algorithm when applied to tumor sample transcriptomes demonstrated significant results only with BAP1 in C1 clusters consisting of epithelioid type histology with a loss of BAP1 locus. Kaplan-Meier survival analyses of C1, C2 classified tumor samples demonstrated significantly different prognoses with long longer survival (of C1 cluster) with an epithelioid histotype and further that within C2 cluster those with epithelioid histotype had a longer survival compared to sarcomatoid type. When C1 and C2 groups were analyzed for differentially expressed Gene Ontology terms and Kyoto encyclopedia of genes and

genomes (KEGG), cell migration and EMT pathways were ranked 3 and 12. Cell adhesion, cell junctions and extracellular matrices were also among top 20 terms. Genes associated with upregulation of EMT were Periostin, Versican (ECM related genes), SNAI2, TCF4, HMGA2 (transcription factors) and CDH1 (E Cadherin), CDH3 (placental Cadherin) were down regulated during EMT. The loss of E Cadherin experession at the protein level was also demonstrated by western blot in C2 cluster of MPM cell lines and by IHC in tumor biopsies [84]. Taken together, these evidence point to a basic mechanism where in transformed malignant cells are enabled for a mesenchymal characteristic of migration, invasion. This characteristic is dependant on multiple genes and pathways leading to an invasive characteristic more evident in sarcomatoid histotype where cells adopt a fibroblast like cell morphology. In the settings of EMT, the restoration of epithelial characteristic in mesothelioma cell models of EMT, Wilms Tumor 1 (WT1) a marker gene expressed in mesothelial and mesothelioma tissue has been reported. In epithelioid cell type H2052 and biphasic cell type MSTO-211H, silencing of WT1 expression with siRNA significantly reduced cell proliferation and EGF induced chemotaxis. Chemoresitance against cisplatin demonstrated WT1 silencing increased the sensitivity in MSTO cell type [85]. This demonstrates the importance of EMT related genes playing a role that influences the histotype of the disease.

3.7. ECM composition from cell culture and tissues.

The composition of cell derived ECM proteins from mesothelioma cell models has been reported previously to mainly consist of fibronectin (“Fn”) and tenascin (Tn) as determined by northern blot and western blot. This study demonstrated the expression

of ECM proteins under the circumstances of exposure to asbestos, H_2O_2 and in response to TNFα and TGF β1 cytokine exposure [86]. Fibronectin (FN), laminin (LM) and collagen type IV (cIV) production in epithelioid, byphasic (biphasic) and fibrous histotypes of mesothelioma cell cultures was assessed by the physiologic incorporation of radio labeled [^{35}S]- Methionine during cell culture and from cell culture supernatant analysis to determine the cellular or extra cellular source of these proteins. The study demonstrated a cell type dependant production of ECM proteins wherein, FN was mainly secreted into the culture media, and highest amount secreted from biphasic histotype followed by epithelioid and fibrous histotypes. LM was mainly secreted as a glycosylated protein produced highest in epithelioid followed by biphasic and then fibrous histotype cells. cIV was secreted as well found in cell lysates in equal fractions in both epithelioid and byphasic histotype while in the fibrous type cIV was mainly a secreted protein [87]. Sarcomatous (Sarcomatoid type) STAV FCS has been demonstrated to actively secrete soluble ECM components, namely Fibronectin, type IV Collagen and Laminin. These proteins were isolated from serum free cell culture media complimented with radio labeled Methionine and then assessed for high molecular weight proteins by fluorography and with peptide specific antibodies by western blot, thus demonstrating the ability of mesothelioma cells to endogenously produce and deposit ECM components [88].

3.8. ECM modification and turnover.

Heparanase (HPSE-1), an ECM modifying enzyme functions to altering the molecular ECM architecture. This enzyme has been investigated in a clinical specimen cohort of pleural effusion and tumors of malignant mesothelioma, and reported to be expressed

in 69 of 80 (86%) samples assessed by IHC with a polyclonal antibody reacting to KKFKNSTYSRSSVDC sequence of the human heparanase enzyme. Further 35 samples showed staining within cytoplasm and the cell membrane, 30 confined only to the cytoplasm while 4 specimens showed restricted staining of the cell membrane. HPSE-1 expression was detectable by RT-PCR in pleural effusion samples to varying degrees. A higher HPSE-1 staining was strongly co-related with solid tumor of mesothelioma [89]. The ECM re-organization and turnover is an essential physiology of the tumor microenvironment. This is an important pre-requisite for the processes of epithelial-mesenchymal transition that are a core feature of tumor invasion into surrounding tissue. The degradation and renewed modeling of the ECM surroundings involves coordinated proteolysis and synthesis, deposition and posttranslational modifications of ECM proteins. Matrix Metalloprotease (MMP) family of proteins are key mediators of basement membrane protein turnover while they are regulated by Tissue Inhibitors of MetalloProteases (TIMPs). To this end mesothelioma and mesothelial cells have been demonstrated to express pro-MMP2 under the stimulus of TGF-β1 in a time and dose dependant manner. The conversion of pro-MMP2 to active MMP2 was limited only to mesothelial cells but not in mesothelioma cell lines [90].

4. AQP1 and ENac channel function and roles in cancer.

4.1. Aquaporins.

Aquaporins are a large family of proteins found to be ubiquitously expressed through out the plant and animal kingdom. The family mainly consists of membrane intrinsic proteins (MIPs) that are involved in water transport across the cell wall (plant kingdom) or plasma membrane (animal kingdom). The evolutionarily conserved function of

water transport is apparent in genome wide studies from various organisms that demonstrated recurrent and independent genetic amplification [91].

Human AQP1 was first discovered in the human erythrocyte and demonstrated to be expressed in as 28 kiloDalton (28kDa) or oligomeric form of 28kDA described as HMW-28kDa. The amino acid composition of AQP1, the protein domains that traverse peptide backbone consisting of intra-cellular and extra-cellular domains, glycosyl modifications that lead to HMW-28kDa protein have been described. Serum from rabbits immunized with this highly purified 28kDa protein demonstrated cross reactivity with various tissues derived from the rat, which was suggestive of a high degree of conservation of this protein in terms of the protein sequence [92, 93]. The same 28kDa protein was later demonstrated to be an oligomer of 28kDA peptide that was a result of N-linked glycosyl modification, and both these peptides 28kDA and HMW 28kDa were demonstrated to be distinct from other membrane proteins prepared from human erythrocytes. Lastly the association between 28kDA and HMW-28 kDa protein was also demonstrated which was suggestive of a tetrameric motif localized on the plasma membrane that could be chemically cross-linked with mild glutaraldehyde treatment [93]. This effectively shows that functional 28kDA and HMW-28kDa oligomers constitute the active complex stabilized through non-covalent interactions.

Functional studies of the 28KDa protein later renamed as CHIP28 began with the isolation, cloning and expression (from fetal liver and adult bone marrow cDNA library) based on the amino terminal peptide sequence [94, Preston, 1991). *In-vitro* transcribed CHIP28 cDNA when injected into Xenopus (African clawed frog) oocytes led to the ability of these oocytes swelling when placed from 200 mOsm to 70mOsm (hypotonic solution) and this effect was demonstrated by videography and water

permeability measurements (P_f) demonstrated that Mercuric chloride significantly reduced P_f and that this effect of Mercuric chloride was reversed by reducing agent mercaptoethanol suggesting the reversible blockade of CHIP28 mediated water transport [95].

By the use of electron microscopy studies in purified human AQP1 it was demonstrated that the molecule can be assembled *in-vitro* with constituent purified 28kDA fragments that are useful for obtaining crystallographic data. The purified and reconstituted peptides have been also demonstrated to form a tertrmeric structure as assessed by optical diffraction and 3D reconstruction from image projections [96]. The AQP1 molecule has been modeled based on X-ray crystallography and NMR methods and is demonstrated to have an hourglass profile with a hydrophobic core lined with 3 hydrophilic nodes that allows the passage of 4 water molecules and further that histidine residue at 182 position is common to all known aquaporin variants and confers selective water transport [97].

The functional aspect of amino residues that confer CHIP28 (now on annoated as AQP1) sensitivity to mercuric chloride have been tied to cys residues (at 87, 102, 152 and 189 positions from N terminus, by mutational replacements) that line the hydrophilic core that permits water transport. The perturbation of cys reside at 189 with larger amino acid tryptophan also abolishes water transport. Lastly, the mutation of amino acid residue aspargine at 42 and 205 positions to threonine abrogates glycosylation of the protein without any loss to water permeability [98]. In terms of genetic ablation of AQP1 in a mouse knock out model, it has been demonstrated that there is severe loss of osmotic water permeability in the erythrocytes lacking AQP1 expression irrespective of AQP3 isoform expression, pointing to a major role of AQP1

for water transport in erythrocytes [99]. Elsewhere it has also been reported that large ionic metal elements such as mercury (Hg^{++}), gold (Au^{+++}) and silver (Ag^{+}) have comparable inhibitory effect (IC50) on water permeability of concentrations of 10 μM, 14 μM and 6 μM respectively. Thus the availability of inorganic, small molecules is advantageous in assessing AQP1 activity in model systems of study for therapeutic development [100].

At the molecular level, AQP1 functions as signal transduction protein through its interaction with Lin7 protein that plays a role of scaffolding, adaptor protein and stabilizes β-catenin and α-catenin complex. The catenin protein complex then plays a critical role in the coordinated assembly of the cytoskeleton that is critical during cell migration, adhesion and cell motility [101]. Elsewhere it has been also demonstrated that through β-catenin and Focal Adhesion Kinase (FAK) physically interact with AQP1, and are released in the event of loss of AQP1 expression, bone marrow mesenchymal stem cells. The cells were severely impacted in the migration abilities [102]. Natural mutations in the AQP1 gene expression have been described in humans but the clinical aspects of AQP1 mutation or complete loss of expression does not cause mortality. Loss of exon1 by deletion in the genomic AQP1 structure, a frame shift mutation due to insertion (A insertion at position 307) and a C to T nucleotide substitution was demonstrated to be homozygous thus leading to complete loss of AQP1 expression. In these individuals osmotic water permeability was reduced by 80% compared to normal erythrocytes [103]. Taken together this demonstrates AQP1 gene and protein functions are largely physiological in nature determining osmotic water permeability. There is limited contextual literature pointing to highly specialized roles

of AQP1 in cell physiology that involve cell volume changes through osmotic maneuvers mainly through protein-protein interaction.

In the context of pathological roles of AQP1 in cancer, there is ample evidence demonstrating an increased disease severity concomitant with the expression of AQP1. Melanoma tumor growth modeling in AQP1 lacking mice compared to wild type type mice has demonstrated a significantly higher survival in mice lacking AQP1, lowered tumor growth and lowered neo-angiogenesis at sites of xenograft implantation [104]. A striking feature of the histology revealed large necrotic patches of the tumor growth asides from the lack of angiogenesis thus suggestive of a role of AQP1 in tumor proliferation and growth. Elsewhere a comparative study on normal and select cancer biopsies evaluated the expression of AQP1. In all normal tissues there was a detectable expression of AQP1 in microvasculature and at the endothelial barriers. Highest expression was observed in kidney chorioid plexus, pancreas and gall bladder epithelium. Moderate expression was observed in lung and peripheral nerve and finally low expression was reported in breast, placenta and endometrium and very low or undetectable in skin and colon. In the cases of prostate and ovarian cancer AQP1 expression was higher capillary endothelium of vasculature surrounding the tumor. Similar trends were of pattern and increased staining intensity was observed in colon, and breast tumor biopsies. This demonstrated the expression of AQP1 in association with neo-angiogenic tissue endothelial barrier in the context of tumor histology and that there is an underlying universal role of AQP1 in oncogenic development in diverse tissues [105].

The specific findings in the context of AQP1 expression in lung and thoracic cavity nesoplasms are: 1) there is a significant AQP1 overexpression in lung

adenocarcinoma and malignant pleural mesothelioma (MPM) and the expression is robust in neo-vasculature associated with the tumor and endothelial lining of capillary beds [106]; 2) the over expression of AQP1 protein (>50% positive cells of the tumor) in MPM diagnosed patients was associated with significantly prolonged survival [107] and 3) AQP1 over expression at the transcript level in epithelioid histotype of MPM has been demonstrated as well [108]. Thus the prognostic value of AQP1 expression is an important aspect of MPM diagnosis, and in a prospective study it was proposed for adoption as diagnostic tool to better manage mesothelioma diagnosis [109].

4.2. ENaC.

The epithelial sodium channel proteins (ENaC) are involved in the active transport of Na+ ions. The channel consists of 4 different subunits namely ENaC α (SCNN1A), ENaC β (SCNN1B), ENaC δ (SCNN1D), and ENaC γ (SCNN1D). The channel facilitates the active transport of Na+ ions in epithelial cells and is a non-voltage gated sodium channel. Na^+ inward transport mainly occurs through the enzymatic activity ENaC α sub-unit and further that this catalytic activity is inhibited by amiloride. The subunits β and γ associate with and stabilize ENaC α activity [110]. The structure, function and mechanism of human ENaC channel proteins have been recently reported employing full length, N and C terminal deletion mutants of α, β and γ subunits from cDNA clones along with GFP fluorescent tags. The human ENaC channel was shown to have the canonical “hand clenching a ball” model and further that a central core sensitive to protease activity provides a path to Na+ ion transport through the channel [111].

The regulation of ENaC channel activity in Xenopus and mouse renal epithelia by proteases demonstrated that local factors are capable of a modulatory effect governing Na^+ reabsorption, rather than a systemic control mechanism through out the body. Channel activating protease (CAP1) activates Na^+ reabsorption and mCAP1 the mouse homolog was also reported [112, 113]. This is a particularly important finding in regards to the respiratory system where airway surface liquid regulation is precisely regulated. In the human airway, extracellular Prostasin and TMPRSS2 have been implicated in regulating ENaC activity [114]. Elsewhere, the regulation of actin cytoskeletal framework has also been implicated in regulating ENaC activity. It was demonstrated that there is an indirect but stable association between actin framework bound to Actin related protein 2/3 (Arp2/3) and ENaC channel through cortactin with Arp2/3 protein. In instances of a stable cytoskeletal framework ENaC activity is minimized, however in the event of loss of cortactin binding with ENaC channel leads to ENaC channel activation. The mechnism of cortactin-ENaC channel disassembly occurs due to dephosphorylation of cortactin from regulartory kinases/phosphatases that affect cell motility and cell shape [115].

Asides from the role of sodium homeostasis during normal physiological processes, there is interesting data pointing to ENaC α subunit interaction with the cell cytoskeleton through its C terminus on the cytoplasmic face of the plasma membrane. There is direct evidence of dual stained ENaC α and actin co-localization along the plasma membrane as determined by laser confocal microscopy. The data also further demonstrates co-immunoprecipitation of actin when ENaC α was the immuno-precipitated target [116].

The roles of ENaC channel proteins in cancer are also well described. In the settings of pulmonary neuroendocrine cancers, transcription factor Achete-Scute homolog 1 (ASCL-1) driven over expression of ENaC α was well correlated in a panel of l11ung cancer cell types of which about 40% (5 cell types) showed robust over expression of ENaC α genetic expression. ENaC α activity abolishment with amiloride demonstrated lower cell survival, colony formation, and tumor volume. Thus ENaC channel proteins are implicated for roles that influence tumor growth and cell proliferation in model lung cancer cells [117]. Several member of the ENaC family of proteins have been observed to be over expressed in glioblastoma, a cancer of the central nervous system. In this regard the over expression of Acid Sensing Ion Channel (ASIC1), ENaC α and ENaC γ in glioblastoma cells compared to normal human primary astrocytes has been demonstrated. Further that, functional silencing of ENaC α expression severly limited invasion and migration capabilities in the glioblastoma cells demonstrating its role in metastasis [118].

The expression of ENaC α (SCNN1A) has also been investigated in a retrospective transcriptomics (by microarray study) study involving a cohort of 85 patients diagnosed with adenocarcinoma. It was found that some patients expressed higher level of SCNN1A gene when unbiased clustering stratified the patient pool. The high expression patients were clustered to be at high risk. The data was further confirmed using a separate set of tissue biopsies with the use of conventional real time PCR. The data demonstrated patients expression of high level of ENaC α transcript had a lowered over all survival compared to low ENaC α expressors [119].

4.3. AQP1 and ENaC in the context of MPM.

Aquaporin-1 is a prime gene of interest for its activity in the pleural physiology. In the settings of mesothelioma, it has been reported that the over-expression of AQP1 protein confers a prognostic survival advantage in surgically managed patients as well as in patients treated conservatively by chemotherapy [120]. The genetic expression of AQP1 transcripts has also been reported where AQP1 is over-expressed in a stratified manner in epithelioid compared to biphasic and sarcomatoid histotypes [108]. While the above two studies were retrospective in nature, a prospective study has demonstrated by immunhistochemical analysis that >50% AQP1 staining was associated with significantly higher survival and further that AQP1 positive cases were predominantly of the epithelioid histotype [109]. In another retrospective study involving fluoro-edenite asbestos exposed individuals, it was demonstrated that significantly high AQP1 (>50%) staining was associated with a median overall survival of 26.3 months as compared to <50% staining with a median survival of 8.9 months [121]. Taken together these data indicate that overexpressed AQP1 in MPM confers overall survival advantage.

As mentioned earlier in the context of AQP1 -/- mouse model wherein amiloride was employed to investigate the role of sodium ion in pleural fluid dynamics. There has been only one study reporting the expression of amiloride sensitive epithelial sodium channel protein α, β, γ, δ subunits in mesothelial cells. Further it was demonstrated the M9K cells human mesothelial cells, that the whole cell current was sensitive to amiloride (inhibitory current $_{50}$ near 10 μM concentration) and that the current was perturbation was dose dependent [122]. Taken together the expression of

AQP1 and ENaC channel protein in mesothelial and mesothelioma cells are important avenues for experimental evaluation.

In the light of the findings of tumor spheroid formation, growth and invasion, the role of TNT during cell culture and EMT playing a developmentally deterministic role, it is apparent to investigate cell adhesion, cell migration, cell proliferation, development of TnTs and EMT phenotypes in mesothelioma cell models. An important variable to consider while evaluating these phenotypes is the critical characterization of the extracellular matrix of homologous origin in cell model studies. In the context of ECM influencing hall mark characteristics in cancer such as metastasis related cell adhesion and cell migration, proliferation related resistance to cell death and EMT governed invasion are relevant models of study. Given the importance of pleural space physiology, the role of channel protein AQP1 and sodium transport inhibitors in pleural fluid turnover it is therefore consequential to determine the roles played by these proteins in the phenotypes described above.

5. Aim of the study

AQP1 and ENaC are water and sodium channels respectively that the pleural mesothelial cells are equipped with. They have a role in regulating the pleural fluid in physiological and patho-physiological conditions. Furthermore, high expression of AQP1 has been shown to confer a survival advantage in MPM patients, although in several cancers a role for AQP1 has been associated with more aggressive malignant phenotype. Regarding ENaC there are only data demonstrating that MPM cells still express the channel while in other cancers it has been shown that ENaC is involved in tumor development as well as progression. AQP1 and ENaC channels can be inhibited pharmacologically by mercury chloride and amiloride respectively. Based on the above, the aim of the current study was to investigate the role of AQP1 and ENaC in MPM cell adhesion, cell migration, tunneling nanotubes formation (TnT), cell proliferation, spheroid formation, spheroid invasion of collagen matrix and collagen gel contraction with embedded cells.

6. Materials and methods

Table 1. List of reagents and instruments

Reagent / instrument name	Catalog number	Company	Abbreviation
24 well culture dish	662 160	Griener Bio-one	
48 well culture dish	677 180	Griener Bio-one	
6 well culture dish	657 160	Griener Bio-one	
96 well culture dish	655 180	Griener Bio-one	
Acetic acid	1.00063.1011	Merck	
Amiloride	A7410-5G	Sigma	
Biotek spectrophotometer	Model-ELx808	BioteK	
Camera	DFC48C	Leica	
Crystal violet	C6158-50G	Sigma	
Di Sodium phosphate	S5136	Sigma	Na_2HPO_4
Eppendorf tubes (1ml)	30722019	Eppendorf	
Ethylenediaminetetraacetic acid	E6758	Sigma	EDTA
Fetal bovine serum	F0804-500	Sigma	FBS
Formaldehyde	33220	Sigma	
Glycine	G7403	Sigma	
L-Glutamine	G7513	Sigma	
Magnesium chloride hexahydrate	A597733	Merck	$MgCl_2.6H_2O$
Mercury (II) Chloride	M1136-25G	Sigma	HgCl2
MicroBCA assay kit	23235	Thermo scientific	
Microscope Nikon Eclipse	TS100	Nikon	
Penicillin-Streptomycin	P4333	Sigma	
Petir dish	BS611	Sterilin	
Plasma fibronectin	341631	Calbiochem	FN
Plasmocin	ANT-MPP	InVivogen	
Potassium chloride	31248	Sigma	KCl
Potassum dihydrogen phosphate	A317873 132	Merck	KH_2PO_4
RPMI 1640	R5886	Sigma	
Sodium bicarbonate	31437	Sigma	$NaHCO_3$
Sodium chlroride	S7653	Sigma	NaCl
Sodium deoxycholate	0970-100G	Sigma	
Sodium dodecyl sulphate	L4390	Sigma	SDS
Sodium Hydroxide	B868698 124	Merck	NaOH
TritonTM X-100	T9284-500ML	Sigma	
Trypan blue	T6146-25G	Sigma	
Trypsin	T4049	Sigma	

Table 2. Buffer compositions

Phosphate buffered saline (PBS)
NaCl - 8 grams (137 mM)
KCl- 0.2 grams (2.7 mM)
Na_2HPO_4 -1.44 grams (10 mM)
KH_2PO_4 - 0.24 grams (1.8 mM)
Final volume - 1 liter, pH 7.4

PBS with Ca^{2+}, Mg^{2+}
NaCl - 8 grams (137 mM)
KCl- 0.2 grams (2.7 mM)
Na_2HPO_4 -1.44 grams (10 mM)
KH_2PO_4 - 0.24 grams (1.8 mM)
$CaCl_2$ – 0.1 grams (1 mM)
$MgCl_2.6H_2O$ – 0.1 grams (0.5 mM)
Final volume - 1 liter, pH 7.4

DNaseI buffer
DTT – 0.1 mM
$MgCl_2$ – 6 mM
TRIS – 40 mM pH 7.5

6.1. Cell culture.

Human cell lines used in this study were a kind gift from Dr Ioannis Kalomenidis (Faculty of Medicine, University of Athens). The human cell lines consisted of a benign immortalized pleural mesothelial cell line (MeT-5A, ATCC catalog #CRL 9444) and 3 malignant pleural mesothelioma (MPM) cell lines of different histotypes: M14K (epithelioid MPM), MSTO-211H (biphasic MPM, ATCC catalog # CRL 2081) and ZL34 (sarcomatoid MPM). The cultures were propagated in 10%FBS - RPMI media with antibiotic additives, which were Penicillin-Streptomycin (1%), Plasmocin (2.5 mg/500 mL), and amino acid supplement L-Glutamine (2 mM) at 37^0C in 5% CO_2 incubator. During cell culture media was replenished every 48 hours after a gentle wash with PBS containing Calcium and Magnesium. For synchronizing purposes the cells

were treated for 24 hours with 0.5% FBS-RPMI. Confluent culture in T-75 flasks for passaging or experimental setup were washed with PBS followed by 2 mL of Trypsin treatment for 5 minutes at 37^0 C and quenching with 8 mL of RPMI with 10% serum. Trypsin was removed by sedimentation of the cells by centrifugation at 4^{o}C, the cell pellets were re-suspended in 5 mL of media for further use. For the purpose of cell counting, cells were diluted 1:10 in Trypan blue and counted on a Neubauer slide at 100X magnification.

6.2. Inhibitor solutions.

AQP1 inhibition was performed by exposure to Mercury (II) Chloride ($HgCl_2$) at a concentration of 10 μM. For experiments a stock solution (filter sterilized) of 1mM was diluted into 10% FBS-RPMI working solution. For ENaC inhibition, Amiloride at a concentration of 10 μM in 10% FBS-RPMI was used. For experiments a filter sterilized stock solution of 1mM was diluted into 10% FBS-RPMI working solution.

6.3. DNaseI treatment and buffer.

DNaseI enzyme was used at a final concentration of 10 mg/mL. The enzyme was dissolved in working buffer that consisted of 0.1 mM dithiothreitol, 6 mM $MgCl_2$, 40mM Tris-HCl (pH 7.5).

6.4. Fixing solution.

4% paraformaldehyde (4%PFA) was prepared from 36.5% PFA in PBS. The solution was stored at room temperature.

6.5. Trypan blue.

0.04% Trypan blue was prepared in PBS. The prepared solution was filtered sterilized and stored at room temperature.

6.6. Crystal violet.

0.5% w/v Crystal violet stain was prepared in 25% methanol in PBS and stored at room temperature.

6.7. 10% Acetic acid.

The distaining solution was prepared in water with glacial acetic acid. The solution was stored at room temperature. De-staining with 10% acetate was subject to optical density (O.D.) measurements at 570 nm wavelength.

6.8. Extra-Cellular Matrix (ECM) extraction buffer.

ECM extraction buffer was formulated in PBS with 0.25% Triton^{TM} X-100 and 1% Sodium deoxycholate. The buffer was autoclave sterilized at 135º C, 15 psi pressure for 40 mins.

6.9. Protein quantitation.

Protein samples from monolayers were subject to MicroBCA assay using a kit. All experimental samples for colorimetric development were diluted in water in a 1:4 or 1:10 ratio. All MicroBCA standard curves had an $\rho^2 \geq 0.995$. All samples had an n=3. O.D. at 570 nm wavelength was measured in 96 well plates using a spectrophotometer (Biotek, ELx100).

6.10. Plasma fibronectin (FN).

FN (1 mg) of bovine origin was dissolved in 20 mL of RPMI. The final concentration was 50 μg/mL. The solution was then filter sterilized with a 0.22 μm pore size filter. The solution was stored at 4ºC.

6.11. Cell derived extracellular matrix preparation.

Cells were seeded at various concentrations according to the total surface area of culture dish/well as shown in **Table 3**. Cells were cultured over 48 hours. The media was removed followed by the application of ECM extraction buffer. The plate was then kept at 37ºC in 5% CO_2 incubator for 10 mins. The ECM buffer was aspirated followed by washing with PBS. The residual ECM was subject to DNaseI treatment for 20 mins in DNaseI buffer. The plate was then washed again with PBS prior to experiments on ECM. The process of cell deposited ECM is illustrated below in **Picture 2**.

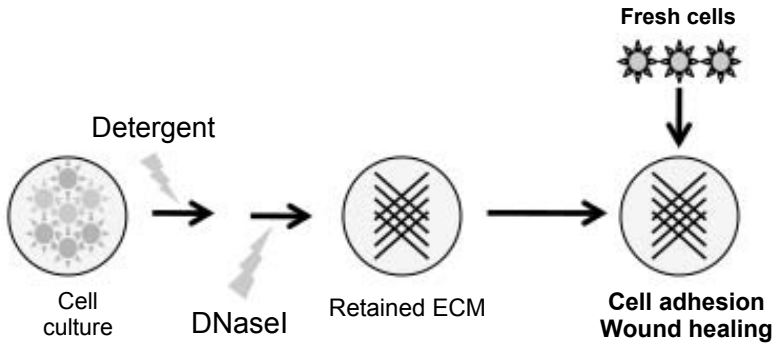

Picture 2: Schematic of ECM generation *in-vitro* followed by cell lysis with detergent, for cell removal, DNaseI treatment for digesting residual genomic DNA. The substratum with retained ECM is used for experimental phenotypes.

6.12. ECM total protein preparation.

$2.5x10^6$ cells were seeded in 10 cm tissue culture dishes. Cells were cultured for 48 hours followed by lysis using ECM buffer and DNaseI treatment. The plates were then air dried in a laminar flow hood and then ECM was extracted by scraping with plastic spatulas using 1mL of citrate buffer. The collected ECM was subject to MicroBCA under defined dilutions to assess the protein concentration.

6.13. Cell surface attachment preparations.

For the purpose of cell adhesion to tissue culture plastic, 2 treatments were performed in a standardized format with plasma fibronectin (FN) of bovine origin (50 μg/mL in RPMI) for 30 minutes or cell derived extracellular matrix (ECM). For the purposes of cell derived ECM depositions, cells were seeded at various cell densities and cultured for 48 hours followed by isolation of cell derived ECM with sterile mild detergent buffer (ECM extraction buffer) for 10 minutes at 37°C. The cell derived ECM was then treated with DNase I for 20 minutes at 37° C. The standardized procedures for plastic treatments are detailed in **Table 3** below.

Table 3: Tissue culture plastic treatment - details of multiwell plates and the volumes of various reagents used.

Treatment type	Plate type	Cells / buffers	Volume (μL)	Time
FN (50 μg / mL)	6, 48, 96	RPMI	200, 100, 50	30 mins
Cell derived ECM	6, 48, 96	10^6, $5x10^4$, 10^4 cells	400, 200, 100	48 hrs
	6, 48, 96	ECM buffer	400, 200, 100	10 mins
	6, 48, 96	DNase I	400, 200, 100	20 mins

6.14. Rat tail collagen preparation.

Tails were obtained from euthanized white Norwegian Sprague-Dawley rats that were designated for disposal, and were kindly provided by Dr. Konstantinos Dimas and Ilias

Begas, Laboratory of Pharmacology, Department of Medicine, UTH. The tails were cut perpendicular to anterior-posterior axis at regular intervals without penetrating the core of the tail. Small 1cm portions of intact tail were pulled apart until cords of white material in-between were stretched. Such strings of collagen were collected, weighed and immersed in 95% ethanol and then air dried in a laminar flow hood. The dried collagen cords were subject to leaching with sterile 0.2 M acetic acid, in a sterile conical flask on a magnetic stir plate for 16 hours at 4^{o}C. The solution was then subject to clarification by centrifuging at 2500g for 20 minutes, two times in order to sediment un-dissolved protein. The resulting collagenous material was then stored in sterilized glass bottles at 4^{o}C.

6.15. Cell adhesion assay.

Cell adhesion assays were performed in 48 well plates under 2 surface treatment conditions (FN or ECM treated). Prior to attachment all cells were serum starved as noted in **Table 3** for 24 hours, followed by trypsinization and quenching. For all adhesion assays 25,000 cells in 200 μL volumes in 10% RPMI without or with $HgCl_2$ or amiloride were plated in 48 well plates. Attachment was carried out at 37^{0}C for 90 minutes in a 5% CO_2 incubator. At the end of the experiment, cell suspension was withdrawn by suction followed by washing with pre-warmed PBS (37^{0}C). The attached cells post washing, were fixed with 100 μL 4% PFA for 10 minutes. The fixative was then removed and the cells were then stained with 0.5% crystal violet for 10 minutes. The stain was then washed out by repeated immersion in a beaker with continuous tap water replenishment. The plates were then dried overnight in an inverted position without the lid. The bound crystal violet was extracted with 100 μL of 10% acetic acid

and then transferred to a 96 well plate for O.D. measurement. All O.D. measurements were adjusted for blank O.D. from untreated wells. For cell adhesion experiments without drugs, O.D. from FN substratum was considered 100%. In experiments with drugs O.D. from controls was considered 100%.

6.16. Cell migration assay.

Assays were performed in 48 well plates under 2 surface treatment conditions (FN or ECM treated). Cells were attached at standardized densities for each cell line in 10% FBS-RPMI medium as shown in **Table 4** below. Cells were cultured for 24 hours followed by serum starvation for 24 hours. Media in each well was aspirated and then the cell monolayer was scratched in a straight line with a sterile 10 μL pipette tip using a ruler as a guide. The detached cells were removed by washing with warm low serum media followed by media change to appropriate treatments i.e. low serum, 10% FBS-RPMI, $HgCl_2$ or amiloride in 10% FBS-RPMI media. Each well was then imaged at 100X, and then the plate was incubated for 4 or, 8 hours at 37°C in 5% CO_2 incubator. Experiments were terminated by media aspiration followed by fixing with 4% PFA for 10 mins at room temp. Each well was imaged again at predefined location as per the marking on the outer bottom. The images were analyzed using ImageJ software and wound migration was calculated as Migration index (MI) = (area t_0 - area $t_{4,8}$) / area t_0. Each condition had a replicate of n=6 or 8, all experiments were performed 2-3 times.

Table 4. Cell migration assay - details of reagents and the volumes used in cell migration assays.

Cell line	FN / well	Cells / well for ECM	Cells / well
MeT-5A	100 μL	50,000 cells	145,000
M14K			145,000
MSTO-211H			130,000
ZL34			110,000

6.17. TnT formation assay.

The cell proliferation assays were performed in sterile 96 well plates. Wells were treated with 50 μL of FN dissolved in RPMI or subject to ECM culture with 10,000 cells/well in 200 μL of 10% RPMI media followed by ECM buffer and DNaseI treatments, 3X washing with sterile PBS. Synchronized cells were then seeded at a concentration of $5x10^4$ cell/mL (200 μL volumes) in 10% FBS-RPMI with/without $HgCl_2$ or amiloride. The cells were allowed to proliferate for 24 hours. At the end of the assay, medium was withdrawn and wells were washed once with PBS, followed by fixing the cells with 50 μL of 4% PFA for 10 mins. The fixing agent was then replaced with 50 μL of 0.5% crystal violet stain for 10 mins. Then the entire plate was repeatedly immersed in a plastic tub continuously replenished with tap water. A minimum of 16 random locations was photographed from two experimental assays. All images were then subject to manual counting with cell-counting plugin of ImageJ.

6.18. Cell proliferation assay.

The cell proliferation assays were performed in sterile 96 well plates. Wells were treated with 50 μL of FN dissolved in RPMI or subject to ECM culture with 10,000 cells/well in 200 μL of 10% RPMI media followed by ECM buffer and DNaseI treatments, 3X washing with sterile PBS. Synchronized cells were then seeded at a concentration of $5x10^4$ cell/mL (200 μL volumes) in low serum-RPMI (0.5% FBS) or 10% FBS-RPMI or 10% FBS-RPMI supplemented with $HgCl_2$ or amiloride. The cells were allowed to proliferate over 3 days with media replenishment at 48 hours. At the end of the assay, medium was withdrawn and wells were washed once with PBS, followed by fixing the cells with 50 μL of 4% PFA for 10 mins. The fixing agent was

then replaced with 50 μL of 0.5% crystal violet stain for 10 mins. Then the entire plate was repeatedly immersed in a plastic tub continuously replenished with tap water to remove unbound stain. The plate was then dried in an inverted position without the lid, overnight. The bound crystal violet was then released by adding 100 μL of 10% Acetic acid. The released dye was then transferred to another 96 well plate and the O.D. was measured at 570 nm using a spectrophotometer. Wells with media alone were used for residual crystal violet binding in order to subtract background due to non-specific plastic staining. Each condition had a replicate of n=8 and all experiments were performed 3-5 times. The O.D. from 10% FBS-RPMI was arbitrarily set at 100% and the O.D. of treatments was normalized accordingly.

6.19. Spheroid formation assay.

Spheroids were generated by the hanging drop method [123]. Synchronized cells $2x10^3$ cells/mL were vortexed thoroughly along with 250 ng/mL FN or cell derived ECM. In some suspensions $HgCl_2$ or amiloride were included in the media. The cells were then spotted on the roof of the lid of a sterile petri plates in 25 μL volumes. The bottom of the petri plate received 2 mL of sterile PBS. The lids with the spotted cultures were gently inverted to form hanging drops and petri plates were thus closed with the bottom plate and placed in standard CO_2 incubator for 48 hours. To assess spheroid formation the plate was opened and the lid re-inverted and allowed to sit for 5-10 mins and then imaged on an inverted tissue culture microscope with camera interfaced (see below under Microscopy and imaging). Each media condition had a replicate of 8-10 and each experiment was repeated at least 3 times. From each image of the spheroid, the

perimeter was measured using polygon tool of ImageJ. The perimeter of the spheroids cultured in media alone was used to normalize the data.

6.20. Spheroid invasion assay.

Spheroids were generated by the hanging drop method as described previously in this section with no addition of FN or cell derived ECM. Neutralized collagen was mixed with 10% FBS RMPI media, and in some mixtures $HgCl_2$ or amiloride were included and set on ice until further use. The lid plates with hanging drops were inverted and each spheroid was over laid with 20 μL of collagen mix. The gels were allowed to congeal over 10-15 mins inside the laminar flow hood. The petri plates were then closed with the spheroids in a hanging state inside the collagen over-lay. The spheroids were cultured for another 48 hours. The spheroids were then imaged by microscopy and the perimeter of each spheroid was assessed using ImageJ.

6.21. Collagen gel contraction.

Synchronized cells were used to perform gel contraction assays. All reagents were kept on ice. Rat tail collagen (1.2 to 1.5 mg/mL) was neutralized with sterile 0.5M NaOH. 10^6 cells/mL were mixed with the neutralized collagen and thoroughly vortexed. In some collagen-cells mixture $HgCl_2$ ($2x10^{-5}$M) or amiloride ($2x10^{-5}$M) were included to account for dilution after additional 10% FBS-RPMI addition. The gel mix was then dispensed in 600 μL volumes in a 24 well cell culture plate and the gels were allowed to polymerize in the laminar flow hood for 30 mins. Additional 600 μL of 10% RPMI was added to each well and then the plates were transferred to a CO_2 incubator to culture for 24 hours. At the end of the assay the plate was scanned on a flat bed Canon

Lide scanner. Each well containing the polymerized gel was then assessed for area measurements by image analysis using ImageJ. Each media condition had a replicate of n=8 and each experiment was performed 3 times. Control gel areas were used to normalize the data sets.

6.22. Microscopy and Imaging.

Microscopy was done on a Nikon Eclipse TS100 instrument. For image capturing, the microscope was interfaced with a Leica CCD camera and the imaging process was controlled with Lieca application suite LAS version 3.6. Imaging was done at 100X, 200X or 400X and indicated where applicable.

6.23. Statistical analyses.

All experiments were subject to statistical analyses. From each experiment the data was subject to normality assessment by the D'Agostino-Pearson omnibus normality test. For comparisons among three groups or more One-way ANOVA was performed with Tukey's multiple comparisons test for parametric data while in case of non-parametric data the Kruskal-Wallis test and Dunn's multiple comparisons test was performed. Two-Way ANOVA with Sidak multiple comparisons test was performed to determine statistically significant differences in cell adhesion, cell migration, TNT formation, cell proliferation, spheroid formation, spheroid invasion, gel contraction during inhibition with $HgCl_2$ or Amiloride on two substratum for comparisons (where applicable) within each cell type. All analyses were performed with Prism 6.0 for Mac. Data were considered to be statistically significant when $p<0.05$.

7. Results

7.1. Sarcomatoid MPM cells produce significantly higher levels of ECM protein.

Cell derived ECM substratum was subject to micro BCA assay in order determine if there are significant differences in the amounts of protein secreted during culture. After ECM isolation, micro-BCA working reagent was directly applied to the treated culture plastic. Benign MeT-5A cells deposited 6.55±0.5 μg/ml protein, M14K cells deposited 6.6±0.4 μg/ml, MSTO cells deposited 9.3±1.0 μg/ml and ZL34 cells deposited 10.7±0.9 μg/ml protein, significantly higher protein deposition compared to MeT-5A and M14K cells ($p<0.01$) as demonstrated in **Figure 1**.

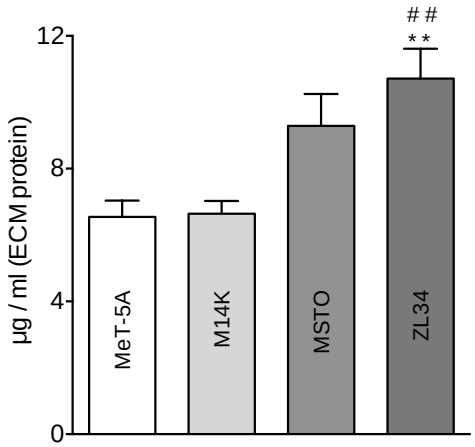

Figure 1: Mean (±SEM) protein content in substratum of all cell lines. *n*=5 or 6, and, ** represents $p<0.01$ compared to MeT-5A and ##compared to M14K $p<0.01$.

7.2. MPM cells demonstrate higher cell adhesion on homologous ECM substratum than on FN.

Single cells in suspension were used for cell adhesion assays **(Figure 2)**. Benign mesothelial cells (MeT-5A) do not show significant differences in cell adhesion based on substratum. All three malignant cell types, M14K, MSTO and ZL34 demonstrated significantly higher cell adhesion on homologous cell derived ECM substratum as compared to FN treated plastic substratum. Cell adhesion on ECM was in comparison to FN (arbitrarily set at 100%). In M14K cell type, the mean adhesion on FN was 100.0±2.55%, while the mean cell adhesion on ECM was significantly higher 125.9±4.1%, ($p<0.001$). In MSTO cell type, mean cell adhesion on FN was 100.0±1.4%, while the mean cell adhesion on ECM was significantly higher 111.6±5.6%, ($p<0.05$). And lastly, in ZL34 the mean cell adhesion on FN was 100.0±1.4%, and on ECM was 141.7±4.2%, significantly higher ($p<0.001$).

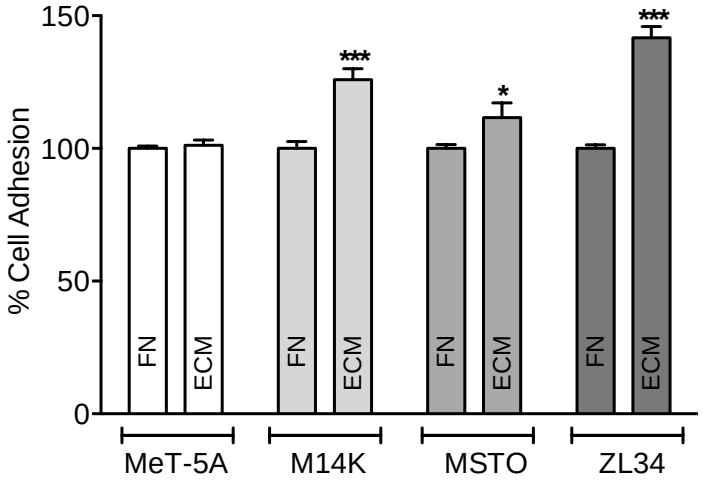

Figure 2: Mean±SEM % cell adhesion on FN or ECM substratum of all cell lines. *n*=40, data combined from 5 experiments. Cell adhesion of each cell line on FN was arbitrarily set to 100%, cell adhesion on ECM was relative to FN, * represents $p<0.05$ and *** $p<0.001$.

7.3. Benign and MPM cell migration was lower on homologous cell derived ECM than on FN.

Cell monolayers were cultured on FN or ECM substratum and subject to wound healing assay to assess cell migration. The MI of each cell type were compared based on the substratum **(Figure 3)**. In MeT-5A cells the mean MI on FN was 0.37±0.01, which was significantly higher than the mean MI on ECM 0.2±0.0 ($p<0.001$). In M14K cells, the mean MI on FN was 0.30±0.01 significantly higher than the mean MI on ECM 0.21±0.0 ($p<0.001$). MSTO cells had a mean MI of 0.5±0.01 on FN, while on ECM the mean MI was 0.4±0.02, the difference was significant with $p<0.001$. The MIs of MeT-5A, M14K and MSTO were assessed at 8 hours, while in ZL34 cells the MI was assessed at 4 hours. Mean MI on FN was 0.63±0.01, significantly higher than the mean MI on ECM, 0.47±0.01, $p<0.001$.

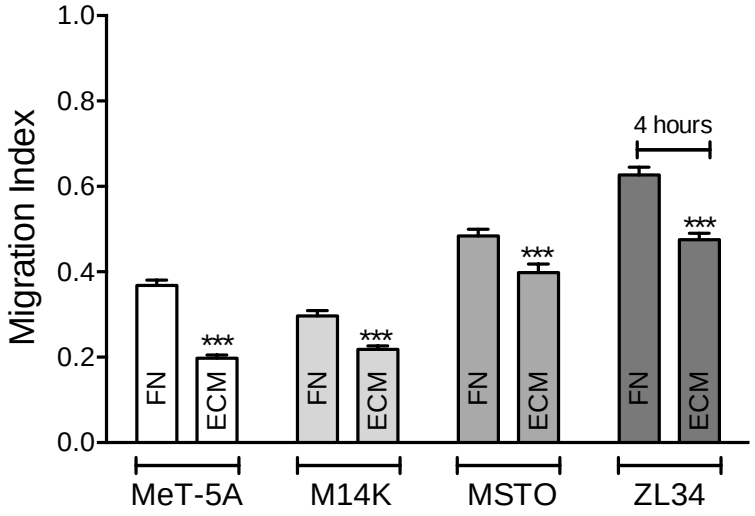

Figure 3: MI on FN and ECM (mean±SEM), n=12, *** indicates $p<0.001$ compared MI on FN of corresponding cell type. MeT-5A, M14K and MSTO experiments span over 8 hours while ZL34 experiments span over 4 hours.

7.4. *Biphasic and sarcomatoid cells develop significantly more TnTs on ECM.*

TnTs were observed in all 4 cell types on both FN **(Figure 4A-D)** and ECM substratum **(Figure 4E-H)** after 24 hours in culture (as indicated with white arrows). While all 4 cell types develop TnTs, significant differences in TnT production were observed in MSTO (on FN, 11.5±0.6, versus ECM, 19.6±1.0, $p<0.01$) and in ZL34 (on FN, 28.6±1.6 versus 35.7±2.2 on ECM, $p<0.01$) as shown in **Figure 4 I**.

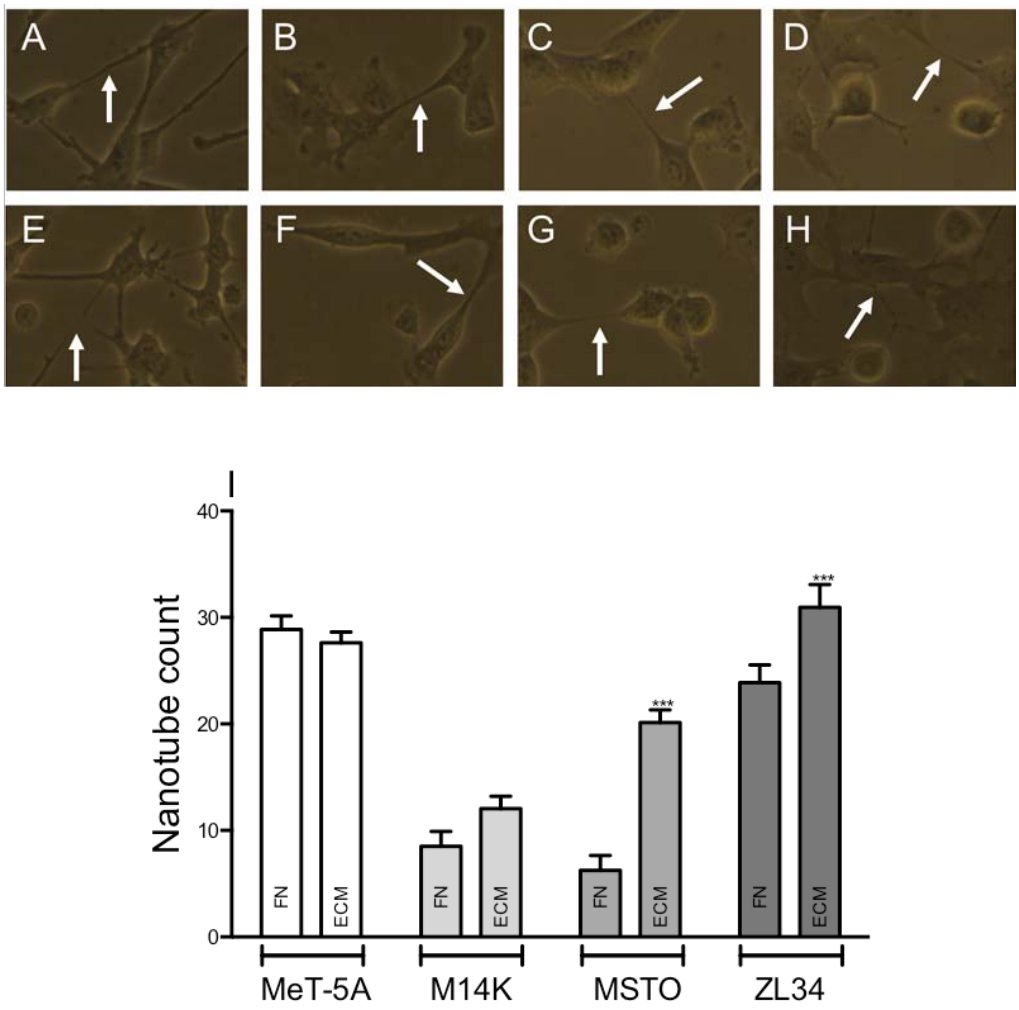

Figure 4: **A**, MeT-5A cells on FN substratum and **E** on ECM, M14K cells, **B** on FN and **F** on ECM, MSTO cells, **C** on FN, **G** on ECM and ZL34 cells **D** on FN, **H** on ECM after 24 hours in culture. **I**: Comparison of Mean±SEM TnT counts / field from all the cell types on FN and ECM, n=16, *** represents $p<0.001$.

7.5. *Benign and MPM cell proliferation is substratum dependant.*

Proliferation after 72 hours on FN was arbitrarily set at 100%. Cell proliferation of MeT-5A on FN was 100±2.3%, on ECM 54.4±3.2%, proliferation of M14K on FN was 100±1.2%, while on ECM was 56.4±2.6%. Cell proliferation of MSTO on FN was 100±1.5%, on ECM was 65.6±3.4%, and that of ZL34 on FN was 100.0±3.0% while on ECM it was 44.8±3.4%. Cell proliferation on FN in all cell lines was significantly higher compared to that of ECM ($p<0.001$) as shown in **Figure 5**.

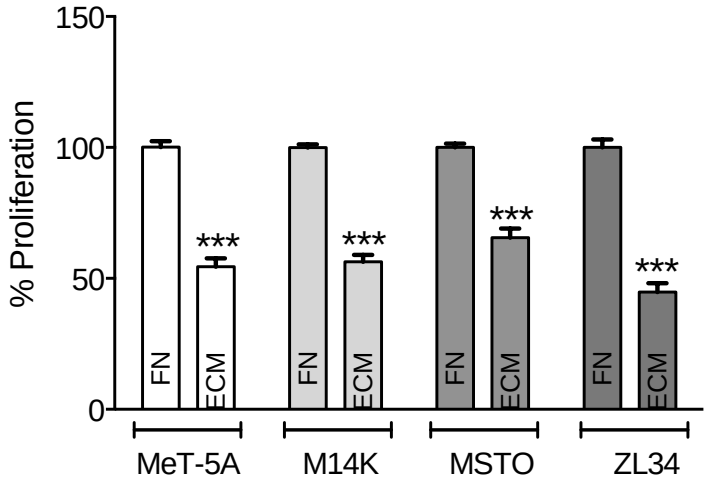

Figure 5: Comparisons of mean±SEM % cell proliferation of each cell line on FN or ECM substratum as indicated. The experiments were performed 3 times with a total n=24 as graphed and shown above, *** represents $p<0.001$.

7.6. Biphasic MPM spheroids were larger in homologous cell derived ECM as compared to FN.

Spheroids cultured in complete media complimented with FN or homologous ECM were compared for differences in the % perimeter as shown in **Figure 6**. The mean perimeter of spheroids grown in FN containing media, were arbitrarily set at 100%. In MeT-5A cells, M14K and ZL34 spheroids formed in FN or ECM do not have

significant differences in the perimeter. In MSTO, the mean spheroid perimeter with FN was 100.0±1.7%, while with ECM the mean spheroid perimeter was 130.0±5.7%, the differences were statistically significant, $p<0.01$. In ZL34, the mean spheroid perimeters differences between FN and ECM were not stastically significant.

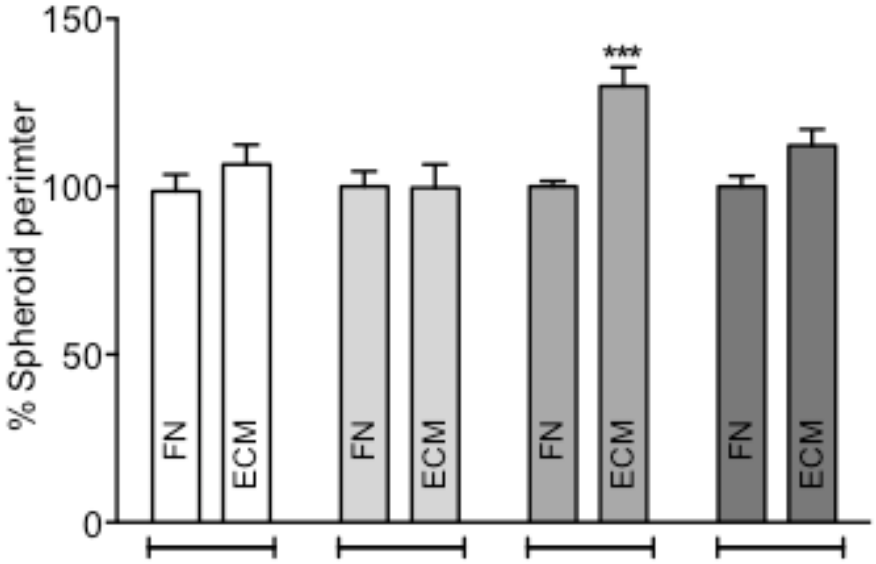

Figure 6: Mean (±SEM) % spheroid perimeter cultured for 48 hours in FN or ECM in media, n=11, *** indicates $p<0.01$ compared to the perimeter of corresponding cell type.

7.7. *MPM cell line tumor spheroids develop invasive protrusions during growth in collagen gel.*

Cells grown under suspension in 3D were subject to invasion assay by an overlay of collagen and further culturing for 48 hours. Benign MeT-5A cells demonstrate spheroids devoid of invasive features with smooth defined edges along the perimeter of the spheroid (**Figure 7A**). In marked contrast MPM cells M14K (**Figure 7B**), MSTO-211H (**Figure 7C**) and ZL34 (**Figure 7D**) tend to develop thin fibrillar structures. Spheroid perimeters were evaluated inclusive of invasive edges. MeT-5A

spheroids were significantly smaller (838.1±37.8) compared to M14K, (1469±151.2, p<0.01), MSTO-211H (2309±128.8, p<0.005) and ZL34 (2441±107.7, p<0.005). Furthermore, M14K spheroids were significantly smaller than MSTO-211H and ZL34 spheroids (p<0.005) as shown in **Figure 7E**.

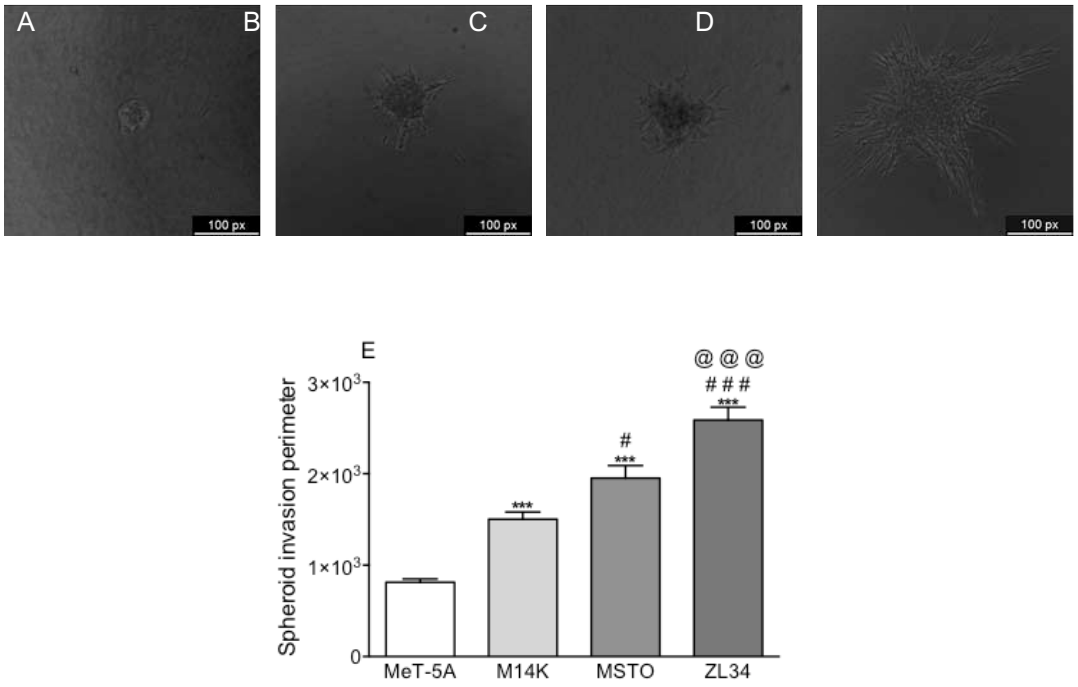

Figure 7: Spheroid invasion microgrpahs of **A**, MeT-5A, **B**, M14K, **C**, MSTO, **D**, ZL34. **E**, Comparison of mean±SEM spheroid perimeters of cell lines relation to MeT-5A *** p<0.005, versus M14K # p<0.05, or ### p<0.001, versus MSTO @@@ p<0.001.

7.8. *Benign and MPM cells demonstrate gel contraction.*

Collagen matrices embedded with benign and MPM cells undergo spontaneous contraction over a period of 24 hours as demonstrated in **Figure 8A-D**. The measured gel area were normalized to areas of MeT-5A embedded gels. MeT-5A gel area (100.0±3.4) was significantly higher (p<0.001) than M14K (54.8±2.4), MSTO-211H (55.7±0.4) and ZL34 (34.3±1.0) as shown in **Figure 8E**. Further, M14K and MSTO-

211H gel areas were significantly higher than ZL34 ($p<0.001$ compared to M14K, $p<0.01$, to MSTO-211H).

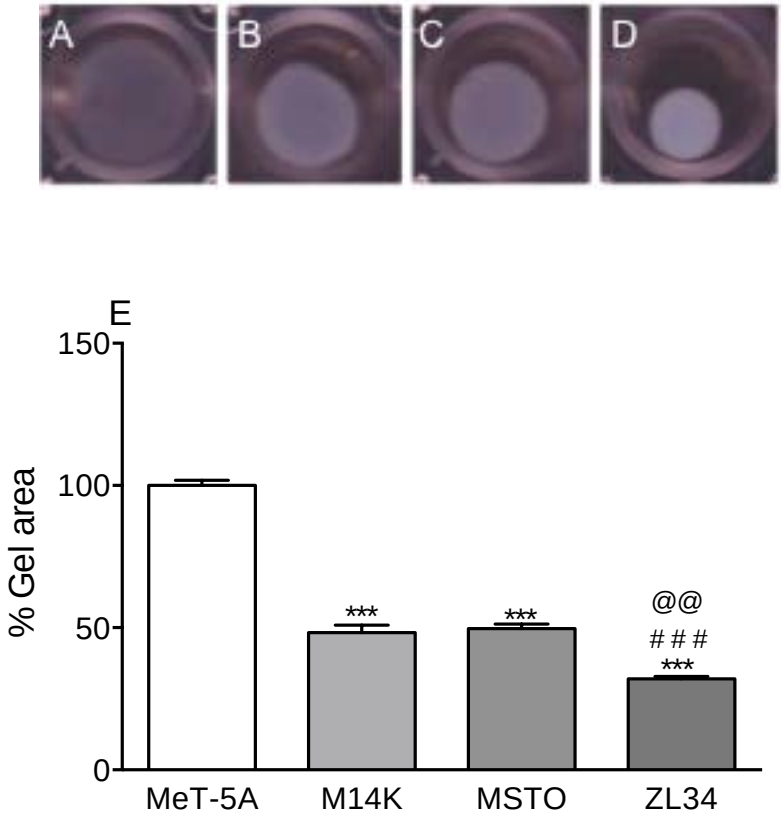

Figure 8: Images of gels containing cells **A**, MeT-5A, **B**, M14K, **C**, MSTO, **D**, ZL34 of AQP1 in collagen matrix **E**: mean±SEM % gel area comparisons between cell lines, *** represents comparison to gels with MeT-5A cells, $p<0.005$, ### represents comparison with M14K, ### $p<0.001$, @@ represents comparison with MSTO-211H, $p<0.01$.

7.9. *AQP1 lowers cell adhesion of MeT5A on FN and of and M14K cells on FN and ECM.*

Cell adhesion on FN and ECM substratum was assessed with $HgCl_2$. MeT-5A cell adhesion was significantly lower on FN with $HgCl_2$ (67.3±3.1%, $p<0.001$) compared to control (100.0±5.1%) as shown in **Figure 9A**. M14K cell adhesion was significantly lower on FN with $HgCl_2$ (71.3±5.9%, $p<0.001$) compared to control (100.7±3.4%) and on ECM with $HgCl_2$ (85.7±3.2%, $p<0.05$) compared to control (100.3±1.5%) as shown

in **Figure 9B**. MSTO-211H and ZL34 cell adhesion was was unaffected with $HgCl_2$ irrespective of the substratum as shown in **Figures 9C** and **9D**.

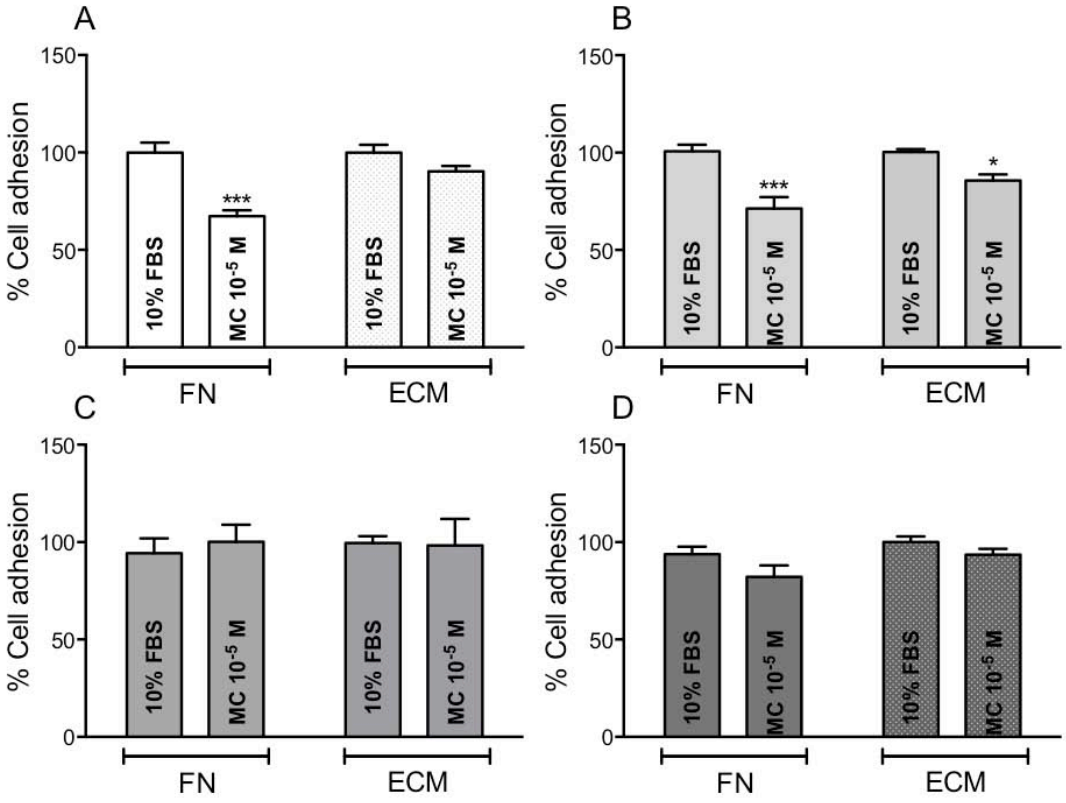

Figure 9: Comparison of mean±SEM % cell adhesion on FN or ECM substratum in the presence of $HgCl_2$. **A**, MeT-5A (n=13), **B**, M14K (n=13), **C**, MSTO-211H (n=13) and **D**, ZL34 cell type (n=14) and * represents $p<0.05$, *** represents $p<0.001$.

7.10. ***AQP1 lowered cell migration in sarcomatoid cell type on FN and ECM substratum.***

Cell migration during AQP1 blockade with $HgCl_2$ was significantly lowered in ZL34 cells on FN, MI=0.45±0.02, $p<0.001$ (in 4 hours) compared to control MI=0.7±0.03, and on ECM with $HgCl_2$ MI=0.86±0.01, $p<0.01$ in 8 hours compared to control MI=0.95±0.01 as shown in **Figure 10D**. MeT-5A **(Figure 10A),** M14K **(Figure10B)** and MSTO-211H **(Figure 10C)** cell types did not show any appreciable lowering of cell migration on FN or ECM substratum during the blockade of APQ1.

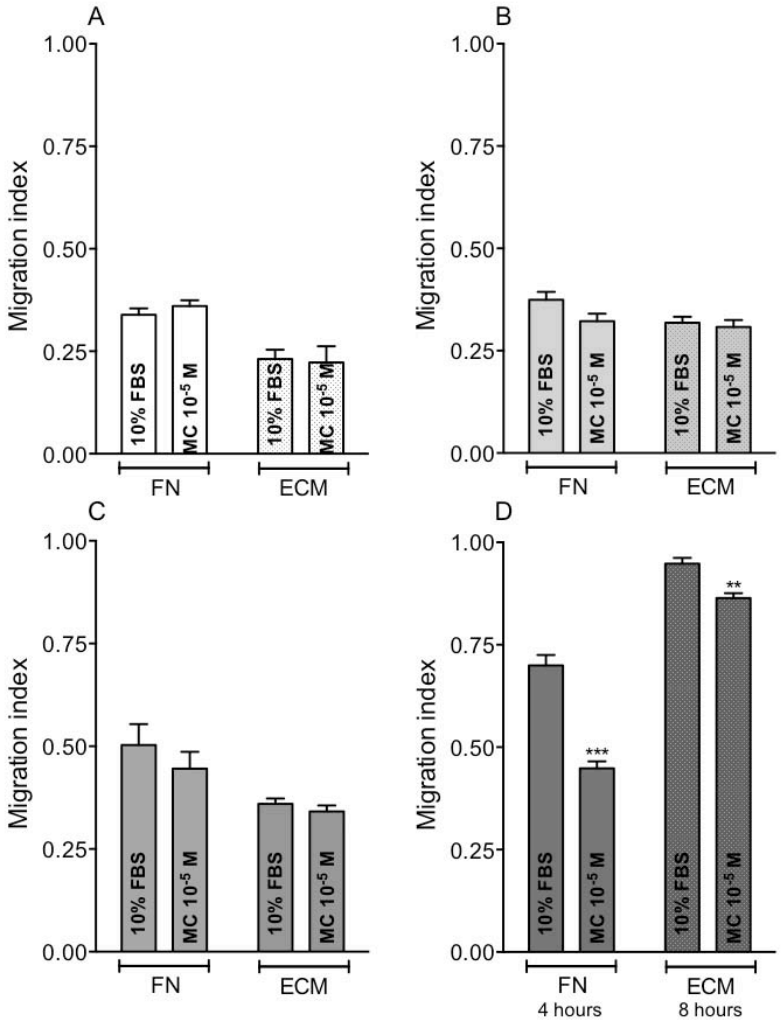

Figure 10: Mean±SEM migration index on FN or ECM substratum. **A**, MeT-5A, n=8 and **B**, M14K, n=8, **C**, MSTO-211H, n=15 and **D**, ZL34, n=14. ** indicates p<0.01, and *** p<0.001.

7.11. *AQP1 inhibition leads to reduced TnT formation in benign mesothelial cells.*

Cells were cultured on FN or homologus cell derived ECM for a period of 24 hours. All 4 cell types demonstrated TnT formation in the presence of $HgCl_2$ as illustrated in **Figures 11A-D**. Benign mesothelial cells MeT-5A demonstrate significantly lower nanotube count (TnT formation) on both FN (control 31.88±1.5 versus $HgCl_2$ 22.75±1.0, p<0.001) and on ECM substratum (control 37.0±1.6 versus $HgCl_2$ 22.38±1.4, p<0.001) as shown below in **Figure 11A**. There were no statistically significant differences in nanotube counts among the MPM cell types with $HgCl_2$ treatment on FN or ECM substratum culture.

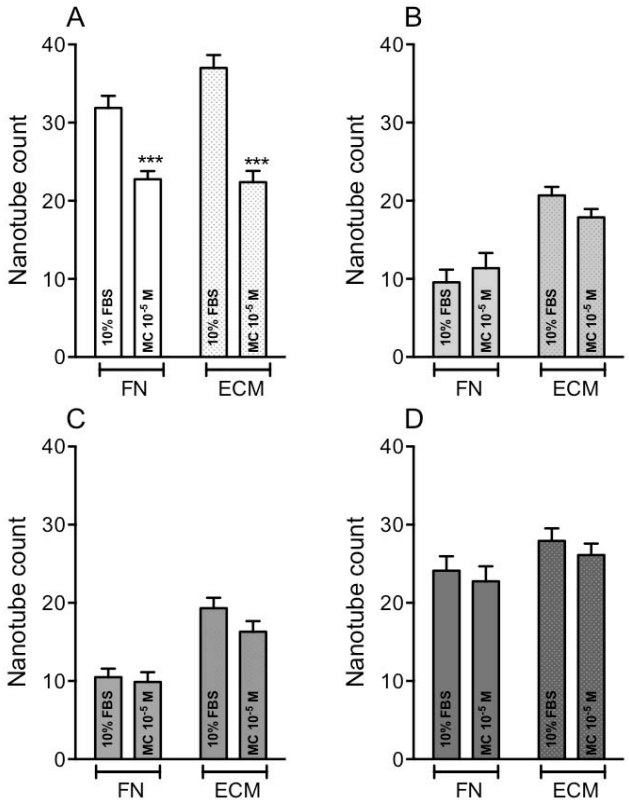

Figure 11: Mean±SEM nanotube count comparisons between control and HgCl2 treated cultures for 24 hours on FN or ECM substratum. **A**, MeT-5A, **B**, M14K, **C**, MSTO-211H and **D**, ZL34 cells. n=16. *** Indicates p<0.001.

7.12. *AQP1 inhibition reduced cell proliferation in all cell types on both FN and ECM substratum*.

Cells were allowed to proliferate over a period of 72 hours on FN or ECM substratum, some wells received $HgCl_2$. The O.D. from 10% FBS RPMI cultures were arbitrarily set at 100%. Benign mesothelial cells MeT-5A, demonstrate significantly lower proliferation on both FN (control 100.0±1.6% versus $HgCl_2$ 38.8±1.9%, p<0.001) and on ECM substratum (control 100.0±2.3% versus $HgCl_2$ 41.5±2.3, p<0.001) as shown below in **Figure 12A.** Epithelioid MPM cells M14K, demonstrate significantly lower proliferation on both FN (control 100.0±1.8% versus $HgCl_2$ 67.1±4.7%, p<0.001) and on ECM substratum (control 100.0±2.5% versus $HgCl_2$ 69.5±2.8, p<0.001) as shown below in **Figure 12B.** Biphasic MPM cells MSTO-211H, demonstrate significantly lower proliferation on both FN (control 100.0±1.3% versus $HgCl_2$ 49.8±3.7%, p<0.001) and on ECM substratum (control 100.0±2.7% versus $HgCl_2$ 67.5±3.5, p<0.001) as shown below in **Figure 12C.** Sarcomatoid MPM cells ZL34, demonstrate significantly lower proliferation on both FN (control 100.0±2.3% versus $HgCl_2$ 83.7±2.5%, p<0.001) and on ECM substratum (control 100.0±1.8% versus $HgCl_2$ 78.4±2.8, p<0.001) as shown below in **Figure 12D.**

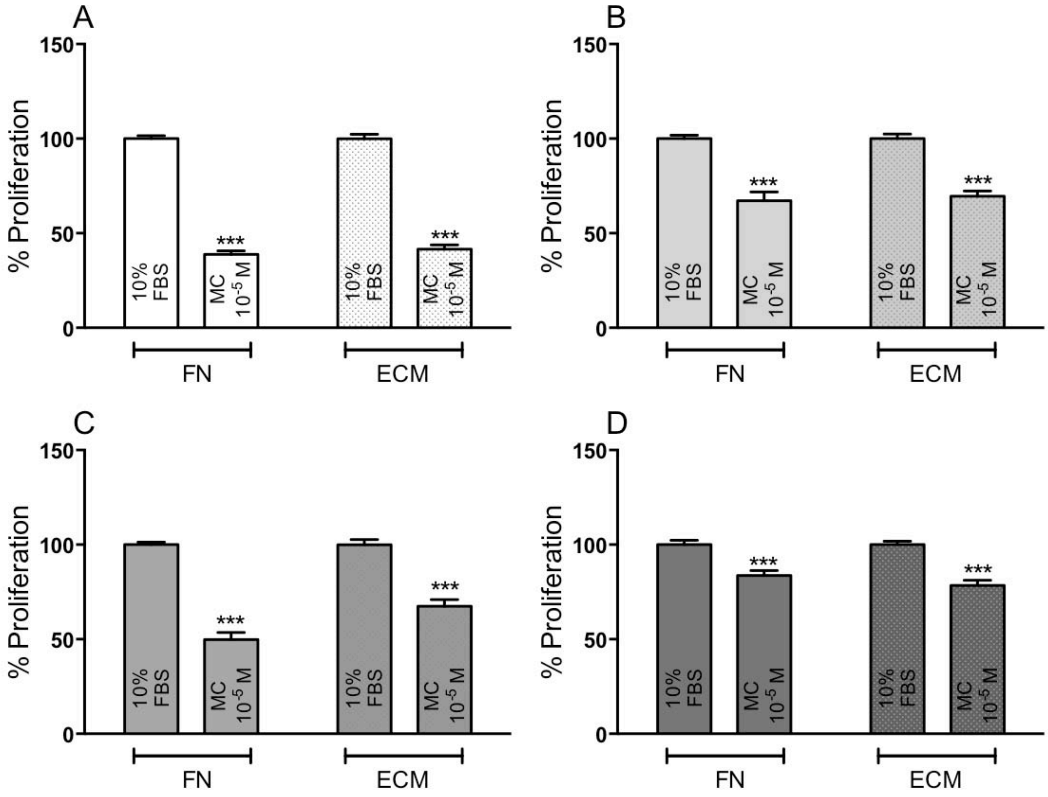

Figure 12: Mean±SEM %proliferation comparisons by two-way ANOVA between 10%FBS and $HgCl_2$ treatment on FN or ECM substratum as indicated on x-axis. **A**, MeT-5A, **B**, M14K, **C**, MSTO-211H and **D**, ZL34 cells. *** Represents $p<0.001$, n=40 from 5 combined experiments.

7.13. *AQP1 blockade with $HgCl_2$ reduces spheroid formation ability.*

Spheroid formation in the presence of $HgCl_2$ with FN or ECM was performed as stated in Materials and Methods. In MeT-5A with ECM the % spheroid perimeter with $HgCl_2$ was significantly lower (44.7±2.4%, $p<0.001$) compared to controls (100.0±2.7%) as shown in **Figure 13A.** In M14K with FN the % spheroid perimeter with $HgCl_2$ was 69.1±8.8%, $p<0.001$, significantly lower than the % spheroid perimeter of the control (100.0%±4.5). With ECM, the % spheroid perimeter with $HgCl_2$ was significantly lowered (35.3±2.1%, $p<0.001$) compared to controls (100.0±6.6%) as shown in **Figure**

13B. In MSTO-211H, with FN the % spheroid perimeter with $HgCl_2$ was 75.0±2.2%, $p<0.001$, significantly lower than the % spheroid perimeter of the control (100%±4.0). $HgCl_2$ significantly lowered the % spheroid perimeter in ECM (73.2±4.4%, $p<0.001$) compared to control % spheroid (100.0±6.3%) as shown in **Figure 13C.** In ZL34 with ECM the % spheroid perimeter with $HgCl_2$ was significantly lower (78.5±4.1%, $p<0.001$) compared to controls (100.0±4.5%) as shown in **Figure 13D,** while with FN spheroid formation was un-effected in the presence of $HgCl_2$.

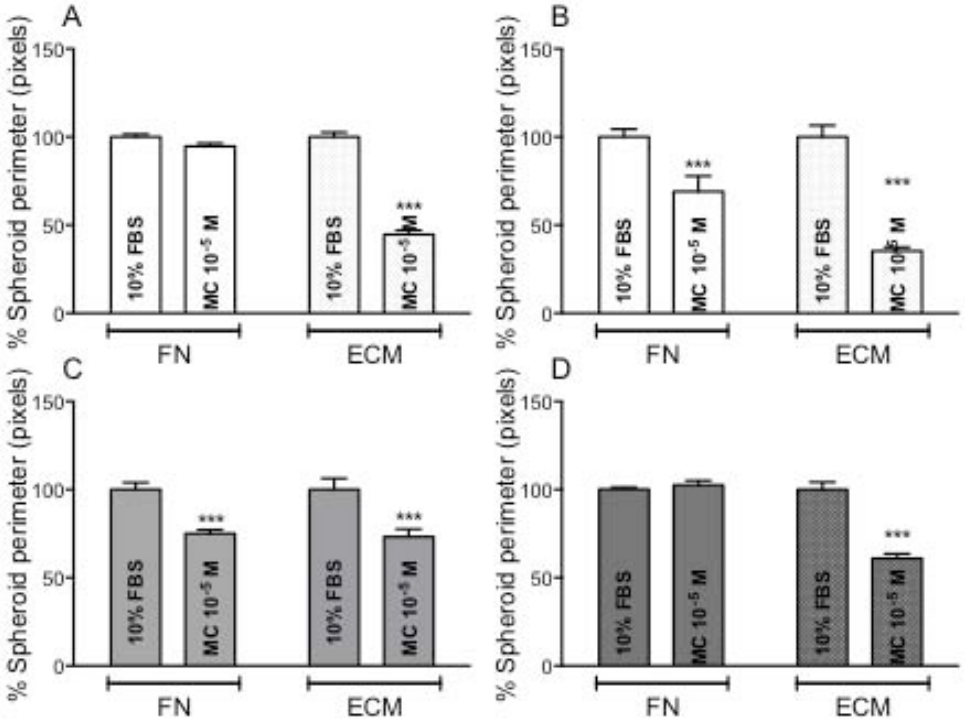

Figure 13: Mean±SEM %spheroid perimeter comparisons by two-way ANOVA between 10%FBS and $HgCl_2$ treatment on FN or ECM substratum as indicated on x-axis. **A**, MeT-5A (n=12), **B**, M14K (n=13), **C**, MSTO-211H (n=9) and **D**, ZL34 cells (n=10). * Represents $p<0.05$ and *** represents $p<0.001$.

7.14. *$HgCl_2$ lowered invasive characteristic of MPM spheroids in collagenous matrix.*

Spheroids occurring from the 48 hours of hanging drop culture were embedded in

neutralized collagen, some spheroids received $HgCl_2$. MeT-5A spheroid growth in collagen containing $HgCl_2$ was unaffected**.** In M14K, spheroids treated with $HgCl_2$ were 67.3±3.0% compared to controls spheroids 100.0±5.8%, $p<0.001$. In MSTO-211H, spheroids treated with $HgCl_2$ were 82.9±4.0% compared to controls spheroids 102.8±6.8%, $p<0.05$. In ZL34, spheroids treated with $HgCl_2$ were 73.1±4.0% compared to controls spheroids 100.0±5.3%, $p<0.001$, as shown below in **Figure 14**.

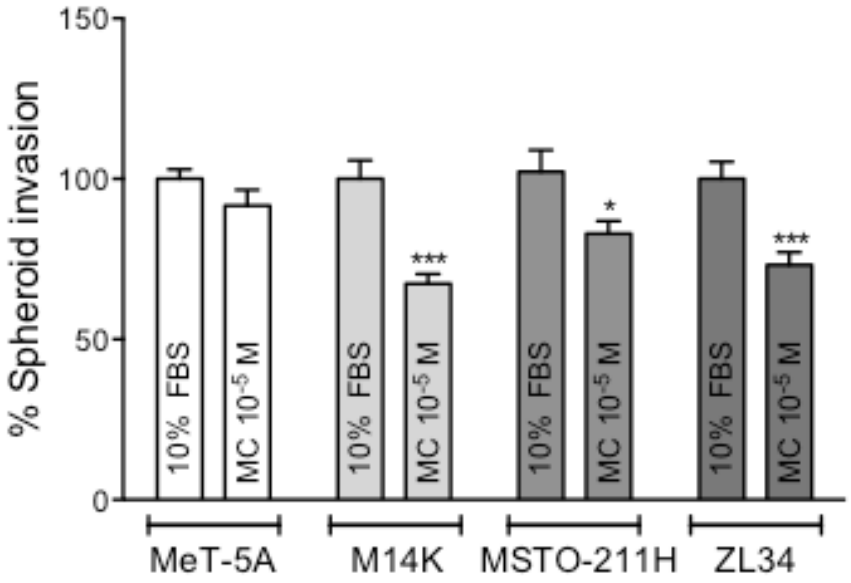

Figure 14: Mean±SEM % spheroid invasion comparisons by two-way ANOVA between 10%FBS and $HgCl_2$ treatment as inside the bars. * Represents $p<0.05$ and *** represents $p<0.001$, n=16.

7.15. *Gel contraction is reduced during AQP1 blockade with $HgCl_2$.*

Cells in suspension were subject to gel contraction assay as described in Materials and Methods. All cell types show significantly higher gel areas when $HgCl_2$ was included in the gels, as shown in **Figure 15.** In MeT-5A cells in $HgCl_2$ treated gels, the % gel areas were 126.8±2.5%, compared to controls 100.0±1.4%, $p<0.005$. In M14K cells in

$HgCl_2$ treated gels, the % gel areas were 163.7±9.0%, compared to controls 100.0±2.5%, p<0.001. In MSTO-211H cells in $HgCl_2$ treated gels, the % gel areas were 126.4±3.1%, compared to controls 100.0±2.0%, p<0.001 and in ZL34 cells in $HgCl_2$ treated gels, the % gel areas were 119.4±3.2%, compared to controls 100.0±1.3%, p<0.01.

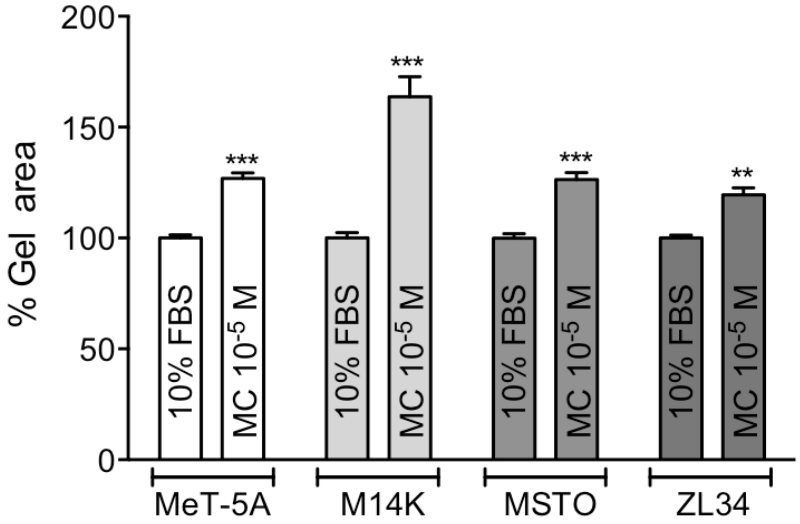

Figure 15: Mean±SEM % gel areas relative to 10% FBS gels, ** represents p<0.01 and *** represents p<0.001 and n=16.

7.16. *Cell adhesion during ENaC blockade with amiloride.*

Cells subjected to cell adhesion assay on FN or ECM substratum with the inclusion of amiloride in complete media, demonstrated variable adhesion. Benign mesothelial cells, MeT-5A had significantly lowered cell adhesion with amiloride (95.5±1.2%, p<0.05) on FN substratum compared to controls (100.0±1.1%) as shown in **Figure 16A,** while adhesion was unaffected on ECM substratum in the presence of amiloride compared to controls. M14K cells had significantly higher cell adhesion with amiloride (108.3±1.8%, p<0.01) on FN substratum compared to controls (100.0±1.9%) (**Figure**

16B), and MSTO-211H cells significantly higher cell adhesion with amiloride (106.0±1.3%, $p<0.05$) on FN substratum compared to controls (100.0±1.1%) (**Figure 16C**)**.** Cell adhesion was unaffected on ECM substratum in the presence of amiloride. In ZL34, cell adhesion was unaffected on FN substratum however, significantly higher cell adhesion with amiloride (111.4±3.8%, $p<0.01$) on ECM substratum compared to controls (100.0±1.1%) was observed as shown in **Figure 16D**.

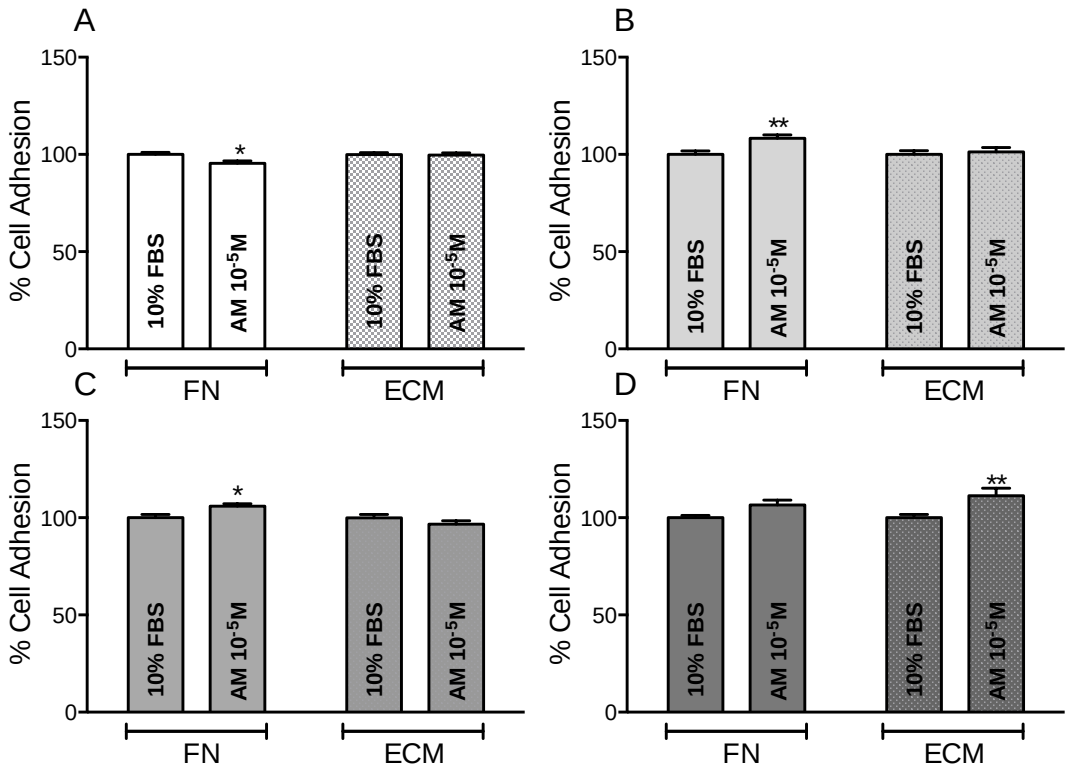

Figure 16: Comparison of mean±SEM % cell adhesion on FN or ECM substratum in the presence of amiloride. **A**, MeT-5A, **B**, M14K, **C**, MSTO-211H and **D**, ZL34 cell type n=32 and * represents $p<0.05$, ** represents $p<0.01$.

7.17. *Cell migration during ENaC blockade with amiloride.*

Cell migration assays were performed to evaluate the migration index under the influence of Amiloride. MeT-5A cells show significantly lower cell migration on FN

substratum in the presence of Amiloride (MI = 0.25±0.01, $p<0.01$) compared to MI in control media (MI = 0.32±0.02) as shown **Figure 17A,** while MI was not significantly affected on ECM substratum in the presence of Amloride. In M14K cells the MI was not significantly affected on FN or ECM substratum in the presence of Amiloride (**Figure 17B**). MSTO-211H cells did not show significantly lower cell migration on FN or ECM substratum in the presence of Amiloride as shown in **Figure 17C**, while MI was not significantly affected on ECM substratum in the presence of Amiloride, ZL34 cells show significantly lower cell migration on FN substratum in the presence of Amiloride (MI = 0.54±0.02, $p<0.01$) compared to MI in control media (MI = 0.66±0.03) as shown **Figure 17D,** while MI was not significantly affected on ECM substratum in the presence of Amiloride.

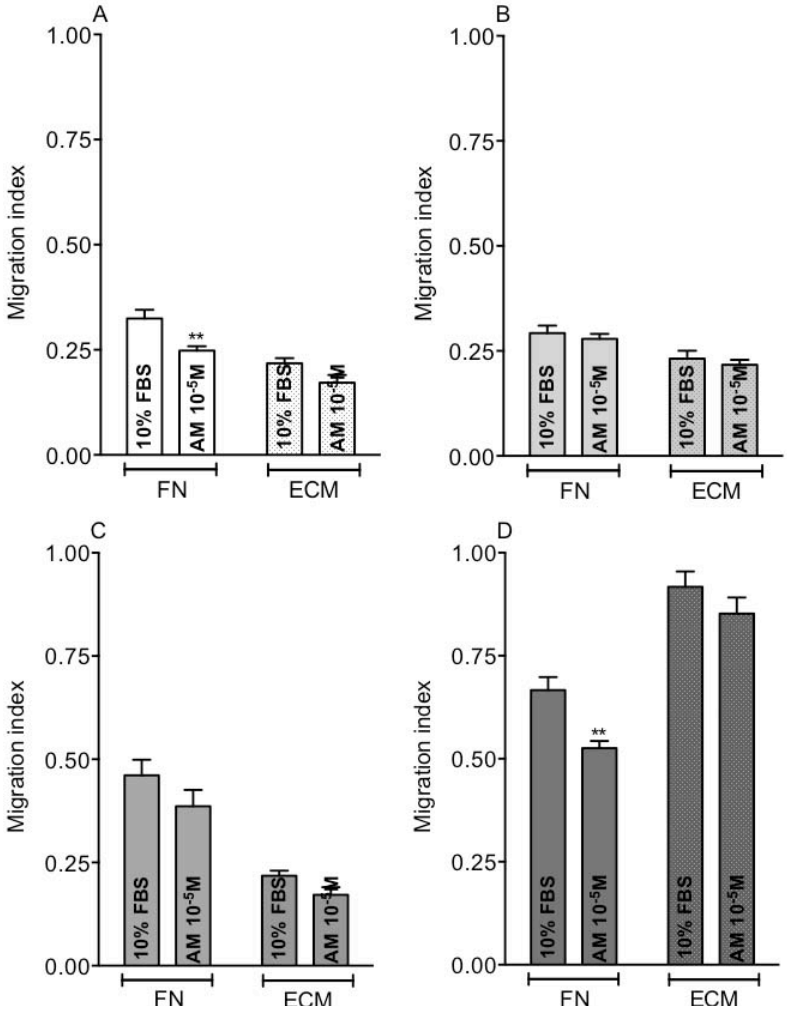

Figure 17: Mean±SEM MI comparisons between control and amiloride treated cells on FN or ECM substratum, **A**, MeT-5A, **B**, M14K, **C**, MSTO-211H and **D**, ZL34 cells. ** Represents p <0.01 and n= 12-16.

7.18. *TnT formation during ENaC blockade with amiloride.*

The formation of TnTs was evaluated during ENaCα inhibition with amiloride during culture on FN and EM substratum. MeT-5A (**Figure 18A**), M14K (**Figure 18B**) and MSTO-211H (**Figure 18C**) cells do not show any statistically significant differences in TnT formation on FN or ECM substratum, however in ZL34 cells, TnT formation is statistically lower during culture on ECM substratum in the presence of amiloride (36.44±1.5) compared to controls (43.1±2, $p<0.05$) as shown below in **Figure 18D.**

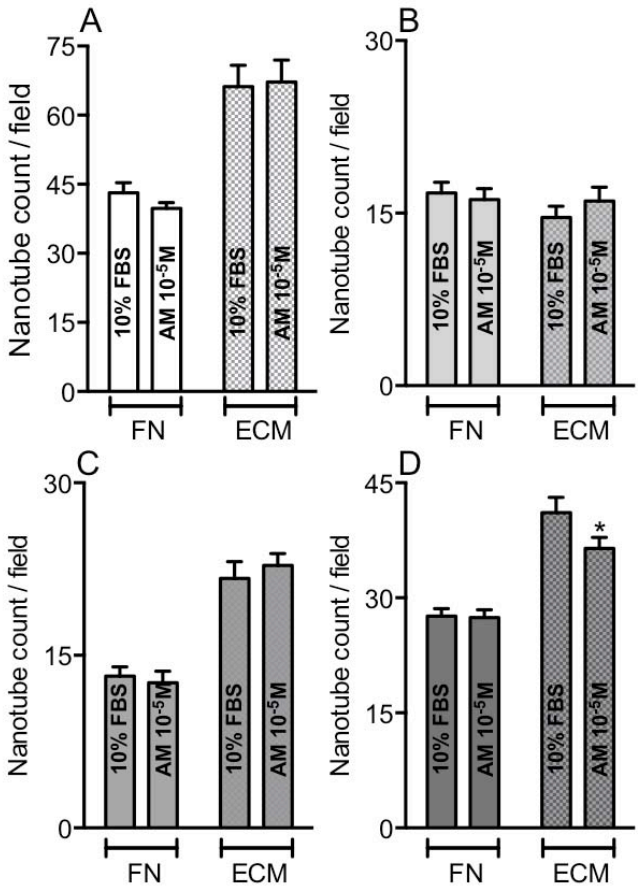

Figure 18: Mean±SEM nanotube count per field on FN or ECM substratum during ENaC inhibition with amiloride in **A**, MeT-5A, **B**, M14K, **C**, MSTO-211H and in **D**, ZL34 cells. * Represents $p<0.05$ and $n=16$.

7.19. *Cell proliferation during ENaC blockade with amiloride.*

Cell proliferation after 72 hours was assessed with the inclusion of amiloride in the media during culture on FN or ECM substratum. MeT-5A cells proliferate significantly lower on FN (78.0±4.1%, $p<0.001$) compared to control (100.0±2.4%), on ECM with amiloride (87.2±4.7%, $p<0.001$) compared to control (100.0±3.3%, $p<0.001$) as shown in **Figure 19A.** M14K cells proliferate significantly lower on ECM with amiloride (81.4±2.8%, $p<0.001$) compared to control (100.0±2.1%, $p<0.001$) as shown in **Figure**

19B. MSTO-211H cells proliferate without any effect of amiloride on FN or ECM substratum as shown in **Figure 19C.** ZL34 cells proliferate significantly lower on FN with amiloride (80.5±2.3%, $p<0.001$) compared to control (100.0±1.0%), on ECM with amiloride (80.3±2.7%, $p<0.001$) compared to control (100.0±2.8%, $p<0.001$) as shown in **Figure 19D.**

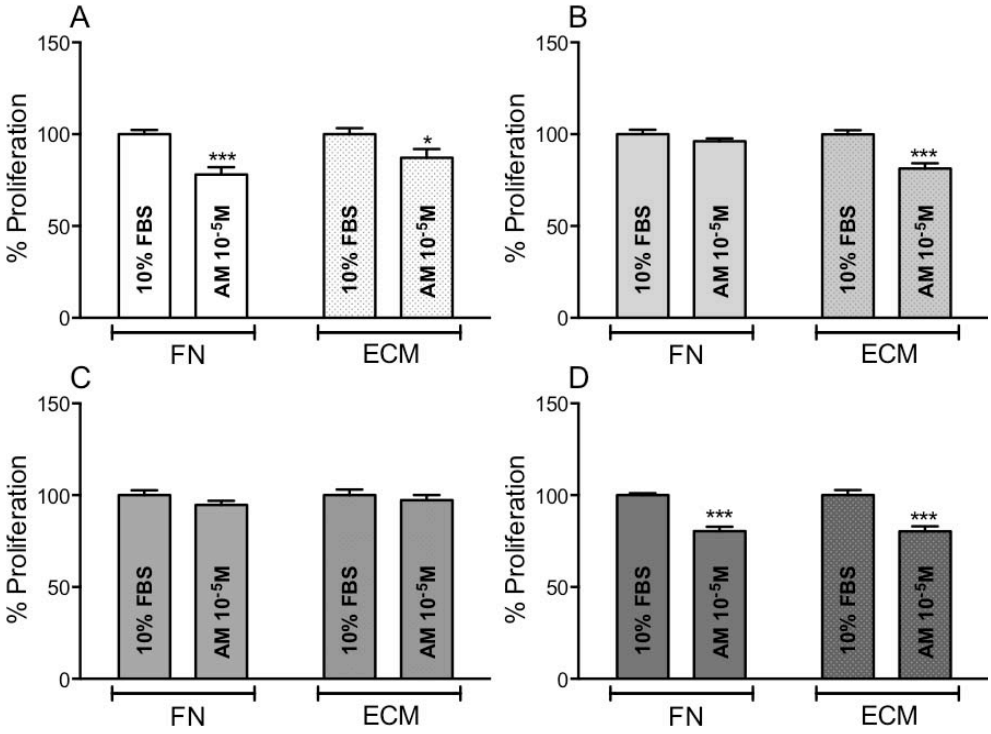

Figure 19: Mean±SEM % proliferation comparisons on FN and ECM substratum with Amiloride. **A**, MeT-5A, **B**, M14K, **C**, MSTO-211H and **D**, ZL34. * Represents $p<0.05$ and *** represents $p<0.001$, n=32. **7.20.**

7.20. Spheroid formation during ENaC blockade with amiloride.

Spheroid formation in the presence of Amiloride with FN or ECM was performed as stated in Materials and Methods. Amiloride does not limit spheroid formation ability with FN in the culture media in any cell type while with ECM in MeT-5A the % spheroid perimeter with amiloride was significantly lower (85.2±5.4%, $p<0.05$)

compared to controls (100.0±3.3%) as shown in **Figure 20A.**

In M14K with ECM the % spheroid perimeter with amiloride was significantly lower (86.4±4.3%, $p<0.05$) compared to controls (100.0±5.2%) as shown in **Figure 20B.** In MSTO-211H, amiloride did not lower the % spheroid perimeter in either FN or ECM as shown in **Figure 20C.** In ZL34 with ECM the % spheroid perimeter with amiloride was significantly lower (78.5±4.1%, $p<0.05$) compared to controls (100.0±4.5%) as shown in **Figure 20D.**

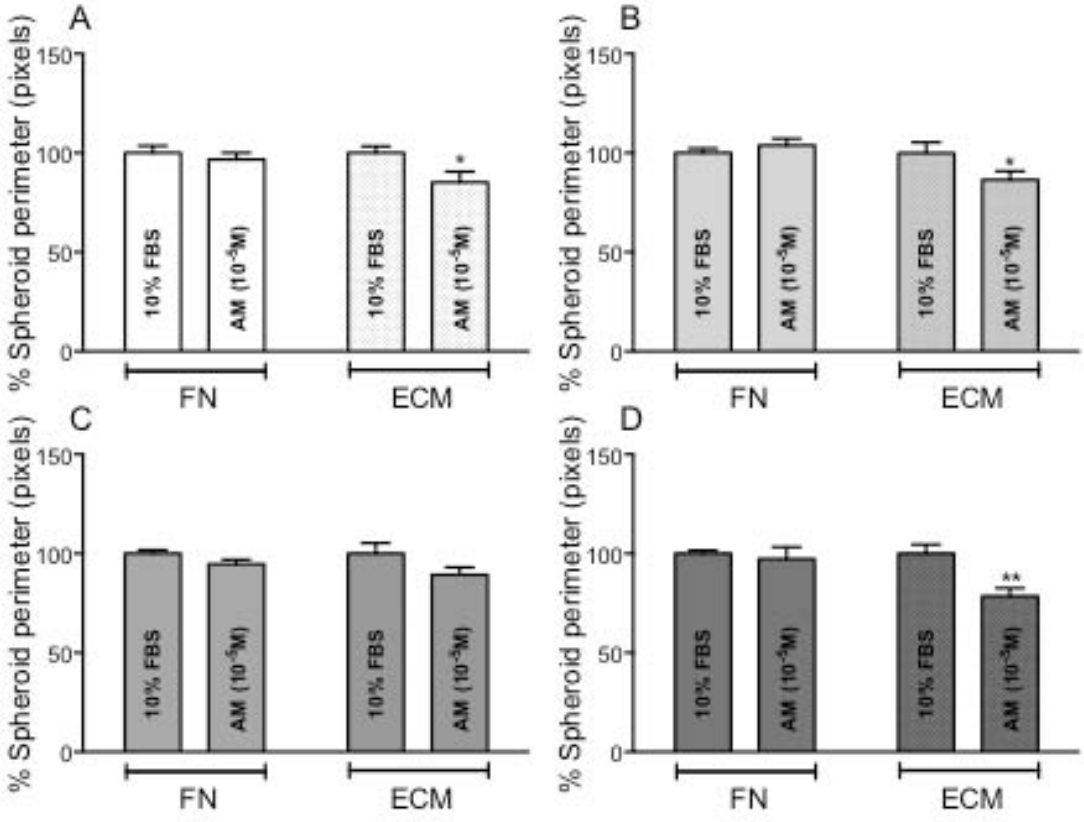

Figure 20: Mean±SEM % spheroid perimeter comparisons between control and amiloride treated cells. **A**, MeT-5A, **B**, M14K, **C**, MSTO-211H and **D**, ZL34. * indicates $p<0.05$ and **, $p<0.01$. n=12.

7.21. *Spheroid invasion during ENaC blockade with amiloride.*

Spheroid cultures were subject to collagen gel invasion assay as detailed in the Materials and Methods section. MSTO-211H spheroids showed a significantly lower spheroid perimeter in amioride treated collagen (69.9±8.0%, $p<0.01$) compared to untreated controls (100.0±5.4%) as shown in **Figure 21.** MeT-5A, M14K and ZL34 spheroids do not show any appreciable changes in spheroid perimeters when cultured with amiloride in collagen.

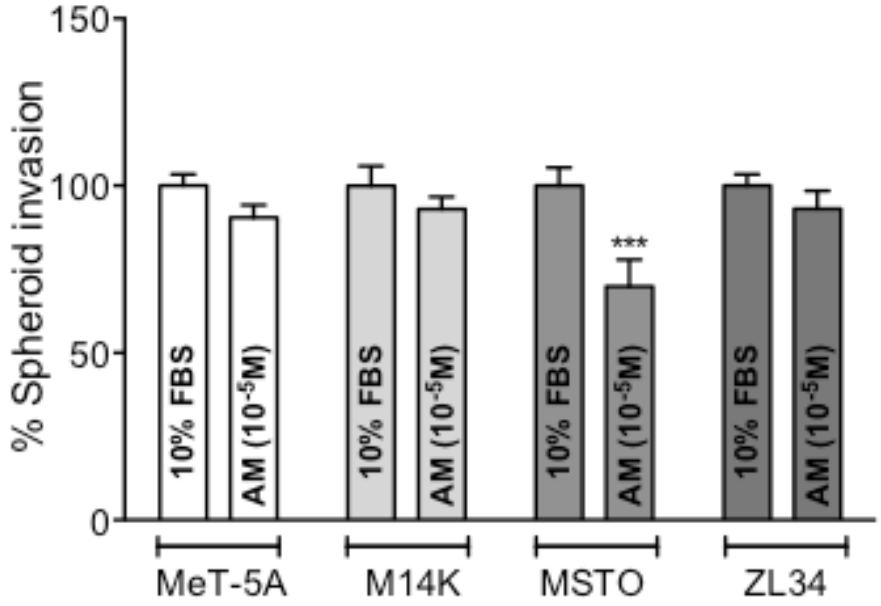

Figure 21: Mean±SEM % spheroid invasion comparisons between control and Amiloride treated collagen overlay cultures. *** represents $p<0.001$ and $n=15$.

7.22. *Gel contraction during ENaC blockade with amiloride.*

Cells were cultured for 24 hours in pH neutral collagen matrices and allowed to contract. In the presence of amiloride, gels with MeT5A cells had a % gel area of 111.3±1.7%, $p<0.01$, significantly higher compared to controls (100.0±1.4%), gels

with M14K cells and amiloride had a % gel area of 126.0±5.4%, p<0.001, significantly higher compared to controls (100.0±3.0%). Amiloride treated gels with MSTO-211H cells had a % gel area of 120.0±1.8%, p<0.001, significantly higher compared to controls (100.0±1.4%), and with ZL34 cells, amiloride treated collagen gels had a % gel area of 132.2±1.3%, p<0.001 compared to control gels (100±1.3) as shown in **Figure 22.**

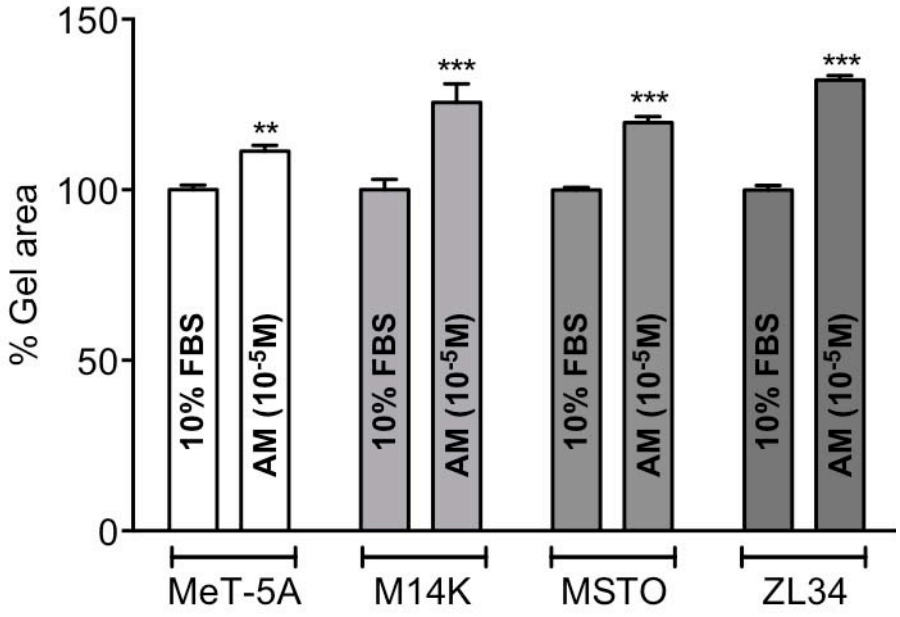

Figure 22: Mean±SEM % gel area comparisons between cells in control and Amiloride treated collagen cultures. ** represents p<0.01 and *** represents p<0.001, n=16.

8. Discussion

8.1. ECM derivation through cell and tissue dissolution.

The extracellular matrix is an important hetero-polymeric protein complex formed during cell culture *in-vitro*. In order to assess the presence of protein, a mild detergent lysis, followed by 2X washes with PBS were performed to remove the detergent that may interfere with subsequent experimental procedures. DNase-I was applied to eliminate any residual DNA after detergent lysis, which may cause inadvertent DNA transformation or might exert toxic effects due to its overall negative charge. In order to ascertain the presence of protein *in-situ* MicroBCA was performed. ECM protein deposition by cell culture was variable among the cell types. MeT-5A, M14K and MSTO-211H cell types did not differ significantly for their ability to produce retained ECM protein. In the model of "sarcomatous cells", STAV FCS (sarcomatoid type), radio-labelled methionine was used to demonstrate the production of cellular and secreted forms of fibronectin, collagen and laminin as assessed by fluorography and immuno-blotting with monoclonal antibodies against laminin, fibronectin and type IV collagen [88]. Previously, a study using bovine corneal endothelial cell derived ECM as an important component has been described. The technique of ECM isolation employs the use of sterile H_2O and a brief exposure to NH_4OH. Lysis of cells occurs due to hypo-osmotic shock and the ammonium hydroxide serves to stabilize protein and prevents the formation of protein aggregates [124]. A similar method to generate cell-derived matrices on polycarbonate substratum has also been reported in the context of invasive lymphoma tumor cell and ECM interaction in a mouse model but without the use of NH_4OH [125]. A modified cell derived ECM but incorporating exogenous soluble fibronectin has been reported. This method involved fibronectin as an additive,

to enhance ECM tensile strength, which provides mechano-sensitivity readouts [126]. ECM isolation from frozen and pulverized rat mammary tissues has also been described. The procedure involves a combination of enzymatic digestion (using trypsin) with the incorporation of mild detergent to prevent protein aggregates and alternatively using sonication along with trypsin [127].

The methodologies developed for ECM isolation from cell cultures, organs or tumor tissues rely on the removal of cellular component by osmotic lysis, or by detergent assisted dissolution, or at times trypsin. The primary purpose of ECM protein isolation is to obtain cell free proteinaceous material. The adoption of ECM as a culture reagent to investigate cell culture based phenotypes and in tissue engineering is gaining traction. This is a key feature mostly overlooked as model cell culture systems are convenient, and require less time and reagents. The implication of ECM based experiments is that there remains the context of native or near native environment of the extracellular space. The ECM framework not only allows cell-substratum interaction but also plays an important role during cell-cell contact during culture by providing a complex organized space. Interactions of the cells via membrane embedded receptors are critical for organ homeostasis. In physiological tissue renewal and wound healing, the ECM status provides critical information that in turn enables cells to perform necessary maintenance and repair. In context of disease progression such as during cancer metastasis, cell surface receptor engagement with ECM determines cell adhesion, invasion and ultimately forming distant neoplastic tissues during metastasis.

8.2. Mesothelial and mesothelioma cells adhesion.

In order to evaluate cell-ECM interaction, cell adhesion on FN and ECM was compared. We employed the use of crystal violet staining as a means to stain adhered cells, followed by de-staining to estimate cell adhesion. Cell adhesion on FN substratum was arbitrarily considered to be 100% and adhesion on ECM substratum was transformed accordingly. This allows comparison of adhesion between the substratum types. In experiments regarding inhibition with $HgCl_2$ or amiloride, cell adhesion of each cell types in media with no inhibitors was considered to be 100% and then adhesion in the presence of either inhibitors was accordingly transformed in-order to evaluate statistically significant changes in cell adhesion. The data indicates that benign mesothelial cells do not show a preferential cell adhesion on FN or homologous cell derived ECM comparatively. In the case of the mesothelioma cell types there was a consistent higher cell adhesion on homologous cell derived ECM substratum. This is an important finding as it indicates that oncogenic transformed cell lines develop a higher affinity to bind ECM proteins in comparison to purified FN protein. In the instance of cell adhesion comparisons between cell types, we have previously published that on FN, ZL34, sarcomatoid cell type adhesion was significantly higher than benign and epithelial cell types on both FN and ECM substratum compared to benign mesothelial cell adhesion used as controls. Epithelioid cell type had lowered cell adhesion compared to benign cell type on FN while this differential was lost when cell adhesion was compared on ECM substratum [128]. The finding that ZL34 cells showed highest cell adhesion in comparison to MeT-5A and M14K cells is suggestive of a strong cell adhesion characteristic, a necessity to invade and colonize efficiently. This behavior is perhaps one characteristic that lends sarcomatoid histotype of mesothelioma a very aggressive variant. ECM was long recognized to be a critical

component for the successful isolation and study of cancerous cell lines. Broad ranges of cell types were first reported to be well responsive to *in-vitro* conditions of propagation when ECM components such as fibronectin and fibrino-peptides were included in agar substratum [129]. This finding was a key to understanding the bases of cell adhesion and cell viability during primary culture of cancer explants for *in-vitro* propagation and characterization. In the context of sarcomatous type STAV FCS cell adhesion had been demonstrated to have a high affinity for fibronectin and collagen type IV coated plastics during cell adhesion as against cell adhesion on laminin coated plastic surface [88]. Asbestos induced mesothelioma cells from a rat model have been described for their adhesion characteristics on glass, and with fibronectin or laminin treatments. Two cell types, epithelioid and sarcomatoid were assessed. Irrespective of the substratum treatment, sarcomatoid cell types exhibited higher cell adhesion and cell spreading compared to epithelioid cell types, and that, cell adhesion and spreading on fibronectin was always significantly higher compared to laminin in both cell types [130]. This demonstrates that each cell type interaction with the ECM protein substratum has a differential and that each ECM protein by itself has a unique adhesive property. These two variables of cell type and ECM protein composition determine the success of cell adhesion at a single cell level. Mesothelial and mesothelioma cells are shown to express a wide variety of cell surface receptors that mediate cell adhesion to ECM substratum. In the M14K and ZL34 cell types it has been demonstrated that integrin β1, β4 are both expressed but β1 is highly expressed among mesothelioma sub types. Of the integrin α isoforms, α3 (most abundant), α5 and α6 (least abundant) and αV are detectable. The α, β isoforms are thought to be promiscuous but they impose preferential binding to ECM proteins. There is a preferential binding to Fibronectin and

Collagen type IV substratum compared to Laminin and further that β1 binding antibody completely (>90%) abrogated cell adhesion in these cells [131]. While the interaction of single cells in suspension with a supporting substratum are important in determining cell adhesion behavior, the *in-vivo* aspect of cell adhesion is far more complex involving the establishment of a stable adhesion between disseminated tumor cell and the ECM of the naïve regions of a target tissue where invasion processes begin. This phenomenon has been demonstrated elegantly *in-vitro* where in, benign mesothelial cell monolayers were used as a substratum for oncogenic ovarian tumor cells attachment. Scanning electron microscopy demonstrated invasive edges of the adherent cells on a monolayer, penetrating inter-cellular spaces of the underlying substratum [124]. Tenascin (TN), yet another ECM protein has been reported for its activity during cell adhesion processes *in-vitro* on defined substratum. The study demonstrated that mesothelial cell types (epithelioid, biphasic and sarcomatoid) have very limited interaction with TN μg/mL at 1 or 10 μg/mL substratum. However, there was a 5 -old higher cell adhesion on fibronectin (FN) (10 μg/mL) treated substratum [132]. The observation that there exists a preferential adhesion to ECM molecules is indicative of the cells to discern between individual ECM substratum components through cell surface receptors. In a study involving benign, biphasic and sarcomatoid cells, integrin αVβ3 was differentially expressed (with highest in sarcomatoid cell type, H28, least in epithelioid type, H2452). αVβ3 integrin interacts with and binds to Osteopontin (OPN). Cell adhesion was dose dependant in H28, while in H2452, cell adhesion was preferential on poly-L-Lysine as opposed to OPN treated substratum. This observation of integrin dependant sarcomatoid mesothelioma cell adhesion was further proved by the use of antibodies against αVβ3 integrin, which significantly abolished cell adhesion

[133]. The transmission of cell interaction with the external environment through intracellular signal cascade enables cell adhesion. In this regard integrin complexes convey cytoskeleton modulating signals to Integrin Linked Kinases (ILK) and Kindlin family of proteins that's enable the maturation of focal adhesions. Kindlin-2 over-expression has been demonstrated in mesothelioma cell lines compared to benign mesothelial cells. siRNA mediated silencing of Kindlin-2 led to decreased areas of cell spreading, cell adhesion, cell migration and cell motility in STAV AB epithelioid MPM cells [134]. The practical application of reversing cell adhesion bears remarkable outcomes. Cilengitide, a cyclic synthetic protein consisting of Arg-Gly-Asp (RGD) residues is a specific antagonist of Integrin αV. The incorporation of Cilengitide in cell culture (benign as well as epithelioid, biphasic and sarcomatoid) media reverses adhesion of cells in a monolayer culture and induces anoikis and reduces cell viability [135]. Taken together these findings are important clues in mesothelioma studies. Cell adhesion as an *in-vitro* model along with the incorporation of ECM components is an important tool to validate therapeutic strategies given their utility in detection of circulating tumor cells and assessing new therapeutic drug studies in pre-clinical settings. To this end, adhesion on cell derived homologous ECM is an important, first step. This methodology characterizes cell adhesion within the context of ECM that was previously synthesized by cell culture.

8.3. AQP1 role in cell adhesion of mesothelial and mesothelioma cells.

Cell adhesion is not only an interaction between the surface and the substratum but also well co-coordinated with the underlying cytosolic compartment, i.e., cytoskeletal re-organization, cytosol fluidic changes and osmotic tempering that enables a firm and

stable interaction of the cells to the substratum. These changes are necessary physiological adjustments that enable cells to adhere and spread to stabilize. The aspect of osmotic balancing and water expulsion are intuitive in that they confer cytosolic rigidity. In our experiments we blocked AQP1 with $HgCl_2$ during cell adhesion and we demonstrated that cell adhesion was sensitive to AQP1 blockade in MeT-5A on FN and M14K cells regardless of the nature of the substratum (FN or ECM). In MSTO and ZL34 cells the adhesion in the presence of AQP1 was not perturbed whether the substratum was FN or ECM. Aqb050, a synthetic inhibitor of AQP1 has been reported in the literature with modulating effects on cell proliferation and cell migration, its effects on cell adhesion has not been reported [136]. Conversely, the over-expression of AQP1 in 4T1 (breast cancer) and B16F10 (melanoma) did not lead to significant differences in cell adhesion on purified Fibronectin, Collagen or Laminin treated substratum [137]. Chondrocytes from AQP1-/- mice demonstrated lowered cell adhesion to type II collagen substratum as compared to AQP1 wild type mouse chondrocytes [138]. By the use of transient silencing of AQP1 expression in osteosarcoma cells, it has been demonstrated that cell adhesion to FN substratum was significantly reduced. In this study, high throughput assay of osteosarcoma RNA by gene set enrichment analysis generated a positive correlation between the expression of TGF-β1 signaling pathway, KEGG focal adhesion genes with AQP1 expression and further that similar patterns were demonstrated in-vitro with AQP1 silencing [139]. Thus the role of AQP1 during its forced expression or deletion is well reflected depending on the cell type and the substratum with which the cells interact.

8.4. ENaC role in cell adhesion of mesothelial and mesothelioma cells.

Cell adhesion in the context of mesothelial or mesothelioma cells with an emphasis on ENaC proteins has not been reported in the literature. Our data is the first instance of addressing the role of ENaC during cell adhesion in benign and mesothelioma cell adhesion assay. In MeT-5A cells, adhesion in the presence of amiloride (10 μM concentration) was significantly lowered during adhesion to FN treated substratum however adhesion was unaffected on ECM substratum. This affect was reversed (in mesothelioma cells) in that there was a significantly higher cell adhesion in M14K and MSTO-211H cells on FN substratum while cell adhesion on ECM was unaffected. In ZL34 cells, cell adhesion on ECM was higher during ENaC inhibition with amiloride while adhesion on FN was unaffected. In all other cases the differences insignificant. The role of ENaC channel in cell adhesion is not well described in the literature with only one report demonstrating the affect of amiloride on changes in ECM proteins that aid adhesion. Cell adhesion interactions between HepG2 (liver cancer) cells overlaid on HUVEC cell monolayer has been demonstrated in a prolonged cell adhesion assay lasting 24 hours. This method demonstrated the interaction of amiloride treated live cell substratum abrogated cell adhesion interaction with cells seeded atop. The study emphasized the role of E-Selectin, an adhesion protein molecule, playing a role on the substratum side of cell adhesion complex between the cells and substratum. This is in contrast to our data where in at 10 fold lower concentration (of amiloride), cell adhesion was significantly higher and in a time period of 90 minutes. The study demonstrated that amiloride at 100 μM dose, down-regulates the expression of E-Selectin proteins [140]. In the physiological context of cell-cell adhesion, the immune cells form multi-cellular complexes in processes related to soluble antigen clearance, and during the

developmental processes of B/T cell lineages. In order to evaluate Na^+/H^+ dependency during peripheral blood mononuclear cells (PBMC) aggregation, amiloride was assessed for cell-cell adhesion on cells from heparinized, healthy human PBMCs. 200 μM dose of amiloride did not show any significant effects in cell adhesion assay on ECM substratum where amiloride at higher concentrations was used for the inhibition of Na^+/H^+ exchanger and Urokinase Plasminogen Activator. The data on cell adhesion experiments with higher amiloride concentration during experimental conditions are interesting, however amiloride specific effects at lower doses that specifically inhibit ENaC activity are not reported. In the context of mesothelial cell adhesion, a dose dependant effect on adhesion was observed over a longer period of cell adhesion at 6, 12 and 24 hours with doses of 10 μM, 100 μM and 1 mM concentration. Negligible effects were observed with the smallest dose at 6 hours, but, prolonged exposure (24 hours) to amiloride significantly reduced cell adhesion [141]. Conditional or knockout studies of ENaC subunit genes are not reported in the literature. The interaction of ENaC channel proteins with cell surface proteins has also been reported in the context of lung injury of alveolar epithelial cell model. During influenza infection it has been demonstrated that patients diagnosed with H7N9 infection produce a significantly higher level of osteopontin (OPN) thus demonstrating the role of OPN as an inflammatory cytokine. When OPN was used as a cytokine stimulant in mouse epithelial cells, ENaC α subunit expression was significantly lowered as assessed by real-timePCR and further that inclusion of agonizing antibodies against integrin β3 and CD44 during OPN stimulus abrogated the affect of OPN on ENaC expression. There this is indirect evidence of ECM proteins regulating ENaC α subunit [142]. Therefore during cell adhesion of MeT-5A, M14K and MSTO-211H cells on ECM during ENaC

activity inhibition with amiloride can be reconciled such that, cell adhesion through ligation with CD44 to hyaluronan and integrins involving β3 subunit with proteins of the cell derived ECM might override any loss of cell adhesion due to amiloride.

8.5. Mesothelial and mesothelioma cell migration during wound healing.

Cell migration was assessed after inflicting a scratch wounding the monolayers. We have adopted migration index as a measure of cell migration. The migration index (MI) formulated as $MI = (A_0 – A_F) / A_0$ (where A_0 and A_F are area at the start and termination of the experiment respectively) evaluates the differential of wound closure with respect to the area of the initial wound scratch and thus allows a uniform measure based on the initial area. This is a technically adaptive approach that takes into account that there are inherent differences in the speed of migration between cell types and the time of wound closure that signals the end of migration. In the context migration on either FN or ECM substratum, the data indicated that MI was significantly higher on FN substratum when compared to that on ECM substratum, this is suggestive of a stimulatory effect from FN on the underlying surface and in the case of migration on ECM substratum, the cell surface adhesion and cell surface receptor engagement possibly predominate migratory behavior and thus lower the MI of each cell type. As mentioned previously in regards to cell adhesion experiments, the adhesion on ECM substratum being more compared to FN helps partially reconcile differences in MI due to a stronger cell adhesion on ECM while cells migrate [128]. Migration of SiHa cells (cervical cancer) on FN as a stimulating factor during cell migration has been demonstrated. There was an enhanced and active recruitment and phosphorylation of Integrin Linked kinase (ILK) through engagement with α5β1 integrin as demonstrated by co-immuno-precipitation of ILK

with anti-α5 antibody. Moreover, supplementing FN into the media during wound healing enhanced cell migration [143]. During the wound healing process, immuno-florescent double staining for actin (with phalloidin) and pan-cadherin (with anti pan-cadherin antibody) was demonstrated. Actin assembly along the wounded edges with characteristic lamellar protrusions, cadherin staining demonstrated a stable pattern remaining between the edges of neighboring cells [144]. Taken together the principle of cell migration during wound healing assay relies on continual modulation of cell-cell and cell-ECM interaction along with cytoskeletal changes that reinforce an advancing edge of the wound. In the context of wound healing on ECM substratum it is likely that the complex ECM substratum effectively engages cell surface receptors more avidly imposing retardation, and, possibly stabilizing cytoskeletal re-organization.

8.6. AQP1 activity during mesothelial and mesothelioma cell migration during wound healing.

Active cell migration during wound healing is a complex process with rapid rearrangements of cellular extensions and cytosolic dynamism in terms of density. During the blockade of AQP1 with $HgCl_2$, ZL34 cells migration showed a significantly lower MI on both FN and ECM substratum with $HgCl_2$ treatment. The role of AQP1 in cell migration in wound scratch model is thus limited to one out the 4 cell types tested since no differences were found regarding MeT-5A, M14K and MSTO cells. In the broader context of wound healing in 2 cancer cell models both overexpressing AQP1 have demonstrated significantly enhanced cell migration during wound healing in B16F10 melanoma cells and in 4T10 mammary gland tumor cells. The study further demonstrated that, at the leading edge of the wound there was a significantly increased

width of the lamella (protrusions), together this demonstrated the facilitation of cell migration involving AQP1 over-expression [137]. The role of AQP1 is an essential feature during cell migration in diverse tissue types for example, mouse aorta cells, in the epithelial, Chinese hamster ovary (CHO) cells and in Fisher rat thyroid cells. In these cell types, the genetic over-expression of AQP1 demonstrated significantly faster cell migration. In the CHO cells, AQP1 over-expression also demonstrated increased membrane ruffles at the edge of the wound suggestive of dynamic cytoskeletal and membrane changes that result in cell migration while attached on a substratum [104]. This points to a conserved mechanism of cell migration where in water transport underlies the migratory mechanism. Conversely, the silencing of AQP1 by small interfering RNA in lung adenocarcinoma cell lines LTEP-A2 and Lewis Lung Carcinoma cells significantly diminished cell migration in the wound scratch model. The lowering of cell migration was associated with a decrease in the production of MMP2, MMP9, which actively modify the homologous ECM during wound healing [145]. The non-toxic pharmacological blockade of AQP1 with Bumetanide derivatives (loop diuretic) has also been reported to have inhibitory effects on cell migration. Bumetanide derivative compounds AqB007 and AqB011 do not have any effect on osmotic water permeability but specifically block AQP1 in HT29 human colorectal adenocarcinoma cells [146]. AqB013, another derivative bumetanide has been shown to retard cell migration during wound healing in HT29 cells [147]. In the settings of mesothelioma cell models, AqB050 has been demonstrated to reduce epthelioid cell type H226 cell migration [136]. From these findings it is very apparent that AQP1 function is a significant part of cell migratory process. It’s function in modulating cell

migration is an important component that may determine invasion along the perimeter of mesothelioma tumor foci.

8.7. ENaC activity in mesothelial and mesothelioma cell migration during wound healing. During ENaC inhibition by amiloride it was found that in MeT-5A cells and ZL34 cells, the MI was significantly lowered on FN substratum. This points to cell type dependant sensitivity to amiloride during the process of wound healing. In the context of epithelial cells derived from bovine cornea it was demonstrated that upon the infliction of an initial wound there occurs a wave of electrical depolarization across the cell monolayer as assessed by an increase in the fluorescence of oxanol dye progressively inwards away from the wounded edge over a time period of 3 to 24 hours. This depolarization was dependant upon the presence of external Na^+ ions. This was demonstrated by replacing the Na^+ ions in the saline used during wound healing assay with equimolar choline. In the choline replacement conditions there was marked reduction in actin cable formation and fewer lamellar extensions. The monolayers were also demonstrated to have positive staining for ENaCα subunit expression and further that, treatment with phenamil, ENaC channel specific blocker significantly reduced the migratory speed to 3.2 μm/h compared to 8.7 μm/h in control monolayers. During the wound healing assay there were striking differences in the pattern of αENaC subunit. Immediately after wounding the florescent signal from ENaC staining was diffuse, however staining after a period of 2 hours the intensity of the stain dramatically increased at the edge of the wound [144]. The role of ENaC subunits in vascular smooth muscle cell migration has been demonstrated. Rat aortic vascular smooth muscle cells were subject to wound healing assays with benzamil (10μM dose), a derivative of

amiloride had an inhibitory effect on cell migration at 8 hours after initial wounding. These data are similiar to the lowered migration index of MeT-5A (8 hours) and ZL34 cell migration (4 hours) on FN substratum. Interestingly, transient silencing of ENaC subunits β, γ led to significant reduction in wound healing at 8 and 4 hours respectively. No reduction in wound healing was observed during the silencing of α ENaCsubunit [148]. The role of ENaC in BeWo cells (human placental carcinoma) has been reported previously. The study demonstrated that there is localized induction of ENaC subunits α,β,γ at the wounded edges of the cell monolayers as detectable by immuno-florescence microscopy. Aldosterone, a potent inducer of ENaCα subunit expression exerts faster wound closure effect and this effect was abolished when combined with amiloride. Importantly, amiloride alone did not lower the wound closure during reinvasion. When amiloride was replaced with anti-sense oligonucleotides against ENaCα during wound healing, the effect of aldosterone in increased wound healing was abolished [149]. The effect of amiloride pre-treatment prior to and during wound healing in epithelial tissues from cornea of bovine, rabbit, bovine aorta and canine kidney cells at 1 μM dose significantly reduced cell migration during wound healing assay at 6 hours, 12 hours and 16 hours respectively [150]. In the context of benign cells, the trophoblasts are developmental precursors of the placenta. The trophoblast cells function by invasion and migration during the implantation of embryo into the uterine endothelium and develop into the placental tissue. Trophoblasts have been demonstrated to be express ENaC channel and the α subunit expression was inhibited by estrogen (1 μM) and progesterone (5 μM). When trophoblasts transfected with siRNA antagonizing ENaCα subunit expression were subject to wound healing assay, there was significantly lowered number of cells migrating into the cleared area [151]. This data demonstrates

a variability of wound closure rates in various cell types but in all of them the characteristic amiloride blocking effect of reduced wound healing is a key feature.

8.8. Tunneling nanotube (TnT) formation in mesothelial and mesothelioma cells.

Tunneling nanotubes are membranous conduits between two cells that are apart with a few cell diameters of space between them. The TnTs are a specialized means of bidirectional, biomaterial exchange that may include cell organelles such as mitochondria, proteins, etc. A remarkable feature of TnTs is that they traverse through space over cell surfaces and the “connect” between two cells is not well understood. TnTs are considered to be inducible due to metabolic stress. TnT formation starts by budding protrusions and a progressive increase in the length of the TnT structure itself, therefore it is likely that cell surface receptor interaction with the substratum, cytoskeletal reorganization and accompanying changes in the fluidity of the cytoplasm are well orchestrated within the cells during the formation and maturation of TnTs. Regarding TnT formation under normal cell culture conditions, the TnT formation in mesothelial and mesothelioma cells, it was found that substratum likely plays a role in their formation. MSTO-211H and ZL34 cells form significantly more TnTs during 24 hour culture on ECM substratum as compared against culture on FN. This demonstrates a supportive feature of homologous cell derived ECM substratum in the formation of TnTs during cell culture. The mechanism of TnT biogenesis with various ECM substrata has been described in hematopoietic stem cells and leukemic KG1a cells. The study showed that cell migration over distances of 60-80 microns immediately after seeding cells on monolayer of feeder cells or fibronectin treated surfaces enabled TnTs but not on substratum coated with collagen-I or poly-L-lysine. Further the formation of

TnTs in KG1a cells was mediated by Rho associated coiled-coil containing protein kinase (ROCK) that was inhibited by pharmacologic blockade. Phalloidin staining of actin was prominent and was maintained when cells were treated with Nocodazole, a potent microtubule inhibitor. Taken together, this study demonstrated that cell migration prior to adhesion and actin cytoskeleton are two important factors that promote TnT formation in the context of leukemic cells [152]. In the context of B cell function, TnT formation was enabled only in mature B cell when compared to immature B cells in both human and mouse, dependant on temperature of cell culture i.e., lowered TnT formation at 24°C and 30°C as opposed to 37°C and significantly higher in number on fibronectin and laminin treated surfaces. The differentiating factor between immature and mature B cells responsible for TnT formation was the expression of α5 and β1 integrin subunits found only in mature B cells. Blockade of individual integrin alone was insufficient to alter TnT formation but simultaneous antagonistic blocking of both integrins lowered TnT formation and lowered cell spreading during cell adhesion. TnT formation was stimulated upon antigenic stimulus with bacterial lipo-polysaccharide [153]. Thus TnT formation is dependant on cues such as the extracellular matrix or presence of diffusible stimulus.

8.9. AQP1 role during TnT formation in mesothelial and mesothelioma cells.

In order to assess the role of AQP1 during TnT formation $HgCl_2$ was included in the media. The data indicated that MeT-5A cells alone show a diminished ability to form TnTs on both FN and ECM substratum. The mesothelioma cell types in contrast, developed TnTs during $HgCl_2$ exposure on both FN and ECM substratum without any significant differences. This demonstrates AQP1 activity is essential in the formation

of TnTs in the context of benign cells while in that of the MPM cell types AQP1 function does not seem to influence TnT formation. A possible explanation is that benign cells tend to be more sensitive to AQP1 activity such that TnT formation is affected. In regards to AQP1 function during TnT formation there are no published data.

8.10. ENaC activity requirements during TnT formation in mesothelial and mesothelioma cells.

During ENaC inhibition with amiloride, it was found that TnT formation was sensitive only in the context of ZL34 cells type during culture on ECM substratum. All other cell types showed no appreciable changes in their ability to form TnTs. This is suggestive of Na^+ ion transport through ENaC channel as a dependency for TnT formation in ZL34 cells alone. Studies in TnT development are sparse and most data on TnT formative mechanisms are based in cytoskeletal dynamics, cell-ECM interaction or cell electrophysiology but lacking in the context of Na+ ions and Na^+ channel family members.

8.11. Cell proliferation is modulated based on the composition of substratum.

Cell proliferation over 72 hours was performed in order to assess if the substratum played a role during culture on FN or ECM substratum. FN is known to be a proliferation-stimulating agent, among other ECM molecules. Cell surface receptor engagement with extracellular environment provides important stimuli that regulate mitogenic signaling; hence the effect of homologous ECM during cell proliferation is an important factor that influences tumor growth in the context of mesothelioma tumor

burden. Cell proliferation was assessed by crystal violet staining after culture of 72 hours on FN or ECM substratum. In order to assess the differential effects of the substratum, the O.D. of de-stained crystal violet from cells cultured on FN was arbitrarily set to 100%. In all cell types the data consistently demonstrated that cell proliferation was lowered on ECM substratum compared to that of FN. Our method relies on assessing cell proliferation by staining cells accumulated at the end of the assay thus providing a direct measure of cell populations. The ability of FN as an inducer of mitogenic signaling resulting in cell proliferation was demonstrated through leukemic cell line K562. These cells were shown to express fibronectin receptor (FNR) which consists of a heterodimer of integrin α5β1. The FNR specifically recognizes Arginine-Glycine-Aspartate (RGD) motif in the FN peptide. A variant of K562 cell line termed FA-K562, which over expresses FNR has been demonstrated to show higher colony formation in response to RGD containing GRGDS peptide. Further, FA-K562 cells showed a significant shift in cell cycle from G1 to S phase in response to GRGDS inclusion in the culture media as assessed by propidium iodide staining by flow cytometry. Stimulation of FA-K562 cells with GRGDS peptide demonstrated a 11-fold incorporation of ^{3}H Thymidine (into DNA) in as little as 5 hours. In agreement with the observations of increased colony formation, DNA synthesis and shift from G to S phase populations in response to GRGDS treatments, it was further demonstrated that immuno-precipitated Cyclin dependant kinase (CDK2) was sufficiently high in phosphorylating immobilized Histone H1 after western blotting. Retinoblastoma protein phosphorylation was also higher in GRGDS treated FA-K562 lysates. Taken together this demonstrates that there are multiple, co-coordinated events that arise due to the ligation of FN receptors on the cell surface that eventually stimulate cell

proliferation [154]. The proliferation of glioblastoma cancer cells A172 and T98G was assessed on culture surface coated with individual, purified ECM proteins Laminin (LN), Fibronectin (FN), collagen type I, IV and V. It was demonstrated by cell counting assay (using coulter counter) that cells enter a logarithmic proliferation on LN and FN treated surfaces by day 3, which was significantly higher than those cultured on collagen types I, IV and V in both cell types. And, further that in as little as 2 hours in A172 cells, BrdU incorporation was significantly higher in cells plated on LN and FN substratum compared to collagen type I, type V. The authors demonstrated lowered cell proliferation effect on collagen substratum due to intense staining of F actin with phalloidin stain on cell cultures on collagen substrata which possibly hindered cytoskeletal re-organization required during cell cycle progression and cytokinesis [155]. While these *in-vitro* data are valuable in assessing the individual roles of various ECM molecules for their affects on cell proliferation, the tumor microenvironment exerts significant influences on cell proliferation that determines tumor growth. In the context of mesothelioma tumor microenvironment it has been shown that conditioned media from fibroblasts consists of nanogram and microgram quantities of FN and Hepatocyte Growth Factor respectively which influence pro-migratory and invasive behavior that expands the tumor niche [156].

The ECM in its complexity however has indirect effects on cell proliferation *in-vivo* as compared to individual ECM proteins in their purified state. Our data indicated that in comparison to FN, cell proliferation on ECM was lowered. This might be perhaps due to lower amounts of FN produced and incorporated during extracellular matrix deposition. Specific data on integrins and their associated down stream mitogenic signaling pathways are lacking in the literature. In a study it was

demonstrated that hyaluronan-and-proteoglycan linked protein 1 (HAPLN1) which binds to hyaluronic acid (HA) was over-expressed in a cohort of matched normal and mesothelioma samples as assessed by qPCR and further that high HAPLN1 expression of >75% was observed in mesothelioma versus lung cancer microarray experiment. Forced over-expression with HAPLN1 vector in low HPLN1 cells namely H2595 (epithelioid) and HP1 (biphasic) significantly enhanced cell proliferation by 1.7 and 4-fold increase as compared to empty vector. While there is no specific role of HAPLN1 that stimulates cell division, it was demonstrated that functional domains containing signal peptide and IgV within HAPLN1 gene were essential to cell proliferation. It was speculated that the interaction of HAPLN1 with HA *in-vivo* enables proliferation from cytokine stimulus from tumor invading immune cells [157]. Cell proliferation and tumor growth are intricately linked. The aspect of cell-cell adhesion and cell-ECM adhesion determines tumor integrity. These interactions are mediated through integrin proteins and thus enable focal adhesion complexes that influence down stream signaling that enables eventual cell proliferation. Merlin, the product of NF2 gene determines cell-cell adhesion. There is a bi-allelic loss of NF2 is observed in >50% of human MPM tumors. NF2 gene disruption sensitizes cells to FAK inhibition at very low doses and hence NF2 status has been implicated in adopting targeted FAK inhibition with VS-418 therapeutic compound highly specific for FAK inhibition. The blockade of N-cadherin (with antibodies) in NF2 positive cells and subsequent inhibition of FAK with VS-418 demonstrated a 60-fold sensitivity to cell proliferation in 3D cultures. To address the role of cell-ECM interaction during NF2 genetic lesions, antibodies against β1 increased the sensitivity to VS-418 compound. This effectively demonstrated the crux of cell proliferation that integrates cues from ECM during cell

proliferation. This study demonstrated that in mesothelioma cells with intact NF2 expression, cell-cell adhesion negates sensitivity to therapeutic FAK inhibition while cell-ECM interaction negates anti-proliferative effects of FAK inhibition [158].

8.12. AQP1 inhibition attenuates cell proliferation.

When $HgCl_2$ was included in the media during cell proliferation, data indicated a significantly lower cell proliferation in all cell types on FN and ECM substratum. AQP1 blockade is an important factor as water availability determines several cellular activities such as in enzymatic reactions, stages in mitosis where cell shape is condensed with the dissolution of membranous organelles such as Golgi, endoplasmic reticulum for example and the essential maneuver of partitioning condensed genome into two halves followed by cytokinesis. A dynamic balance of cytoplasmic contents and the cytoplasm composition of ions, solutes and water are critical to a complete progression through the cell cycle. Hence, AQP1 activity during mesothelial and mesothelioma cell proliferation is understandably critical. In context of AQP1 in mesothelioma cells it has been demonstrated that increased proliferative activity as measured by chromogenic MTS assay was positively correlated with the expression of AQP1. This was demonstrated in a cohort of 14 samples, and, all the malignant cells were isolated from pleural effusion samples. When pharmacologic blockade of AQP1 with Abq050 was performed there was a dose dependant (20μM, 40μM and 80μM) lowering of cell proliferation in H226 cells (epithelioid type) and further that the blockade of AQP1 only in high AQP1 expression cells from pleural effusions were responsive to proliferation blockade but not the low AQP1 expressing cells except at higher concentrations of 80 μM. The silencing of AQP1 expression with siRNA in

H226 and primary cell culture isolates also significantly reduced cell proliferation. In growth independent cultures of colony formation, the significant lowering of colonies in terms of dose dependence was observed and the size of the colonies was also significantly reduced. However, the *in-vivo* tumors of H226 cells in subcutaneous xenograft model did not show any appreciable reduction in tumor size [136]. This demonstrated that Aqb050 mediated AQP1 inhibition was limited to *in vitro* proliferation assay in cell culture. A detailed study regarding the role of AQP1 in cell proliferation and apoptosis has been reported in blood vascular system. Carotid body (CB) is an organ that senses pO_2 in the blood stream [159], CB location is biologically strategic in that it is found at the bifurcation of carotid artery into arches. CB is shown to have a robust AQP1 expression [160]. The link between hypoxia and cell proliferation of CB has also been modeled. In the AQP1 deletion mutants in mice, CB was demonstrated to have same number of TH^+ cells specific to CB tissue irrespective of the AQP1 status. When AQP1 knockout mice and wild type mice were exposed to hypoxia for 12 days or 21 days (10% O_2), and orally administered with water containing BrdU and tail injections of BrdU, there was significantly lower double positive TH^+ and $BrdU^+$ cell count (in AQP1 -/- mice compared to wild type mice) as assessed by immuno florescence (on histological slide preparations) at both time points. This was indicative of lowered cell proliferation in AQP1 -/- CB cells during hypoxia. PC12 cells belong to the same lineage as CB cells and in this cell type the over-expression of AQP1 demonstrated a 10% higher (significant) BrdU stained cells in the PC12-AQP1 cells as compared to PC12 wild type cells assessed by flow cytometry. In response to mitogenic stimuli there was significantly higher cell count estimated by hemocytometer counting as early as 2 hours after mitogenic stimulus with serum complemented media

containing BrdU. A significantly higher rate of cell proliferation in PC12-AQP1 cells was demonstrated in comparison to wild type PC12 cells after 3 days of culture. By DNA staining and flow cytometry analyses, it was demonstrated that in PC12-AQP1 cells, there was a significantly higher proportion of cells in G2/M and further that the S phase was shorter as compared to PC12 wild type cells. By western blot analysis it was also demonstrated that the expression of S phase specific cyclin D1 and cyclin E1 proteins was significantly higher in PC12-AQP1 cells compared to wild type cells. Nocodazole is a drug used in cell cycle synchronizing. Nocodazole inhibits cell proliferation by limiting viable cells from entering mitotsis phase due to inhibition of microtubule spindle fibers that partition the genome into two. The accumulation of dead cells is observed as an additional subG1 phase consisting of G1/G0 stage cells committed to apoptotic cell death. PC12-AQP1 cells when exposed to Nocodazole demonstrated a small subG1 peak, and G1 peak was significantly higher compared to G2/M transitioning cells. In the wild type cells however there was a marked increase in subG1 cells and higher number of cells in G2/M phase compared to G1/G0 phase, a reverse in the trend as compared to that of AQP1 over expressing cells. This demonstrated the ability of AQP1 in rescuing apoptotic cells away into G1/GO phase. By flow cytometric analysis it was also demonstrated that in response to Nocodazole treatment the AQP1 over expressing cells were significantly less stained for Annexin V as compared to that of the wild type PC12 cells. Moreover western blot analysis demonstrated a lower activated PARP, a marker of apoptosis in AQP1 over expressing cells. PC12-AQP1 cells and wild type PC12 cells were also assessed for cell size, cell volume and cellular complexity. By assessing forward scatter characteristics by flow cytometry AQP1 over expression cells were demonstrated to significantly larger than

wild type cells, there was a significantly higher complexity as determined by side scatter. Taken together these data point that through AQP1 over expression, faster cycling through cell cycle, a significant increase of S phase specific cell cycle markers, apoptotic resistance, better cell volume regulation along with cytoplasmic complexity are some notable features. A microarray analyses comparing AQP1 over expressing and wild type cells were also performed. Ingenuity Pathway analyses revealed significant differences of genes responsible for cell growth and proliferation, and further that this was highest ranked molecular and cellular function category [161]. This finding of AQP1 over expression related higher cell proliferation is a characteristic of many cancers where AQP1 over expression leads to higher cell proliferation. In the dual context of AQP1 over expression and neo-angiogenesis model, it has been demonstrated that mesothelioma cells demonstrate Vascular Mimicry (VM) where upon culturing in matrigel, the mesothelioma cells demonstrate a networked pattern of cell organization with branches and loops. Mesothelioma cells also demonstrate the ability to produce Vasculo Endothelial Growth Factor A (VEGFA). The modulation of AQP1 blockade Aqb050 and VEGF inhibition with bevacizumab (an inhibiting antibody of VEGFA ligation to its receptor VEGFR) was tested in mesothelioma cells. Under hypoxia conditions AQP1 silencing or treatment with Aqb050 led to a significant decrease in branching and loop formation of mesothelioma cells (NCI-H28 and NCI-H226) and mesothelioma primary cells *in vitro*. Under normoxic conditions, the inhibition with bevacizumab had no effect on VM in high VEGFA producing NCI-H28 cells, while AQP1 inhibition in low VEGFA producing NCI-H226 cells had no effect either [162]. This finding is suggestive of AQP1 sensitivity to O_2 and its effect on cell physiology during VM but not VM inhibition with bevacizumab.

8.13. ENaC inhibition attenuates MeT-5A and ZL34 cell proliferation.

While water transport through AQP1 channel bears great importance to the process of cell proliferation, ENaC activity abolishment with amiloride has comparatively limited effect. The data indicated that MeT-5A and ZL34 cell proliferation was significantly lower on both FN and ECM substratum. While in M14K, cell proliferation during ENaC inhibition was lowered on ECM substratum alone. In MSTO-211H cells, amiloride did not affect cell proliferation on FN or ECM substratum. These data are the first instance of ENaC inhibition effect on cell proliferation in the context of mesothelioma cells. Genetic silencing of ENaC subunits has been performed in HepG2 cell model (liver cancer) with siRNA strategy. In this study the silencing of ENaCα demonstrated a significant lowering of cell proliferation after 24 hours as measured by MTT assay and automated cell counting. The cells treated with ENaCα siRNA demonstrated an accumulation of cells in the G2/M phase of the cell cycle. This indicates that ENaC expression is a pre-requisite for uninterrupted cell cycle progression. The ENaCα siRNA transfected cells were demonstrated to have activated caspase 3/7 dependent apoptosis but not due to LDH release, an indicator of necrotic cell death [163]. The role of lineage specific transcription factors that control the expression of ENaC family of proteins has been reported in a large cohort of non-small cell lung cancer, and small cell lung cancers. Achaete-Scute homolog 1(ASCL1) is a basic helix-loop-helix transcription factor that controls the development of lineage specific pulmonary nueroendocrine bodies. Through co-expression analyses it was demonstrated that ASCL-1 expression is strongly correlated with ENaCα expression as demonstrated by chromatin immuno-precipitation with ASCL1 bound at genomic ENaCα intronic regions and by the dual expression ASCL1 and ENaCα on a “both or

none" basis. The knockdown of ASCL1 resulted in loss of ENaCα expression. In this study the pharmacologic blockade of ENaCα with amiloride at 50 μM dose demonstrated activation of PARP, a substrate of activated caspases (and hence apoptosis) during viability assay and further that inclusion of amiloride during colony formation on agar in the presence of amiloride had significantly lowered colony number in ASCL1 positive cells. While the amiloride concentration used was higher than the one used in our study, the entire cohort of lung cancer cell lines showed limited to no expression of uPA, also a target of amiloride. Hence this clearly demonstrated a role of ENaCα in lung cancer cell proliferation during viability and in colony formation [117]. In the context of adult neural stem cells, ENaC activity has been demonstrated in the sub-ependymal zone (SEZ) via ionic changes in the cerebrospinal fluid. ENaCα expression was demonstrated in transgenic harboring GFP reporter driven by Glial Fibrillary Acidic Protein (GFAP, a marker specific to astrocytes) and GFP-Sox2, a marker of stem cell specific transcription factor in the SEZ that forms an epithelial lining of the ventricular system in mammalian brain. This zone harbors adult neural stem cells that support neurogenesis. Primary SEZ cultures when subject to transient silencing of ENaCα gene resulted in significantly lower number of neurospheres and alternatively when subject to pharmacologic blockade of ENaCα with amiloride demonstrated increased apoptosis demonstrated by TUNEL assay (labeling of fragmented DNA ends arising from apoptosis). Further the conditional silencing of ENaCα in a tissue specific manner (i*n-vivo* mouse model) using Cre/Lox with tamoxifen inducible excision of ENaCα, it was demonstrated that in as little as 5 days there was a marked loss of ENaCα expression in SEZ tissue histologically along with a significant loss of Sox2 and Ki67 expression along with an evident loss of thickness

of the SEZ [164]. Taken together, the role of ENaC channel in cell proliferation is demonstrative of imposing a significant influcence on cell proliferation in a wide variety of tissues.

8.14. Spheroid formation from mesothelial and mesothelioma cells.

Spheroid formation is a complex process that is a combination of cell-cell adhesion (due to absence of a physical support) and proliferation. The phenotype of the sphere has a 3 dimensional nature, while most cell culture based assays *in-vitro* are simpler in 2D. During sphere formation with FN and ECM inclusion over 48 hours, the MSTO-211H spheroids demonstrated significantly larger perimeteres when homologous cell derived ECM was included in the media and that the effect was restricted to biphasic mesothelioma cell types only. The aspect of cell adhesion to FN and ECM substratum treated plastic in 2D is identical to sphere formation that suggestively explains the increased cell-cell adhesion during sphere formation. There marked contrast to cell proliferation in 2D with FN or ECM substratum where all cell types demonstrated significantly higher rates of cell proliferation on FN substratum. We have not assayed for cell proliferation in the 3D model but the significantly higher perimeters in biphasic cells is likely to be due to cell proliferation. Biopsy explants of glioblastoma cells have been assessed for their ECM protein components and integrin protein expression in biopsy samples, cell monolayers derived from the same biopsy tissue as well as spheroid culturing on agarose substratum. In this context, immunohistochemical staining for the ECM proteins collagen type I, III, IV, V, VI and Laminin (Lam) was restricted to the vasculature surrounding the tumor core and further that integrin β1 expression was detected in all tumors. When the same biopsy samples were plated in

cultures, the basement membrane proteins collagen type IV and Laminin did not increase in expression however collagen types I, III, V, VI steadily increased through 5 passages and the expression of integrin β1 expression was maintained. A striking feature of spheroids cultured on agarose substratum was that, there was a central core where ECM expression was highest and the proliferative marker Ki-67 was preferentially restricted to the periphery. The integrin expression of β1 was maintained and β4 steadily increased which was in stark contrast to its absence in monolayer cultures. This demonstrated a spheroid forming ability when tumor biopsies were fractionated into smaller fragments and that there are differences in ECM protein and integrins depending on the status of the sample i.e. tissue or monolayer or spheroid [165]. Generation of spheroid cultures has been reported in glioma and thyroid cancer cells. The method reported that cells form spheroidal structures when cultured on agarose substratum containing growth media. Electron microscopy was performed and it was estimated that there was 20-40% of extracellular space between cells in glioma spheroids and a uniform 50% space total extracellular space in thyroid cancer cells. When the spheroids were subject to detergent lysis agent deoxycholate (DOC), thin fibrillar, framework of ECM remnant was apparent and when treated with guanidine. HCl a diffuse structure was obtained. With the use of ^{3}[H] Hyaluronic acid and ^{35}[S] sulfate, it was demonstrated that hyaluronan and chondroitin sulfate were found to be incorporated in the ECM derived from the spheroids after treatment with DOC and guanidine respectively. Further spheroids treated with DOC were shown to be positive for immunoflorescent staining for Fibronectin, Laminin and Collagen peptides. The pattern of immunoflorescent stains also demonstrated that the ECM proteins were sharper in contrast at the periphery and in the central regions the staining was diffuse.

Taken together from this study it was apparent that fibronectin, laminin, collagen, hyaluronan and chondroitin sulfate are some of the ECM components found in cancer spheroids [166]. The use of spheroid cultures has illustrated an important aspect of spheroid adhesion to ECM components and cell monolayer substratum. In ovarian carcinoma spheroid model, it was demonstrated that ovarian cancer spread through ascites consists of heterogeneous sizes and single cells. These spheroids and single cells were amenable to cell culture. The spheroid cultures and cells were subject to adhesion assays on purified fibronectin, collagen type I, type IV and laminin peptides. The spheroids and single cells demonstrated significantly higher adhesion to fibronectin and collagen type I proteins that was significantly higher than adhesion to collagen type IV and laminin, thus indicating a preferential behavior to the ECM proteins. The inclusion of β1 integrin antibody in the spheroid-single cell suspension during adhesion led to a significant decrease in binding to all 4 ECM proteins. Adhesion on hyaluronan peptide and fragmented hyaluronan fragments was also demonstrated. Further the spheroid isolates when pretreated with hyaluronan and hyaluronan fragments failed to adhere to hyaluronan substratum in a dose dependant manner. When the spheroid and single cells were incubated with anti CD44 antibodies and then allowed to adhere there were no significant effects compared to untreated controls, indicating that CD44 – hyaluronan interaction was not critical for adhesion. While the adhesion of spheroid and single cells to individual proteins is an interesting aspect, interaction with cell monolayers of mesothelial cells was also assessed. It was demonstrated that spheroid and single cell adhesion (fluorescently labeled) was significantly higher on unfixed monolayers as opposed to adhesion on formalin fixed monolayers. Additionally, inhibition with anti β1 integrin antibody but not anti CD44 antibody was shown to have a significant

reduction of adhesion. This data taken together demonstrated that adhesion is mediated by integrin receptors to a significant degree with preferential adhesion to fibronectin and collagen type I over collagen type IV and laminin, mediated by β1 integrin and further that native protein but not cross-linked protein (with formaldehyde fixation) is critical to adhesion [167]. Therefore spheroid plus single suspension adhesion data to unfixed monolayers compares well with spheroid cultures reported in this thesis work, as the ECM isolation protocol does not include any fixing agents. Comparisons between three methods 1) by cell suspension over lay on low adhesion polystyrene substratum, 2) in spinner flasks by continuous agitation of cell suspension or by 3) simple hanging drop of single suspension to generate multi cellular tumor spheroids (MCTS) has also been reported. Spheroid formation methods revealed that there was consistent size and sphericity (a measure of sphere shape) when cultured by hanging drop as opposed to cultures in spinner flasks or polystyrene surface. Further the hanging drop method was demonstrated to be versatile in a broad range of cancer cell types of hepatic cancer (HepG2), mammary gland fibrocystic disease (MCF-10a), breast cancer (MCF7), prostate cancer (DU145), cervical cancer (HeLa), colon adenocarcinoma (Caco-2), connective tissue fibrosarcoma (HT-1080). Electron microscope reveled that the MCTSs were tightly aggregated with a continuous surfaces and at time individual cells within the spheres were indistinguishable (Hep2G and MCF7). Of particular note in the hanging drop method is that cell-cell aggregation was time dependant and there was a progressive compaction and MCTS enlargement [168]. The hanging drop method relies on the natural ability of cells to cluster in the absence of a substratum that aids cell-cell adhesion without the prerequisite of ECM or ionic charge to aid cell adhesion. Moreover the MCTS formation required very little starter cell population that is

advantageous to consider when clinical samples are limited by cell counts. The technical advantage behind sphere cultures by suspension has also been evaluated in comparison to monolayer culture in NCI-H226 cells, an epithelioid histotype mesothelioma cell line derived from primary culture of pleural effusion. The study showed that there are significant differences in the transcriptome as assessed by microarray technique. Genes associated with biological functions were over expressed in specific clusters by function, namely, cell movement (17 genes), cell growth and proliferation (16 genes), cell-cell signaling (13 genes) and 13 morphological function genes, significantly higher in spheres compared to monolayer culture. By gene ontology analyses there was a significant higher enrichment for immune response, wound healing, immune related stimulus. Conversely, significant down regulation of apoptosis related ontologies of anti-apoptosis, regulation of apoptosis, regulation of programmed cell death were reported in sphere versus monolayer comparisons. Hence the sphere cultures are an important in determining the response to chemotherapeutics that are aimed at regulating tumor proliferation, tumor growth and tumor apoptosis [74].

8.15. AQP1 blockade during spheroid formation.

With the inclusion of $HgCl_2$ in the media during sphere formation with FN, the data indicated that spheroid sizes were significantly lowered in M14K and MSTO-211H cells while with the inclusion of ECM the spheroid sizes were significantly lower in all cell lines. The role of AQP1 in regards to sphere formation with a component of cell proliferation contributing in part to sphere growth also bears similarities compared to cell proliferation in 2D cultures on a ECM treated plastic substratum. $HgCl_2$ significantly lowers cell proliferation in 3D cultures. Elsewhere, the expression of

AQP1 and AQP5 has been demonstrated in spheres induced by recombinant cytokines insulin growth factor (IGF), epidermal growth factor (EGF) and recombinant fibroblast growth factor (FGF). The expression of AQP1 and AQP5 was shown to be retained in both monolayer and sphere cultures and further that the expression was observed in Notch2 expressing cells which are thought to be cancer stem-like cells [169]. In the context of forced AQP1 expression, it has been demonstrated that in NIH-3T3 fibroblasts, anchorage independent growth on agarose substratum demonstrated a significantly lower rate of apoptosis and not an increase in mitogenic signaling was responsible to larger colony formation when compared to mock transfectants [170]. In the context of mesothelioma suspension cultures on agarose, it was demonstrated that, with the blockade of AQP1 using Aqb050, there was a dose dependant reduction in the number of colonies formed at concentrations of 20 μM, 40 μM and 80 μM concentrations and further that the colony sizes were significantly reduced to less than half compared to no inhibition with Aqb050 [136]. Taken together this points to the fact that cell size and growth are modulated by AQP1 in 3D cultures mainly via apoptotic mechanisms that influence the size of the spheroid structures.

8.16. ENaC blockade during spheroid formation.

Amiloride inclusion in the media along with FN or ECM had limited effects in spheroid formation. The effects were mainly restricted to spheroids generated with ECM in the MeT-5A cells, in M14K, and ZL34 cells. The spheroids were significantly smaller in their perimeter. The lowering of cell proliferation component of sphere growth in the presence of amiloride is in good agreement with that of proliferation on 2D substratum with ECM. With regards to sphere formation with amiloride and FN, there were no

appreciable differences in sphere sizes. In the settings of amiloride and its anti-proliferative effect, it is over-ridden when compared to cell proliferation in 2D substratum with FN. There is little data in regards to the effects of ENaC on the process of spheroid formation. Anchorage independent growth of breast cancer cells MDA 468 was determined on agarose surfaces with two amiloride analogs (modified with ethyl-propyl modification to amiloride base; EPA) was tested. It was demonstrated that in MDA 468 cells, exogenous EGF enhanced anchorage independent colony formation and that with EPA, 15 μM dose completely abrogated plating efficiency (no anchorage independent colony formation) and at concentrations lower than 7.5 μM to 0.1 μM there was a significant suppression of the number of colonies. Of particular note was the fact that this low dose was sufficient to disrupt Na^+/H^+ antiport [171], and there was no mention of ENaC activity or gene expression. It is noteworthy that most literature citing the use of amiloride or its derivates during anchorage independent colony growth was reported in the context of uPA and NHE1.

8.17. Spheroid invasion characteristics of mesothelial and mesothelioma cells.

Spheroid were generated in 10% FBS RPMI media alone over 48 hours. The spheres were then overlaid with neutralized collagen. This experimental setup was designed to determine sphere growth in a collagen rich matrix, which bears some similarities to the basement membrane of the visceral and parietal pleura in principle. The data indicated that MeT-5A cells maintained spherical morphology while M14K, MSTO-211H and ZL34 cells develop invasive protrusions radiating away from the main sphere body. This represents invasive characteristic of metastatic potential of mesothelioma cells and further that the representative mesothelioma cells show an increasing perimeter of

invasion, yet another capitulation on their increasing tendencies between histotypes during invasion into the matrix in 3D. This phenotype demonstrated the growth of the sphere edge as characteristic invading structures. The invasive capacity of pre-formed spheroids into collagenous matrix demonstrates an important aspect of the spheroid interacting with external environment and the formation of invasive outgrowths. The interaction of cells in a co-culture model of mammary tumor spheroids and a monolayer of endothelial cells with a component of collagen has been reported. It was demonstrated that mammary tumor spheroids generated on agarose substratum when over laid on a monolayer of endothelial cells cultured on collagen substratum. It was demonstrated that there is a dependant adhesion of tumor spheroids to the collagen rich monolayer of endothelial cells, along with a cleared zone of 20 μm peripheral to each implanted tumor spheroid. After a period of 24 hours it was also demonstrated that the spheroids maintained their morphology and developed invasive cords still attached to the main spheroid body [172]. Spheroid and benign cell co-culture has been reported in the context of ovarian tumor ascites and mesothelial LP9 cell monolayer. In this model it has been demonstrated that ovarian ascites tend to spontaneously resolve into a monolayer by disaggregation. This was demonstrated firstly with select ECM proteins such as collagen type I, type IV, Laminin, Fibronectin and Hyaluronan on tissue culture plates. The disaggregation was also demonstrated when ascites were seeded on top of LP9 cell monolayers. The ascite spheroids demonstrated and intial enlargement in size followed by proliferation over 4-7 days of culture and maintained homologous cell-cell to contact occasionally [167]. The ascites spheroid invasion model is contrast to most invasion assays where the spheroid structures maintain 3D morphology. In an invasive spreading model on glass cover slip (2D) surfaces, it has been demonstrated that

spheroids derived from glioma cells (SNB19) tend to preferentially spread out on glass slips pre-treated with collagen type I, collagen type IV and fibronectin but not laminin [173]. This behavior of spreading appeared as a continuous cord emerging from the periphery of the spheroid structure. The ability of spheroids invading a collagenous matrix has been mechanistically employed to determine if there arise characteristics of protein expression that are similar to the ones observed in pathological specimens, namely heterogeneity of protein expression. This is particularly relevant since it has been demonstrated that monolayers of melanoma cells do not show corresponding protein expression of an important axis involving two proteins Brain-2 (BRN2) that correlates with increased melanoma cell proliferation and Melanogenesis Associated Transcription Factor (MITF) that regulates melanocyte development. The expression of these proteins is reciprocal in nature. In melanoma monolayer model BRN2 and MITF expression is dual while in biopsy samples, it is reciprocal i.e. $BRN2^{+}/MITF^{-}$ or $BRN2^{-}/MTIF^{+}$. The reciprocity is re-capitulated in spheroid cultures which when used as xenograft demonstrated the staining characteristics of human melanoma biopsy samples. With permanent BRN2 deletion there was a significant loss of invasive features with preformed spheroids embedded in collagen [174]. This demonstrates the importance of heterogeneity observed in pathological specimens that can be evaluated through *in-vitro* model of 3D and invasion into a collagen matrix. The generation of spheroid culture from monolayer culture with the application of growth factors has been reported in a mouse glioma cell line, RSV-M that produces tumor spheroids RSV-TM with basic Fibroblast Growth Factor (bFGF), EGF, and Leukemia Inhibitory Factor (LIF). The RSV-TMs were demonstrated to stable and did not require any growth factors when sub cultured for more than a year. The stable RSV-TM (labeled with red

florescent Vybrant dye) cell type was then subject to invasion assays in to the mouse brain through intracranial allograft. In comparison to RSV-M the RSV-TM variant was significantly higher for its migration into the brain. Interestingly, the overexpression of Tenascin (TN) was demonstrated to be at the tumor front of the invasion when examined by histology [175]. Taken together it was demonstrated that, the method of tumor spheroid formation does not influence tissue invasion and further that there is a component of the ECM protein that guides invasive process. A recent advancement in modeling tumor behavior in the setting of tumor microenvironment has employed the use of heterotypic cultures in 3D configuration. In this method fibroblasts and cancer cells are propagated embedded in a collagenous matrix. By prior expression with florescent markers in non-invasive tumor spheroid and their co-culture with tumor derived myofibroblasts it was demonstrated that, real time invasion tracking can be achieved with florescent microscope and further that this method is amenable for mathematical modeling purpose [176]. Complex co-culture models are advantageous in gaining better insights into tumor invasion processes that incorporates ECM, cancerous cells along with myofibroblasts that constitute the heterogenous cellular population within a tumor biopsy. In the context of mesothelioma studies, it has been demonstrated that, tissue biopsies subject to drug treatments during 3D culture in collagen matrix is an excellent method to predict drug sensitivity. The method evaluated samples of the same origin for multiple drug sensitivity and it was demonstrated that there was a marginal correlation between the drug sensitivity test and patient response in terms of disease status of the patient. An important part of the platform was the use of chemotherapy regimen guided by sensitivity and resistance *in vitro* on biopsy samples [77]. The invasion assay model with 3D tumor spheroid in

collagenous matrix represents a technique that is adaptable to tissue or cell suspension derived spheroids. The versatile nature of incorporating drugs and chemotherapeutics and at times, tumor associated myofibroblast cells is a feature that can be easily adapted for clinical evaluation.

8.18. AQP1 inhibition limits invasive capacity of spheroids in collagen matrix.

AQP1 inhibition with $HgCl_2$ inclusion in the overlaid collagen demonstrated a significant lowering of invasive perimeter in all mesothelioma cell types. The affect of AQP1 blockade was not significant in mesothelial cells. The reduction in invasive development in collagen matrix in mesothelioma cells due to loss of AQP1 activity can be an attributed to the lowered ability of the cells to orchestrate biomechanical penetration. With a reduction in H_2O transport, tensile invasion is reduced suggestive of the inability to regulate cytosolic rigidity. In the context of spheroid invasion in mesothelioma or other cancer types there are no data. However, the use of collagen as a barrier during cell migration is a technique often employed to assess single cell invasion. It involves the use of a chemotactic gradient, usually 10% FBS complemented media that influences cells to migrate through a gelatinous protein material of choice such as collagen or matrigel. In regards to HT20 human colon cancer cells, the role of AQP1 expression has been characterized. These cells express AQP1 and the forced overexpression of AQP1 results in a significantly higher rate of migration during wound healing assays as compared to wild type cells and further that silencing of AQP1 expression using shRNA targeting exonic sequences the migration was significantly lower than wild type cells. In the settings of single cell suspension and migration through fibronectin coated porous substratum, the over expression and silencing were

significantly higher and lower respectively compared to wild type HT20 cells. The invasive ability through cleared space and through pores was further tested. Tail vein injection with over expressing AQP1 (with CMRA, red florescence agent) and AQP1 wild type expressing (labeled with CMFDA, green florescence reagent). 15 minutes post injection red and green florescent cells were observed attached to the lung endothelium. However after 7 hours of injection AQP1 over expressing fluorescently labeled cells were 2.5 times significantly higher in the lung parenchyma [177]. This data demonstrates the role of AQP1 (in colon cancer) during the processes of invasion and migration. The differential expression of AQP1 in lung cancer cells has been reported in LTEP-A2 and LLC cells where in LLC cells show a significantly higher level of AQP1 expression compared to LTEP-A2 cells. The two cell lines were demonstrated to show no significant differences in migration through a matrigel substratum (ECM from a sarcoma basement membrane coated on Boyden chamber filters) however upon the transient silencing AQP1 gene expression with siRNA it was demonstrated that the invasion through matrigel was significantly reduced. Migration through nude Boyden chambers was also significantly lowered when AQP1 expression was silenced [178]. This demonstrated the activity of AQP1 contributing significantly towards lung cancer cell invasion through basement membrane. In contrast to soft tissue tumors such as colon and lung cancer as mentioned above, osteosarcoma is a neoplasm of the bone. Significant AQP1 overexpression was demonstrated in osteosarcoma by microarray analyses on normal versus tumor and real time PCR analyses. By employing lentiviral mediated APQ1 silencing it was shown that <30% of cells (statistically significant) invaded through Matrigel [139]. Hence it is apparent that AQP1 activity plays a crucial role irrespective of the anatomical source of the

neoplasm. The invasion of colon cancer spheroids has been reported in the setting of AQP1 activity with pharmacologic inhibitor AqB013. It was demonstrated that spheroids derived from cells with low or high AQP1 expression had a differential response to AqB013 mediated AQP1 activity abolishment. Specifically, high AQP1 expressing cells (HT29 cells) were sensitive to AqB013 treatment at doses of 80 μM and 160 μM showed a proportional and significantly lower growth and invasion into matrigel however this AqB013 inhibition was ineffective in limiting growth and invasion of low AQP1 expressing HCT116 cells. This is suggestive of a limited role of AQP1 in HCT116 colon cancer cells [147]. Thus it is reasonable to reconcile AQP1 protein activity such that it may have limiting effects on invasion but may be cell type dependant as was demonstrated in our study where MeT-5A cells show no inhibition of sphere growth in collagen matrix. The genetic expression of AQP1 has been demonstrated to be under the regulation of miR320. The loss of miR320 has been demonstrated in breast cancer patient samples by in situ hybridization technique along with over expression of AQP1 in matched normal and tumor histological sections. Moreover, MCF7 breast cancer cells when transfected with miR320, AQP1 expression was down regulated. To demonstrate the causal mechanism of AQP1 degradation through miR320 mediated decay involving the 3' UTR, AQP1 mutant of 3' UTR when over over expressed was not silenced miR320 transfection. The over expression of miR320 was also demonstrated to have a significant lowering of invasion through Boyden chamber [179]. Taken together, the role of AQP1 is conserved in terms of its influence on cell invasion and this has been demonstrated through genetic silencing of AQP1 gene, pharmacological blockade of AQP1 protein and through miRNA mediated control of AQP1 mRNA stability.

8.19. ENaC inhibition during spheroid invasion.

Amiloride induced blockade of ENaC demonstrated a lowered invasive perimeter only in the MSTO-211H tumor spheroids. All other cell types did not show appreciable decrease in the perimeter of the spheroid. This is suggestive of a limited role for ENaC channel activity during spheroid invasion given that MeT-5A, M14K and ZL34 tumor spheroids demonstrated to be less invasive in the presence of amiloride but not significantly. The spheroid invasion assay is mainly reported in the settings of evaluating drug action in limiting the growth and invasion of patient derived spheroids or tissue fragments. In the context of trophoblast invasion during embryo implantation, it was demonstrated the cell invasion was significantly reduced during ENaCα subunit silencing [151]. Subsequently trophoblast cells were also evaluated for their invasive ability through Matrigel towards a chemotactic gradient of serum. During ENaCα mRNA ablation with siRNA, the trophoblast cells were demonstrated to migrate lower than untreated cells and non-targeting siRNA control. Moreover, a comparison of the expression of ENaCα and ENaCβ was demonstrated to be significantly lower in patients with preeclampsia compared to normal placental biopsy sample [151]. Collectively, this demonstrates the expression and activity of ENaC is a specialized function, fundamental to migration and invasion of trophoblast cells. The induction of ENaCα mRNA is also reported in HTR8/SVneo cells (extravillous trophoblast cells). Cells when treated with aldosterone, a potent inducer of ENaCα expression as mentioned earlier, demonstrated a signifiicantly higher invasion through Matrigel in Boyden chamber assay compared to untreated cells. When aldosterone treated cells with amiloride were subject to invasion there was significantly lower invasion compared to aldosterone treated cells. Amiloride treatment alone significantly reduced

invasion compared to untreated controls. In control non-targeting siRNA transfected cells, the migration was significantly higher than siRNA ENaCα transfected cells, thus demonstrating the importance of ENaC channel activation and mRNA expression as a requirement of gel invasion. The study further demonstrated the expression of MMP2, a matrix modifying enzyme that is required for migration and invasion ability of cells. Silencing of ENaCα or amiloride treatments significantly lowered the expression of MMP2 transcript (by qPCR assay) and protein activity as measured by in gel zymography. This is indicative of ENaC playing an important role in the secretion of MMP2 that in turn facilitates migration and invasion [180]. Thus ENaC activity has a complex function in the context of trophoblast activities.

8.20. Contraction of collagen gels embedded with mesothelial and mesothelioma cells.

Mesothelial and mesothelioma cells in a suspension of neutral collagen and media demonstrate a contractile ability. After a 24-hour incubation in culture conditions the collagenous matrix was visible as a disc with a clear periphery, suspended in the media. This is indicative of cells interacting with each other and the collagenous matrix to form a contracted complex that is opaque (unlike the clear, un-polymerized collagen solution). More over the defined circular edge of this collagenous disc retracted from the edges of the well and is indicative of a contracted state. This is attributable to the ability of the cells that have developed a mesenchymal characteristic and is visible only in a 3 dimensional model without a substratum. The characteristic of cells of mesothelial origin showing a mesenchymal, contractile behavior is alternatively described as mesothelial-mesenchymal transition (MMT), akin to epithelial mesenchymal (EMT) often described in neoplastic development. In our model the data

demonstrated that gel contraction (as a phenotype of MMT) was increased in the most aggressive ZL34 cells compared to MeT-5A, M14K and MSTO-211H cells. MMT is evident with other phenotypes as well where cell motility during wound healing and gel invasion are apparent and are well correlated with histotype in a stratified manner with increased wound healing and increased tumor spheroid invasion. In the context of EMT/MMT and gel contraction by mesothelioma cells is not reported in the literature. However mesothelial cells that are stimulated to undergo MMT by TGFβ stimulus or primary mesothelial cell isolated from human fibrotic lungs have been demonstrated for their contractile ability [181]. Along the lines of evaluating EMT characteristics in mesothelioma microarray study (consisting of 40 mesothelioma patients and 9 normal lung or pleura), a list of manually curated transcription factors that govern EMT was compiled. SNAI1, SNAI2, E47/TCF3, TWIST1, ZEB1, ZEB2, FOXC1, and FOXC2 were analyzed by principle component analysis. It was demonstrated that most epithelial samples were negatively associated with EMT genes while biphasic MPM samples were associated with SNAI1, ZEB1, ZEB2, FOXC1, FOXC2 and weakly associated with SNAI2, TWIST1, E47/TCF3 [182]. Therefore the transcriptional apparatus supporting the EMT characteristic is an evidence of the genetic machinery that turns on EMT in mesothelioma. Among other cancer types, colonic carcinoma cells HCA-7 were further purified to generate isolated colonies from single cell islands. Cells from colony were demonstrated to have a mesenchymal characteristic of gel contraction after 14 days of culture inside a collagen suspension. Further that the contracted gels were lowest in their weight indicating lower fluid retention after gel contraction. When integrin α2 and integrin α3 functional blocking antibodies were included in the collagenous mix, contraction was lowered and dose dependant with anti

integrin α2 antibody and was concentration dependant [183]. Therefore it indicates that contractile behavior of the collagenous matrix required the engagement of cell surface receptors. In the context of collagen gel contraction by glioma cells and fibrosarcoma cells, it was demonstrated that the gel contraction was enhanced due to activation of Matrix-Metallo-protease-2 (MMP2). MMP2 is expressed in an inert form designated as pro-MMP2. Pro-MMP2 to MMP2 conversion is catalyzed by membrane type (MT) MMP. The interaction of integrins with the exterior collagen matrix was also demonstrated to be dependent through integrin α2, α3 and β1. Gel contraction was significantly reduced when appropriate function blocking antibodies were included in the cell-collagen suspension. Lastly, the inhibition of actin polymerization with phalloidin or microtuble assembly with nocodazole completely abolished gel contraction [184]. The contraction mediated by glioma and fibrosarcoma cells elucidated the requirement of enzymatic activity external to the cells, necessary for gel contraction, requirement of cell-ECM interaction through integrins and the involvement of cytoskeletal proteins during gel contraction. In breast cancer cells T47D and MCF10-A, the collagen concentration during gel contraction and attachment of collagen matrix itself to the walls of culture wells was demonstrated to have differential effects. When collagen concentration was increased there was a decrease in contraction and when collagen was left attached to the walls there was enhanced proliferation compared to collagen gels that were allowed to float during contraction. The mechano-transduction behind floating or anchored (attached) gels was shown to be modulated through Rho-ROCK signaling pathway that differentially activated FAK at Y397 when gels were dense or rigid and negligible FAK phosphorylation when gels were flexible and free floating [185]. Elsewhere it has been demonstrated that both mesenchymal

fibroblasts and epithelial cells that have undergone EMT are capable of contracting collagen gels and further that α smooth muscle actin expression was not a requirement for epithelial EMT cells to cause collagen gel contraction. Analysis of the height of the cells after contraction was significantly different and hence this was propose as a method to discriminate mesenchymal cells with epithelial cells having mesenchymal-like phenotype due to EMT [186]. In the context of mesothelial and mesothelioma cells it might be expected that despite the epithelial characteristic of MeT-5A and M14K cells, there exists a potential of these cells to contract the collagen gel. EMT and MMT based collagen gel contraction is an important variable to consider based on the above observations where in cell-ECM interaction determines the ability of transformed cells to respond differently based on ECM composition and ECM rigidity. The MMT observed in our work is the first example in the setting of mesothelioma model *in vitro*. Gel contraction with cells embedded in a collagenous medium with retinal pigment cells (ARPE-19 cells) has been described in terms of integrin protein expression, focal adhesion kinase (FAK) protein activation dependant manner. It was demonstrated that ARPE-19E cells expression integrin α1, α2, α3, α4, α5, α6, αvβ3 and αvβ5. Functional blockade of integrins with anti α2, α3 prior to embedding the cells in collagen matrix significantly inhibited gel contraction. When FAK activation was interfered with PP2 a FAK specific small molecule inhibitor there was a significant loss of gel contraction in a dose dependent manner. And moreover FAK silencing with siRNA also abolished gel contraction [187]. Taken together it is apparent that integrin and FAK mediate gel contraction in concert. The contractile apparatus within the cytoplasm is a network of actin-myosin assembly, disassembly and stabilization through phosphorylation modifications. Actomyosin contraction is a balance of

repeated phosphorylation and phosphatase modifications on myosin light chain (MLC). MLC is phosphorylated by Myosin light chain kinase (MLCK) while de-phosphorylation occurs via MLC phosphatase (MLCP). Continued action of MLCK and MLCP sustains contractile state through collective action of integrin-linked kinases, protein kinases and ROCK, a member of Rho family proteins (Rho associate coiled coil containing protein kinase). In trabecular meshwork cells of the eye have been demonstrated to show gel contraction model. It was demonstrated that ROCK inhibtion with small molecule inhibitor Y27632 and Y39983 led to lowered gel contraction in a dose dependant manner. Further more with the use of Myosin II ATPase inhibitor blebbistatin also significantly reduced gel contraction [188]. Thus action-myosin based mechaism of contraction is dependant on ROCK activity. Together, the activation of FAK and RHO family ROCK govern contractile abilities when cells are embedded in a collagen rich matrix.

8.21. AQP1 regulates the ability of gel contraction mediated by mesothelial and mesothelioma cells.

$HgCl_2$ inclusion in the neutral collagen, mixed with cells consistently lowered the ability of cells to contract the gels in all mesothelioma cell types. This is indicative of a basic requirement of AQP1 activity that is necessary to express H_2O from the cell cytoplasm in-order for cells themselves to progressively contract during collagen polymerization and the formation of collagen-cell heterogeneous polymerized structures. Therefore the MMT of mesothelioma cells in the context of the 3D collagen model is of significance wherein the contractile behavior is modulated due to a limitation in H_2O expulsion. The benign cells demonstrated less contraction in

comparison to mesothelioma cell types. The AQP1 blockade during inherent contraction after collagen polymerization demonstrating significant differences in the context of AQP1 inactivation is suggestive of AQP1 activity influencing the contraction from mesothelial cells in collagen matrices. This points to a more biomechanical role of AQP1 activity essential to MMT dependant phenotype of contraction. EMT in the context of miRNA influenced gene expression has been described in the human pterygium (ocular degeneration due to conjuctival tissue invasion into cornea). In a disease versus normal tissue microarray experiment, it was demonstrated that 5 members of miR200 family (miR200a, miR200b, miR429, miR200c and miR141) were differentially expressed and down regulated (-1.5 to -2.0 fold change). The functional targets of de-repressed miRNAs were identified as 3 discrete categories of EMT related transcription factor genes (range of 2.3 to 2.6 fold change), fibrosis related genes (range of 1.7 to 2.7 fold change, AQP1 2.7 fold) and angiogenesis (2.3-2.7 fold). This demonstrates there is a concerted mechanism underlying the process of EMT that in this case, elevated the AQP1 gene expression [189]. AQP1 has also been demonstrated to interact with proteins on the cytoplasmic side of plasma membrane. In an epithelioid melanoma cell line model it has been demonstrated that upon AQP1 silencing there was marked disorganization of actin cytoskeleton as demonstrated by immuno-fluorescence. Lin7, β-Catenin proteins were demonstrated to be down regulated as a result of AQP1 silencing and further that Lin7 from whole cell protein lysate co-immuno precipitated AQP1 and β-Catenin protein. The co-immuno precipitation of Lin7 in APQ1 silenced cells (with siRNA) was significantly lowered and further that inhibtion of proteasomes with MG132 increased the Lin7 yield in AQP1 silenced cells, this demonstrates the role of AQP1 protein in

stabilizing Lin7 and β-Catenin protein [101]. The interaction of FAK and β-Catenin has been mechanistically described in the context of AQP1 function. In immortalzed rat bone marrow mesenechymal stem cells AQP1 silencing or over expression was resulted in decreased or increased migration into bone fracture sites, a model to demonstrate invasion and healing processes at the cellular level. It was further demonstrated that there was a linear relationship between the expression of AQP1 and β-Catenin where in β-Catenin expression was considerably lowered during silencing of AQP1 expression. Similar relationship was described between AQP1 and FAK expression. Further immuno precipitation of AQP1 also demonstrated positive signals for β-Catenin and FAK. This described a direction interaction of AQP1 with β-Catenin and FAK that in concert influence migration into wounded tissue, an ability reliant on cytoskeletal modulation through AQP1 activity [102]. AQP1 activity also modulates Rho dependant cell cytoskeletal changes. In HT20 colon cancer model cell line, it has been demonstrated that the silencing of AQP1 expression lower invasion and migration. The phosphorylation of RhoA and GTP-Rac expression are significantly lowered during AQP1 silencing and conversely the over expression of AQP1 increased their expression. Thus there is an underlying mechanism of cell cytoskeletal changes that are subject to AQP1 activity. Taken together it can be inferred that AQP1 influences both FAK and Rho dependant mechanism that regulate the contractile properties of benign and mesothelioma cells.

8.22. ENaC regulates the ability of gel contraction mediated by mesothelial and mesothelioma cells.

Amiloride inclusion in the collagen matrices along with the cells also demonstrated a diminished ability of the cells to contract. The effect of ENaC activity blockade was apparent in all cell lines. It was demonstrated that ENaC activity is essential for gel contraction via the embedded cells. These results in mesothelial and mesothelioma cell contractile apparatus are suggestive of sensitivity to Na^+ availability. In the context of embryonic chondrocytes of mouse limb bud cultured as organoids, the physical interaction of integrin β1 was interrogated. By immuno co-precipitation method it was demonstrated that integrin β1 formed complexes with α subunit of Na-K ATPase, α subunit of ENaC and with α subunit of Voltage Activated Calcium Channel (VACC). The immuno co-precipitates were demonstrated by western blot. Alternatively, dual immuno fluorescence staining revealed the co-localization of integrin β1 stain with α subunits of Na-K ATPase, ENaC and with VACC [190]. This effectively demonstrates the physical interaction of integrin β1 with ENaCα subunit and localized feature along the cell membrane. Elsewhere in melanoma cells (MV3 and BLM cells) mediated collagen gel contraction the role of integrin α2 and integrin β1 has been reported using a highly aggressive cell line for collagen gel contraction. Functional blockade with anti integrin α2 or integrin β1 completely abolished gel contraction and further that there was a marked expression of integrin α2 in lysates obtained from [^{35}S] Methionine label supplemented media [191]. Taken together this demonstrates gel contraction is also subject to ENaC activity through its association with integrin although the precise mechanism are yet to be determined in the context of gel contraction in mesothelioma and mesothelial cells involving transcript and protein expression along with effectors of contraction such as integrin linked kinases, Rho/ROCK and FAK kinases.

9. PhD Thesis Synopsis

Below are the important findings in this thesis work titled: “Dissecting the role of aquaporin-1 (AQP1) and amiloride sensitive epithelial sodium channel (ENaC) in pleural mesothelioma biology”. This thesis investigated benign mesothelial and malignant pleural mesothelioma cell models of cell adhesion, cell migration during wound scratch, tunneling nanotube (TnT) development, cell proliferation, spheroid formation and invasion and gel contractility to evaluate EMT characteristics of the mentioned cell types. This work incorporated the homologous cell derived extra-cellular matrix (ECM) as a substratum. Firstly, the assays were characterized on a comparative basis between 2 substrata, FN or ECM in 2 dimensional phenotypes of cell adhesion, cell migration, TnT formation, cell proliferation and spheroid formation (3D). Using collagen, spheroid invasion and cell-mediated contraction of collagen gels were performed in 3D.

- *Malignant mesothelioma cell types demonstrated a higher affinity of adhesion on homologous ECM compared to fibronectin. The cell adhesion of M14K, MSTO-211H and ZL34 cells was significantly higher on ECM compared to cell adhesion on fibronectin.*
- *Cell migration during wound scratch was significantly higher on FN substratum compared to ECM substratum in all cell types.*
- *MeT-5A, M14K, MSTO-211H and ZL34 cells develop tunneling nanotubes during culture. MSTO-211H and ZL34 cells develop significantly higher TnTs when cultured on ECM substratum compared to those on FN.*

- *Cell proliferation of MeT-5A, M14K, MSTO-211H and ZL34 cells was assessed after 3 days of cell culture. In all cell lines, proliferation was significantly higher on FN substratum compared to ECM substratum.*
- *Spheroid formation was assessed after 2 days of cell culture with FN and ECM added to culture media by hanging drop technique. Mesothelioma cell type MSTO-211H formed significantly larger spheroids with ECM.*
- *Pre-formed spheroids were assessed for invasion in collagen matrices. Only M14K, MSTO-211H and ZL34 cells develop invasive morphology. MeT-5A cell spheroid perimeter was significantly smaller compared to M14K, MSTO-211H and ZL34 cell types.*
- *EMT was assessed through embedding the cells in collagen gel matrix. MeT-5A, M14K, MSTO-211H and ZL34 cells demonstrated visible gel contraction after 24 hours. ZL34 cells demonstrate significantly least gel area (highest contraction), followed by MSTO-211H, M14K and MeT-5A the highest gel area (least contraction).*

In order to determine the role of AQP1 during cell adhesion, cell migration, TnT formation, cell proliferation, spheroid formation and invasion and gel contraction, the activity of AQP1 was inhibited with the inclusion of Mercuric chloride (MC, 10 μM) in the culture media during the experimental investigations.

- *Cell adhesion was significantly lowered in MeT-5A and M14K cells during inhibition with MC on FN substratum. During cell adhesion with MC on ECM substratum only M14K cell adhesion was significantly lowered.*
- *Cell migration on FN and ECM substratum with MC was significantly lowered in ZL34 cells only.*

- *TnT development in MeT-5A cells was significantly lowered irrespective of the substratum of culture, while in M14K, MSTO-211H and ZL34 cells TnT development was unperturbed.*
- *Cell proliferation during blockade of AQP1 with MC was significantly lowered. All cell types irrespective of the substratum proliferated significantly lower than controls without MC.*
- *Spheroid formation with MC lowered the perimeters in M14K and MSTO-211H cell types in media with FN, while MC treatment in all cell types lowered spheroid perimeter when ECM was present.*
- *Spheroid invasion into collagen matrices with MC significantly lowered spheroid perimeter in M14K, MSTO-211H and ZL34 cell types.*
- *During gel contraction, MC included in the gel mixture led to significantly relaxed gels in all cell types.*

To determine the role of ENaC during cell adhesion, cell migration, TnT formation, cell proliferation, spheroid formation and invasion and gel contraction, the activity of ENaC was inhibited with the inclusion of Amiloride (AM, 10 μM) in the culture media during the phenotype assays.

- *Cell adhesion was significantly lowered in MeT-5A cells during inhibition with AM but significantly enhanced in M14K and MSTO-211H cells on FN substratum. During cell adhesion with AM on ECM substratum ZL34 cell adhesion was significantly increased.*
- *Cell migration with AM was significantly lowered in MeT-5A and ZL34 cells during wound healing on FN substratum.*

- *TnT development in ZL34 cells was significantly lowered with ENaC blockade on ECM substratum.*
- *Blockade with AM significantly lowered cell proliferation on FN substratum in MeT-5A and ZL34 cells. While with AM, on ECM substratum proliferation was significantly lower in MeT-5A, M14K and ZL34 cells.*
- *Spheroid formation with AM lowered the perimeters in MeT-5A, M14K and ZL34 cell types when ECM was present.*
- *Spheroid invasion into collagen matrices with AM significantly lowered spheroid perimeter only in MSTO-211H cell type.*
- *Gel contraction with AM included in the gel led to significantly relaxed gels in MeT-5A, M14K, MSTO-211H and ZL34 cells.*

In this body of work on mesothelioma cell models, cell adhesion, cell migration, cell proliferation, spheroid formation, spheroid invasion and gel contraction phenotypes were characteristised. The phenoytpes represent characteristics that contribute towards malignant growth and development.

In the aspect of AQP1 blockade with $HgCl_2$, the malignant phenotypes of cell proliferation, spheroid invasion and gel contraction were significantly inhibited in all cell types. AQP1 inhibition was not key to lowering cell adhesion, migration and spheroid formation in all cell types. In aspect of ENaC bloackade with amiloride only gel contraction was sensitive in all cell types. In the remaining phenotypes, the affect of amiloride was variable depending on the cell type.

The prevailing hypothesis on the role of AQP1 in MPM currently is that it's over-expression is associated with a survival advantage as reported in the literature.

Our body of work tested the role of AQP1 in different MPM cell types. When inhibited pharmacologically, loss of AQP1 activity led to a diminished malignancy potential which contradicts the clinical data. Therefore, the AQP1 overexpression conferred advantage in MPM patients may be the result of a role of AQP1 in the pleural fluid turnover in the pleural cavity, suggestive of the notion that decreased pleural effusion burden leads to lowered number of tumor foci the cavity and thus less local tumor dissemination. In order to reconcile the role of AQP1 *in vivo*, inducible and conditional silencing of AQP1 in immune competent mice with allogenic mesothelioma model cell types will help in a better understanding of AQP1 expression at the tissue (normal or malignant type) level.

The role of ENaC needs to be further explored with studies on the genetic and protein expression levels in model cells and human tumor biopsies. From the data produced in the current work, amiloride could be considered as a neoadjuvant but this would require initially *in vivo* studies in mouse mesothelioma models in order to further evaluate its potential.

10. References

1. **Wang N.** Anatomy of the pleura. Clin Chest Med. 1998;19:229–240.
2. **Agostoni E., Zocchi L.** Pleural liquid and its exchanges. Respir Physiol Neurobiol 2007;159:311-323.
3. **Light R.** Pleural Diseases. (Lippincott Williams & Wilkins, 2007).
4. **Michailova K.N., Usunoff K.G.** Serosal membranes (pleura, pericardium, peritoneum). Normal structure, development and experimental pathology. Adv Anat Embryol Cell Biol 2006;83: i-vii, 1-144.
5. **Zarogiannis S., et al.** Comparison of the electrophysiological properties of the sheep isolated costal and diaphragmatic parietal pleura. Clin Exp Pharmacol Physiol. 2007 Jan-Feb;34(1-2):129-31.
6. **Mutsaers S.E.** Mesothelial cells: their structure, function and role in serosal repair. Respirology 2002;7:171-191.
7. **Bird S.D., Legge M., Walker R.J.** Cultured peritoneal mesothelial cells exhibit apical primary cilia. Cell Biol Int. 2004;28:79-92.
8. **Heldin P., Pertoft H.** Synthesis and assembly of the hyaluronan-containing coats around normal human mesothelial cells. Exp Cell Res. 1993;208:422–429.
9. **Noppen et al.** Volume and Cellular Content of Normal Pleural Fluid in Humans Examined by Pleural Lavage. AJRCCM 2000;162:1023-1026.
10. **Zocchi L.** Physiology and pathophysiology of pleural fluid turnover. Eur Respir J. 2002;20:1545-1558.
11. **Liakopoulos V., et al.** Inhibition by mercuric chloride of aquaporin-1 in the parietal sheep peritoneum: an electrophysiologic study. Adv Perit Dial. 2006;22:7-10.
12. **Du H., et al.** Increased expression of aquaporin-1 on the pleura of rats with a tuberculous pleural effusion. Lung. 2007;185:325-336.
13. **Hatzoglou C.H., Gourgoulianis K.I., Molyvdas P.A.** Effects of SNP, ouabain, and amiloride on electrical potential profile of isolated sheep pleura. J Appl Physiol. 2001;90:1565–1569.
14. **Sarkos S., et al.** Effect of amiloride in human and sheep parietal pleura. Respir Physiol Neurobiol. 2002;132:233-237.
15. **Zarogiannis S., et al.** Influence of the sodium transport inhibition by amiloride on the transmesothelial resistance of isolated visceral sheep peritoneum. Adv Perit Dial. 2005;21:5-8.
16. **Stefanidis I., et al.** Amiloride-sensitive sodium channels on the parietal human peritoneum: evidence by ussing-type chamber experiments. ASAIO J. 2007;53:335-338.
17. **Zarogiannis S., et al.** Comparison of the electrophysiological properties of the sheep isolated costal and diaphragmatic parietal pleura. Clin Exp Pharmacol Physiol. 2007;34:129-131.
18. **Kouritas V.K., et al.** Human parietal pleura present electrophysiology variations according to location in pleural cavity. Interact Cardiovasc Thorac Surg. 2008;7:544-547.
19. **Zarogiannis S., et al.** Dexamethasone decreases the transmesothelial electrical resistance of the parietal and visceral pleura. J Physiol Sci. 2009;59:335-339.
20. **Peppa V.I., et al.** VEGF increases the permeability of sheep pleura ex vivo through VEGFR2 stimulation. Cytokine. 2014;69:284-288.

21. **King L., Nielsen S., Agre P.** Aquaporin-1 water channel protein in lung: ontogeny, steroid-induced expression, and distribution in rat. J Clin Invest. 1996;97:2183–2191.
22. **Song Y., et al.** Role of aquaporin water channels in pleural fluid dynamics. Am J Physiol Cell Physiol. 2000;279:1744–1750.
23. **Jiang J., et al.** Effect of aquaporin-1 deletion on pleural fluid transport. Acta Pharmacol Sin. 2003;24:301–305.
24. **Jiang J., Hu J., Bai, C.** Role of aquaporin and sodium channel in pleural water movement. Respir Physiol Neurobiol 2003;139:83–88.
25. **Kinasewitz G.** Transudative effusions. Eur Respir J. 1997;10:714–718.
26. **Baikati K., et al.** Hepatic hydrothorax. Am J Ther. 2014;21: 43–51.
27. **Lal C., Huggins J., Sahn, S.** Parasitic diseases of the pleura. Am J Med Sci. 2013;345:385–389.
28. **Nestor J. et al.** Viral diseases affecting the pleura. J Clin Virol. 2013;58:367–373.
29. **Fenton K., Richardson, J.** Diagnosis and management of malignant pleural effusions. Am J Surg. 1995;170:69–74.
30. **Lynch T.J.** Management of malignant pleural effusions. Chest. 1993;103: 385S–389S.
31. **Thieke C. et al.** Long-term results in malignant pleural mesothelioma treated with neoadjuvant chemotherapy, extrapleural pneumonectomy and intensity-modulated radiotherapy. Radiat Oncol. 2015;30:267.
32. **Marshall A. et al.** Survival from malignant mesothelioma: where are we now? J R Coll Physicians Edinb. 2015;45;123–126.
33. **Wagner J., Sleggs C., Marchand P.** Diffuse pleural mesothelioma and asbestos exposure in the North Western Cape Province. Br J Ind Med. 1960;17:260–271.
34. **Musk A., de Klerk N., Brims F.** Mesothelioma in Australia: a review. Med J Aust. 2017;207:449–452.
35. **Sakai K. et al.** Trends in asbestos and non-asbestos fibre concentrations in the lung tissues of Japanese patients with mesothelioma. Ann Occup Hyg. 2014;58:103–120.
36. **Mao W. et al.** Association of Asbestos Exposure With Malignant Mesothelioma Incidence in Eastern China. JAMA Oncol. 2017;3:562–564.
37. **Metintaş S. et al.** Turkey National Mesothelioma Surveillance and Environmental Asbestos Exposure Control Program. Int J Env Res Public Heal. 2017;14(11).
38. **Sakellariou, K. et al.** Malignant pleural mesothelioma from nonoccupational asbestos exposure in Metsovo (north-west Greece): slow end of an epidemic? Eur Respir J. 1996;9:1206–1210.
39. **Gogali A. et al.** Evidence Suggesting the End of Universal Domestic Asbestos Exposure in Metsovo, NW Greece. Respiration. 2917;94:510–517.
40. **Marinaccio A., et al.** Regional Operating Centres. Epidemiology of malignant mesothelioma in Italy: surveillance systems, territorial clusters and occupations involved. J Thorac Dis. 2018;10:S221-227.
41. **Berry M.** Mesothelioma incidence and community asbestos exposure. Env Res. 1997;75:34–40.

42. **Peterson J.J., Greenberg S., Buffler P.** Non-asbestos-related malignant mesothelioma. A review. Cancer. 1984;54:951–960.
43. **Attanoos R., et al.** Malignant Mesothelioma and Its Non-Asbestos Causes. Arch Pathol Lab Med 2018;142:753–760.
44. **Bianco A., et al.** Clinical diagnosis of malignant pleural mesothelioma. J Thorac Dis. 2018; S253-261.
45. **Xu, L. et al.** Malignant pleural mesothelioma: diagnostic value of medical thoracoscopy and long-term prognostic analysis. BMC Pulm Med. 2018;18:56.
46. **Odisio E. et al.** Malignant Pleural Mesothelioma: Diagnosis, Staging, Pitfalls and Follow-up. Semin Ultrasound CT MR. 2017;38:559–570.
47. **Rossini M. et al.** New Perspectives on Diagnosis and Therapy of Malignant Pleural Mesothelioma. Front Oncol. 2018;8:91.
48. **Katzman D., Sterman, D**. Updates in the diagnosis and treatment of malignant pleural mesothelioma. Curr Opin Pulm Med. 2018;24:319–326.
49. **Kapeles M. et al**. Trimodality Treatment of Malignant Pleural Mesothelioma: An Institutional Review. Am J Clin Oncol. 2018;41:30–35.
50. **Chang S.S.**, **et al,**. Mutations in subunits of the epithelial sodium channel cause salt wasting with hyperkalaemic acidosis, pseudohypoaldosteronism type 1. Nat Genet 1996;12:248-253.
51. **Beyer H**, **et al.** MESOMARK: a potential test for malignant pleural mesothelioma. Clin Chem 2007;53:666–672.
52. Ferro P., et al. Mesothelin is more useful in pleural effusion than in serum in the diagnosis of pleural mesothelioma. Anticancer Res. 2013;33:2707–2713.
53. **Franceschini M., et al.** Mesothelin in serum and pleural effusion in the diagnosis of malignant pleural mesothelioma with non-positive cytology. Anticancer Res. 2014;34:7425–7429.
54. **Inaguma S., et al.** Comprehensive immunohistochemical study of mesothelin (MSLN) using different monoclonal antibodies 5B2 and MN-1 in 1562 tumors with evaluation of its prognostic value in malignant pleural mesothelioma. Oncotarget 2017;8:26744–26754.
55. **Hassan R.**, **et al.** Phase II clinical trial of amatuximab, a chimeric antimesothelin antibody with pemetrexed and cisplatin in advanced unresectable pleural mesothelioma. Clin Cancer Res 2014;20:5927–5936.
56. **Cappia S.**, **et al.** Prognostic role of osteopontin expression in malignant pleural mesothelioma. Am J Clin Pathol. 2008;130:58–64.
57. **Grigoriu B.**, **et al.** Utility of osteopontin and serum mesothelin in malignant pleural mesothelioma diagnosis and prognosis assessment. Clin Cancer Res. 2007;13:2928–2935.
58. **Tajima K.**, **et al**. Osteopontin-mediated enhanced hyaluronan binding induces multidrug resistance in mesothelioma cells. Oncogene 2010;29:1941–1951.
59. **Qi F**, **et al.** Continuous exposure to chrysotile asbestos can cause transformation of human mesothelial cells via HMGB1 and TNF-α signaling. Am J Pathol. 2013;183:1654–1666.
60. **Napolitano A.**, **et al**. HMGB1 and Its Hyperacetylated Isoform are Sensitive and Specific Serum Biomarkers to Detect Asbestos Exposure and to Identify Mesothelioma Patients. Clin Cancer Res. 2016;22:3087–3096.
61. **Rrapaj E.**, **et al**. Expression analysis of HMGB1 in histological samples of malignant pleural mesothelioma. Histopatholog*y* 2018;72:1039–1050.

62. **Ying S.**, **et al**. Serum HMGB1 as a Potential Biomarker for Patients with Asbestos-Related Diseases. Dis Markers 2017;2017:5756102.
63. **Pass H**, **et al.** Fibulin-3 as a blood and effusion biomarker for pleural mesothelioma. N Engl J Med. 2012;367:1417–1427.
64. **Battolla E**., et al. Comparison of the Diagnostic Performance of Fibulin-3 and Mesothelin in Patients with Pleural Effusions from Malignant Mesothelioma. Anticancer Res. 2017;37:1387–1391.
65. **Robinson B.**, **Lake R**. Advances in malignant mesothelioma. N Engl J Med. 2005;353:1591–1603.
66. **Stathopoulos G.**, **et al**. Nuclear factor-kappaB affects tumor progression in a mouse model of malignant pleural effusion. Am J Respir Cell Mol Biol. 2006;34: 142–150.
67. **Kaneko O.**, **et al**. A binding domain on mesothelin for CA125/MUC16. J Biol Chem. 2009;284:3739–3749.
68. **Ito A.**, **et al**. Expression of cell adhesion molecule 1 in malignant pleural mesothelioma as a cause of efficient adhesion and growth on mesothelium. Lab Invest. 2008;88:504–514.
69. **Yoneda K.**, **et al.** Circulating tumor cells (CTCs) in malignant pleural mesothelioma (MPM). Ann Surg Oncol. 2014;S4:472–480.
70. **Chowdhury P.**, **Chang K.**, **Pastan I**. Isolation of anti-mesothelin antibodies from a phage display library. Mol Immunol. 1997;34:9–20.
71. **Hassan R.**, **et al.** Preclinical evaluation of MORAb-009, a chimeric antibody targeting tumor-associated mesothelin. Cancer Immun. 2007;7:20.
72. **Hassan R.**, **et al,**. Phase I clinical trial of the chimeric anti-mesothelin monoclonal antibody MORAb-009 in patients with mesothelin-expressing cancers. Clin Cancer Res. 2010;16:6132–6138.
73. **Craighead J., et al.** Characteristics of tumors and tumor cells cultured from experimental asbestos-induced mesotheliomas in rats. Am J Pathol. 1987;129: 448–462.
74. **Kim H.**, **Phung Y.**, **Ho M**. Changes in global gene expression associated with 3D structure of tumors: an ex vivo matrix-free mesothelioma spheroid model. PLoS One 2012;7:e39556.
75. **Hudson A.**, **et al.** Establishing a panel of chemo-resistant mesothelioma models for investigating chemo-resistance and identifying new treatments for mesothelioma. Sci Rep. 2014;4:6152.
76. **Barbone D., et al.** Mammalian target of rapamycin contributes to the acquired apoptotic resistance of human mesothelioma multicellular spheroids. J Biol Chem. 2008;283:13021–13030.
77. **Higashiyama M**, **Oda K**, **Okami J**, **et al,**. In vitro-chemosensitivity test using the collagen gel droplet embedded culture drug test (CD-DST) for malignant pleural mesothelioma: possibility of clinical application. Ann Thorac Cardiovasc Surg. 2008;14:355–362.
78. **Lou E., et al.** Tunneling nanotubes provide a unique conduit for intercellular transfer of cellular contents in human malignant pleural mesothelioma. PLoS One 2012;7:e33093.
79. **Thayanithy V., et al.** Tumor exosomes induce tunneling nanotubes in lipid raft-enriched regions of human mesothelioma cells. Exp Cell Res. 2014;323:178–188.

80. **Ady J., et al.** Intercellular communication in malignant pleural mesothelioma: properties of tunneling nanotubes. Front Physiol. 2014;5:400.
81. **Ady J., et al.** Tunneling nanotubes: an alternate route for propagation of the bystander effect following oncolytic viral infection. Mol Ther Oncolytics 2016;3:16029.
82. **Schramm A., et al.** Prognostic significance of epithelial-mesenchymal transition in malignant pleural mesothelioma. Eur J Cardiothorac Surg. 2010;37:566–572.
83. **Iwanami T., et al.** Clinical significance of epithelial-mesenchymal transition-associated markers in malignant pleural mesothelioma. Oncology 2014;86:109–116.
84. **de Reyniès A., et al.** Molecular Classification of Malignant Pleural Mesothelioma: Identification of a Poor Prognosis Subgroup Linked to the Epithelial-to-Mesenchymal Transition. Clin Cancer Res. 2014;20:1323-1334.
85. **Plönes T., et al.** Turning back the Wheel: Inducing Mesenchymal to Epithelial Transition via Wilms Tumor 1 Knockdown in Human Mesothelioma Cell Lines to Influence Proliferation, Invasiveness, and Chemotaxis. Pathol Oncol Res. 2017;23:723–730.
86. **Kinnula V.**, **et al.** Tenascin and fibronectin expression in human mesothelial cells and pleural mesothelioma cell-line cells. Am J Respir Cell Mol Biol. 1998;19:445–452.
87. **Scarpa S., et al.** Migration of mesothelioma cells correlates with histotype-specific synthesis of extracellular matrix. Int J Mol Med. 1999;4:67–71.
88. **Klominek J., Robért K., Sundqvist K**. Chemotaxis and haptotaxis of human malignant mesothelioma cells: effects of fibronectin, laminin, type IV collagen, and an autocrine motility factor-like substance. Cancer Res. 1993;53:4376–4382.
89. **Davidson B., et al.** Heparanase and basic fibroblast growth factor are co-expressed in malignant mesothelioma. Clin Exp Metastasis 2004;21:469–476.
90. **Zhong J.**, **et al.** ERK1/2 and p38 MAP kinase control MMP-2, MT1-MMP, and TIMP action and affect cell migration: A comparison between mesothelioma and mesothelial cells. J Cell Physiol. 2006;207:540–552.
91. **Abascal F., Irisarri I., Zardoya R.** Diversity and evolution of membrane intrinsic proteins. Biochim Biophys Acta - Gen Subj. 2014;1840:1468–1481.
92. **Denker B., et al.** Identification, purification, and partial characterization of a novel Mr 28,000 integral membrane protein from erythrocytes and renal tubules. J Biol Chem. 1988;263:15634–15642.
93. **Smith B., Agre P.** Erythrocyte Mr 28,000 transmembrane protein exists as a multisubunit oligomer similar to channel proteins. J Biol Chem. 1991;266:6407–6415.
94. **Preston G.M.**, **Agre P.** Isolation of the cDNA for erythrocyte integral membrane protein of 28 kilodaltons: member of an ancient channel family. Proc Natl Acad Sci U S A 1991;88:11110–11114.
95. **Preston G.M., et al.** Appearance of Water Channels in Xenopus Oocytes Expressing Red Cell CHIP28 Protein. Science 1992;256:385-387.
96. **Walz T., et al.** The three-dimensional structure of human erythrocyte aquaporin CHIP. EMBO J 1994;13:2985–2993.

97. **Sui H., et al.** Structural basis of water-specific transport through the AQP1 water channel. Nature 2001;414:872-878.
98. **Zhang R., et al.** A point mutation at cysteine 189 blocks the water permeability of rat kidney water channel CHIP28K. *Biochemistry* 1993;32:2938–2941.
99. **Yang B**, **Ma T**, **Verkman A**. Erythrocyte water permeability and renal function in double knockout mice lacking aquaporin-1 and aquaporin-3. J Biol Chem. 2001;276:624–628.
100. **Yang B., Kim J.K., Verkman A.S.** Comparative efficacy of HgCl2 with candidate aquaporin-1 inhibitors DMSO, gold, TEA+ and acetazolamide. FEBS Lett. 2006;580:6679-6684.
101. **Monzani E., et al.** AQP1 Is Not Only a Water Channel: It Contributes to Cell Migration through Lin7/Beta-Catenin [Online]. PLoS One 2009;4: e6167.
102. **Meng F., et al.** Aqp1 enhances migration of bone marrow mesenchymal stem cells through regulation of FAK and β-catenin. Stem Cells De*v.* 2014;23:66–75.
103. **Preston G.M., et al.** Mutations in aquaporin-1 in phenotypically normal humans without functional CHIP water channels. Science 1994;265:1585-1587.
104. **Saadoun S., et al.** Impairment of angiogenesis and cell migration by targeted aquaporin-1 gene disruption. Nature 2005;434:786-792.
105. **Mobasheri A., et al.** Heterogeneous expression of the aquaporin 1 (AQP1) water channel in tumors of the prostate, breast, ovary, colon and lung: a study using high density multiple human tumor tissue microarrays. Int J Oncol. 2005;26:1149–1158.
106. **López-Campos J., et al.**. Overexpression of Aquaporin-1 in lung adenocarcinomas and pleural mesotheliomas. Histol Histopathol. 2011;26:451–459.
107. **Kao S.C-H., et al.** Aquaporin 1 is an independent prognostic factor in pleural malignant mesothelioma. Cancer 2011;118:2952–2961.
108. **Jagirdar R., et al.**. Gene expression profile of aquaporin 1 and associated interactors in malignant pleural mesothelioma. Gene 2013;517:99–105.
109. **Driml J., et al.** Usefulness of Aquaporin 1 as a Prognostic Marker in a Prospective Cohort of Malignant Mesotheliomas. Int J Mol Sci. 2016;17:E1041.
110. **Canessa M., et al.** Rate of activation and deactivation of K:Cl cotransport by changes in cell volume in hemoglobin SS, CC and AA red cells. J Membr Biol. 1994;142:349-362.
111. **Noreng S., et al.** Structure of the human epithelial sodium channel by cryo-electron microscopy. Elife 2018;7:e39340.
112. **Vallet V., et al.** An epithelial serine protease activates the amiloride-sensitive sodium channel. Nature 1997;389:607-610.
113. **Vuagniaux G., et al.** Activation of the Amiloride-Sensitive Epithelial Sodium Channel by the Serine Protease mCAP1 Expressed in a Mouse Cortical Collecting Duct Cell Line. J Am Soc Nephrol. 2000;11:828-834.
114. **Donaldson S.H., et al.** Regulation of the Epithelial Sodium Channel by Serine Proteases in Human Airways. J Biol Chem. 2002;277:8338–8345.
115. **Ilatovskaya D.V., et al.** Cortical actin binding protein cortactin mediates ENaC activity via Arp2/3 complex. FASEB J 2011;25:2688–2699.

116. **Mazzochi C., et al.** The Carboxyl Terminus of the α-Subunit of the Amiloride-sensitive Epithelial Sodium Channel Binds to F-actin. J Biol Chem. 2006;281:6528–6538.
117. **He M., et al.** The Epithelial Sodium Channel (αENaC) Is a Downstream Therapeutic Target of ASCL1 in Pulmonary Neuroendocrine Tumors. Transl Oncol. 2018;11:292–299.
118. **Kapoor N., et al.** Knockdown of ASIC1 and epithelial sodium channel subunits inhibits glioblastoma whole cell current and cell migration. J Biol Chem. 2009;284:24526–24541.
119. **Endoh H., et al.** Prognostic Model of Pulmonary Adenocarcinoma by Expression Profiling of Eight Genes As Determined by Quantitative Real-Time Reverse Transcriptase Polymerase Chain Reaction. J Clin Oncol 2004;22:811–819.
120. **Kao S.C., et al.** Aquaporin 1 is an independent prognostic factor in pleural malignant mesothelioma. Cancer. 2012;118:2952-2961.
121. **Angelico G., et al.** Aquaporin-1 expression in fluoro-edenite-induced mesothelioma effusions: An approach by cell-block procedure. Cytopathology 2018;29:455–460.
122. **Nie H.G., et al.** Expression and Regulation of Epithelial Na+ Channels by Nucleotides in Pleural Mesothelial Cells. Am J Respir Cell Mol Biol. 2009;40:543–554.
123. **Foty R.** A simple hanging drop cell culture protocol for generation of 3D spheroids. J Vis Exp. 2011;(51).
124. **Niedbala M.**, **Crickard K.**, **Bernacki R**. Interactions of human ovarian tumor cells with human mesothelial cells grown on extracellular matrix. An in vitro model system for studying tumor cell adhesion and invasion. Exp Cell Res. 1985;160:499–513.
125. **Erkell L.**, **Schirrmacher V.** Quantitative in vitro assay for tumor cell invasion through extracellular matrix or into protein gels. Cancer Res. 1988;48:6933–6937.
126. **Kubow K.E., et al.** Crosslinking of cell-derived 3D scaffolds up-regulates the stretching and unfolding of new extracellular matrix assembled by reseeded cells. Integr Biol. 2009;1:635–648.
127. **Hansen K.C., et al.** An In-solution Ultrasonication-assisted Digestion Method for Improved Extracellular Matrix Proteome Coverage. Mol Cell Proteomics 2009;8: 1648-1657.
128. **Jagirdar R., et al.** Influence of AQP1 on cell adhesion, migration, and tumor sphere formation in malignant pleural mesothelioma is substratum- and histological-type dependent. Am J Physiol Lung Cell Mol Physiol. 2016;310:489-495.
129. **Baker F.L., et al.** Drug and Radiation Sensitivity Measurements of Successful Primary Monolayer Culturing of Human Tumor Cells Using Cell-adhesive Matrix and Supplemented Medium. Cancer Res. 1986;46:1263-1274.
130. **Lee M., et al.** Cell-substrate adhesion and metastatic potential of cultured mesothelioma cells induced by asbestos. Biochim Biophys Acta 1994;1226:151–162.

131. **Klominek J., et al.** Differential motile response of human malignant mesothelioma cells to fibronectin, laminin and collagen type IV: The role of β1 integrins. Int J Cancer 1998;72:1034–1044.
132. **Giuffrida A., et al.** The interaction of tenascin-C with fibronectin modulates the migration and specific metalloprotease activity in human mesothelioma cell lines of different histotype. Int J Oncol. 2004;25:745–750.
133. **Ohashi R., et al.** Osteopontin Modulates Malignant Pleural Mesothelioma Cell Functions In Vitro. Anticancer Res. 2009;29:2205–2214.
134. **An Z., et al.** Kindlin-2 is expressed in malignant mesothelioma and is required for tumor cell adhesion and migration. Int J Cancer 2010;127:1999–2008.
135. **Cheng N.C.**, **van Zandwijk N.**, **Reid G**. Cilengitide Inhibits Attachment and Invasion of Malignant Pleural Mesothelioma Cells through Antagonism of Integrins αvβ3 and αvβ5 [Online]. PLoS One 2014;9:e90374.
136. **Klebe S., et al.** Blockade of aquaporin 1 inhibits proliferation, motility, and metastatic potential of mesothelioma in vitro but not in an in vivo model. Dis Markers 2015;2015:286719.
137. **Hu J., Verkman A.** Increased migration and metastatic potential of tumor cells expressing aquaporin water channels. FASEB J. 2006;20:1892–1894.
138. **Liang H.T., Feng X.C., Ma T.H.** Water channel activity of plasma membrane affects chondrocyte migration and adhesion. Clin Exp Pharmacol Physiol. 2007;35:7–10.
139. **Wu Z., et al.** RNAi-mediated silencing of AQP1 expression inhibited the proliferation, invasion and tumorigenesis of osteosarcoma cells. Cancer Biol Ther. 2015;16:1332–1340.
140. **Borentain P., et al.** Inhibition of E-selectin expression on the surface of endothelial cells inhibits hepatocellular carcinoma growth by preventing tumor angiogenesis. Cancer Chemother Pharmacol. 2016;77:847–856.
141. **Ding Y., et al.** u-PA inhibitor amiloride suppresses peritoneal metastasis in gastric cancer. World J Surg Oncol. 2012;10:270.
142. **Zhu Y., et al.** Osteopontin Exacerbates Pulmonary Damage in Influenza-Induced Lung Injury. Jpn J Infect Dis. 2015;68:467–473.
143. **Maity G., et al.** Fibronectin--integrin mediated signaling in human cervical cancer cells (SiHa). Mol Cell Biochem. 2010;336:65–74.
144. **Chifflet S., Hernández J.A., Grasso S.** A possible role for membrane depolarization in epithelial wound healing. Am J Physiol Cell Physiol. 2005;288: 1420–1430.
145. **Wei X., Dong J.** Aquaporin 1 promotes the proliferation and migration of lung cancer cell in vitro. Oncol Rep. 2015;34:1440–1444.
146. **Kourghi M., et al.** Bumetanide Derivatives AqB007 and AqB011 Selectively Block the Aquaporin-1 Ion Channel Conductance and Slow Cancer Cell Migration [Online]. Mol Pharmacol. 2016;89:133-140.
147. **Dorward H.S., et al.** Pharmacological blockade of aquaporin-1 water channel by AqB013 restricts migration and invasiveness of colon cancer cells and prevents endothelial tube formation in vitro. J Exp Clin Cancer Res. 2016;35:36.
148. **Grifoni S.C., et al.** ENaC proteins contribute to VSMC migration. Am J Physiol Circ Physiol 2006;291:3076–3086.

149. **del Mónaco S.M., et al.** Cell Migration in BeWo Cells and the Role of Epithelial Sodium Channels. J Membr Biol. 2009;232:1–13.
150. **Justet C., et al.** ENaC contribution to epithelial wound healing is independent of the healing mode and of any increased expression in the channel. Cell Tissue Res. 2013;353:53–64.
151. **Wang S., et al.** Reduced Expression of Enac in Placenta Tissues of Patients with Severe Preeclampsia Is Related to Compromised Trophoblastic Cell Migration and Invasion during Pregnancy. PLoS One 2013;8:e72153.
152. **Reichert D., et al.** Tunneling nanotubes mediate the transfer of stem cell marker CD133 between hematopoietic progenitor cells. Exp Hematol. 2016;44:1092–1112.
153. **Osteikoetxea-Molnár A., et al.** The growth determinants and transport properties of tunneling nanotube networks between B lymphocytes. Cell Mol Life Sci. 2016;l73:4531–4545.
154. **Symington B.** Fibronectin receptor modulates cyclin-dependent kinase activity. J Biol Chem. 1992;267:25744–25747.
155. **Nagano N., et al.** Organization of F-actin filaments in human glioma cell lines cultured on extracellular matrix proteins. J Neurooncol. 1996;27:215–224.
156. **Kanaji N., et al.** Fibronectin and Hepatocyte Growth Factor Produced by Lung Fibroblasts Augment Migration and Invasion of Malignant Pleural Mesothelioma Cells. Anticancer Res. 2017;37:2393–2400.
157. **Ivanova A.V., et al.** Protumorigenic Role of HAPLN1 and Its IgV Domain in Malignant Pleural Mesothelioma. Clin Cancer Res. 2009;15:2602-2611.
158. **Shapiro I., et al.** Merlin deficiency predicts FAK inhibitor sensitivity: a synthetic lethal relationship. Sci Transl Med. 2014;6:237ra68.
159. **McGregor K., Gil J., Lahiri S.** A morphometric study of the carotid body in chronically hypoxic rats. J Appl Physiol Respir Env Exerc Physiol. 1984;57:1430–1438.
160. **Muñoz-Cabello A.M., et al.** AQP1 mediates water transport in the carotid body. Pflügers Arch - Eur J Physiol. 2010;459:775–783.
161. **Galán-Cobo A., et al.** Aquaporin-1 plays important role in proliferation by affecting cell cycle progression. J Cell Physiol. 2015;231:243–256.
162. **Pulford E., et al.** The Effect of Aquaporin 1-Inhibition on Vasculogenic Mimicry in Malignant Mesothelioma. Int J Mol Sci. 2017;18(11).
163. **Bondarava M., et al.** α-ENaC is a functional element of the hypertonicity-induced cation channel in HepG2 cells and it mediates proliferation. Pflügers Arch - Eur J Physiol. 2009;458:675-687.
164. **Petrik D., et al.** Epithelial Sodium Channel Regulates Adult Neural Stem Cell Proliferation in a Flow-Dependent Manner. Cell Stem Cell 2018;22:865–878.
165. **Paulus W., Huettner C., Tonn J.C.** Collagens, integrins and the mesenchymal drift in glioblastomas: A comparison of biopsy specimens, spheroid and early monolayer cultures. Int J Cancer 2018;58:841–846.
166. **Nederman T., et al.** Demonstration of an Extracellular Matrix in Multicellular Tumor Spheroids. Cancer Res. 1984;44:3090-3097.
167. **Burleson K.M., et al.** Ovarian carcinoma ascites spheroids adhere to extracellular matrix components and mesothelial cell monolayers. Gynecol Oncol 2004;93:170–181.

168. **Kelm J.M., et al.** Method for generation of homogeneous multicellular tumor spheroids applicable to a wide variety of cell types. Biotechnol Bioeng 2003;83:173–180.
169. **Zhou Z.C., et al.** Characteristics of Notch2+ pancreatic cancer stem-like cells and the relationship with centroacinar cells. Cell Biol Int. 2013;37:805–811.
170. **Hoque M.O., et al.** Aquaporin 1 Is Overexpressed in Lung Cancer and Stimulates NIH-3T3 Cell Proliferation and Anchorage-Independent Growth. Am J Pathol. 2006;168:1345–1353.
171. **Church J.G., Mills G.B., Buick R.N.** Activation of the Na+/H+; antiport is not required for epidermal growth factor-dependent gene expression, growth inhibition or proliferation in human breast cancer cells. Biochem J. 1989;257:151-157.
172. **Zamora P.O., Danielson K.G., Hosick H.L.** Invasion of Endothelial Cell Monolayers on Collagen Gels by Cells from Mammary Tumor Spheroids. Cancer Res. 1980;40:4631-4639.
173. **Chintala S., et al.** Role of extracellular matrix proteins in regulation of human glioma cell invasion in vitro. Clin Exp Metastasis 1996;14:358–366.
174. **Thurber A.E., et al.** Inverse expression states of the BRN2 and MITF transcription factors in melanoma spheres and tumour xenografts regulate the NOTCH pathway. Oncogene 2011;30:3036-3048.
175. **Nonaka M., et al.** Elevated cell invasion in a tumor sphere culture of RSV-M mouse glioma cells. Neurol Med Chir (Tokyo) 2015;55:60–70.
176. **De Wever O., et al.** Modeling and quantification of cancer cell invasion through collagen type I matrices. Int J Dev Biol. 2010;54:887–896.
177. **Jiang Y.** Aquaporin-1 activity of plasma membrane affects HT20 colon cancer cell migration. IUBMB Life. 2009;61:1001-1009.
178. **Wei X., Dong J.** Aquaporin 1 promotes the proliferation and migration of lung cancer cell in vitro. Oncol Rep 2015;34:1440–1448.
179. **Luo L., et al.** Decreased miR-320 expression is associated with breast cancer progression, cell migration, and invasiveness via targeting Aquaporin 1. Acta Biochim Biophys Sin (Shanghai) 2018;50:473–480.
180. **Yang Y., et al.** ENaC mediates human extravillous trophblast cell line (HTR8/SVneo) invasion by regulating levels of matrix metalloproteinase 2 (MMP2). Placenta 2015;36:587–593.
181. **Zolak J., et al.** Pleural mesothelial cell differentiation and invasion in fibrogenic lung injury. Am J Pathol. 2013;182:1239–1247.
182. **Casarsa C., et al.** Epithelial-to-mesenchymal transition, cell polarity and stemness-associated features in malignant pleural mesothelioma. Cancer Lett. 2011;302:136–143.
183. **Kirkland S.C., et al.** Organisation and gel contraction by human colonic carcinoma (HCA-7) sublines grown in 3-dimensional collagen gel. Int J Cancer 2018;60:877–882.
184. **Deryugina E.I., et al.** Remodeling of Collagen Matrix by Human Tumor Cells Requires Activation and Cell Surface Association of Matrix Metalloproteinase-2. Cancer Res 1998;58:3743-3750.
185. **Wozniak M.A., et al.** ROCK-generated contractility regulates breast epithelial cell differentiation in response to the physical properties of a three-dimensional collagen matrix. J Cell Biol. 2003;163:583-595.

186. **Nielsen H., et al.** Collagen gel contraction serves to rapidly distinguish epithelial- and mesenchymal-derived cells irrespective of alpha-smooth muscle actin expression. Vitr Cell Dev Biol Anim. 2003;39:297–303.
187. **Morales S.A., et al.** Collagen gel contraction by ARPE-19 cells is mediated by a FAK-Src dependent pathway. Exp Eye Res. 2007;85:790–798.
188. **Ramachandran C., et al.** Rho-Rho kinase pathway in the actomyosin contraction and cell-matrix adhesion in immortalized human trabecular meshwork cells. Mol Vis. 2011;17:1877–1890.
189. **Engelsvold D., et al.** miRNA and mRNA expression profiling identifies members of the miR-200 family as potential regulators of epithelial-mesenchymal transition in pterygium. Exp Eye Res. 2013;115:189–198.
190. **Shakibaei M., Mobasheri A.** Beta1-integrins co-localize with Na, K-ATPase, epithelial sodium channels (ENaC) and voltage activated calcium channels (VACC) in mechanoreceptor complexes of mouse limb-bud chondrocytes. Histol Histopathol. 2003;18:343–351.
191. **Klein C.E., et al.** Integrin alpha 2 beta 1 is upregulated in fibroblasts and highly aggressive melanoma cells in three-dimensional collagen lattices and mediates the reorganization of collagen I fibrils. J Cell Biol. 1991;115:1427–1436.